WADC TECHNICAL REPORT 54-113
Part III
ASTIA DOCUMENT NO. AD-118052

(UNCLASSIFIED TITLE)

THREE-DIMENSIONAL SUPERSONIC FLUTTER MODEL TEST NEAR MACH NUMBER 1.5

Part III: Experimental and Theoretical Data for Wings with Control Surfaces

Gifford W. Asher
Warren H. Weatherill

Massachusetts Institute of Technology

JANUARY 1958

AIRCRAFT LABORATORY
CONTRACT AF 33(038)-22955
PROJECT No. 1370

WRIGHT AIR DEVELOPMENT CENTER
AIR RESEARCH AND DEVELOPMENT COMMAND
UNITED STATES AIR FORCE
WRIGHT-PATTERSON AIR FORCE BASE, OHIO

[redacted]

FOREWORD

This report, which presents the experimental and theoretical results of a program of supersonic flutter testing, was prepared by the Aeroelastic and Structures Research Laboratory, Massachusetts Institute of Technology, Cambridge 39, Massachusetts for the Aircraft Laboratory, Wright Air Development Center, Wright-Patterson Air Force Base, Ohio. The work was performed at M. I. T. under the direction of Professor R. L. Halfman, and the project was supervised by Mr. G. W. Asher. The research and development work was accomplished under Air Force Contract No. AF33(038)-22955, Project No. 1370, (UNCLASSIFIED TITLE) "Aeroelasticity, Vibration and Noise," and Task No. 13474, (UNCLASSIFIED TITLE) "Three Dimensional Supersonic Flutter Model Tests at Mach Number 1.5." Mr. Niles R. Hoffman of the Dynamics Branch, Aircraft Laboratory, is task engineer. This task covers a continuing effort on flutter research at supersonic speeds which started in March 1951. This is Part III of a report published in three separate parts. WADC TR 54-113, Part I. (UNCLASSIFIED TITLE) "Model Design and Testing Techniques" was published in December 1955; WADC TR 54-113, Part II, (UNCLASSIFIED TITLE) "Experimental and Theoretical Data For Bare Wings and Wings With Tip Tanks" was published in December 1955; and WADC TR 54-114, (UNCLASSIFIED TITLE) "A Variable Mach Number Supersonic Test Section for Flutter Research" was published in December 1954.

The authors are indebted to Mr. O. Wallin and Mr. C. Fall for their help in the model construction and testing programs; to Mr. G. M. Falla for his help in the high speed photography; to Messrs. A. Heller, J. R. Martuccelli, J. R. Friery, H. Moser, and G. Zartarian for their help in preparing the calculations and data of this program; and to all the other members of the Aeroelastic and Structures Research Laboratory Staff for their help in obtaining the data for this report.

This document is classified CONFIDENTIAL in its entirety (excepting the title) because results of supersonic flutter tests are presented and these results have application in the determination of flutter prevention criteria for present and future military aircraft.

[redacted]

ABSTRACT

This report presents the results of experimental supersonic wind tunnel flutter model tests and the associated theoretical calculations made on a series of low-aspect-ratio models of straight, swept, and delta wing planform with trailing edge control surfaces. Models of each planform were designed to be free from flutter without the control surface. Flutter was then obtained by adding a control surface to the basic wing and lowering the flapping frequency of the surface until flutter occurred. The following results were obtained.

1. For the straight wing planform, high-frequency flutter involving mainly the aileron generally occurred for unbalanced but not for balanced ailerons. This type of flutter occurred for all values of control surface frequency that could be attained on the models at Mach numbers at or below $\sqrt{2}$. Low-frequency flutter, similar to classical bending-torsion-aileron flutter also occurred at lower supersonic Mach numbers for two models.

2. For the swept wing planform, high-frequency flutter involving mainly the aileron occurred when the aileron frequency was lowered sufficiently for both balanced and unbalanced ailerons. No cases of flutter similar to classical bending-torsion-aileron flutter occurred for the swept planform.

3. For the delta wing planform, flutter involving the elevon and wing degrees of freedom was found when the elevon frequency was lowered sufficiently.

Some calculations using linearized supersonic, two-dimensional aerodynamic coefficients were also made for the straight wing configurations with three degrees of freedom, wing bending, wing torsion, and aileron flapping, and with a single-degree-of-freedom aileron flapping. Both types of calculation predicted high-frequency flutters of the type observed experimentally, and the quantitative correlation between the theoretical and experimental results is quite good in some instances.

PUBLICATION REVIEW

This report has been reviewed and is approved.

FOR THE COMMANDER:

For RANDALL D. KEATOR
Colonel, USAF
Chief, Aircraft Laboratory

TABLE OF CONTENTS

LIST OF ILLUSTRATIONS

LIST OF ILLUSTRATIONS (Cont.)

LIST OF ILLUSTRATIONS (Cont.)

LIST OF TABLES

LIST OF SYMBOLS

Unswept coordinate directions x, y, z are used in the definition of all quantities except EI and GJ which are related to the elastic axis direction.

a	Distance aileron hinge line lies aft of elastic axis, positive aft (Fig. 23)
b	Semichord of a surface
c	Chord of a surface
C	Flexibility influence coefficient
(cg)	Center of gravity position, percent chord
(ea)	Elastic axis position, percent chord
EI	Bending stiffness
g	Coefficient of structural damping
GJ	Torsional stiffness
I_{HL}	Mass moment of inertia of the aileron about the hinge line
I_α	Mass moment of inertia of the wing and aileron about the elastic axis
K	Spring stiffness (Fig. 23)
k	Reduced frequency, $k = \omega b/V$
ℓ	Semispan of wing
m	Mass per unit span
M	Mach number
M_β, M_3', M_4'	Theoretical aerodynamic moments for the aileron (see Eqs. 1, 3 and 4 of Appendix I)
r_α	Radius of gyration of the wing and aileron about the elastic axis (nondimensionalized with respect to the semichord)

List of Symbols (Cont.)

r_{HL}	Dimensionless radius of gyration of the aileron about the hinge line
S_α	Static unbalance of the wing and aileron about the elastic axis
S_{HL}	Static unbalance of the aileron about the hinge line
V	Velocity
x	Coordinate axis along the wing chord with origin at the elastic axis (Fig. 23)
y	Coordinate axis along the wing span with origin at the wing root
z	Coordinate in vertical direction with origin at the elastic axis
α	Angle of attack of the wing, positive when nose up
β	Angle of flapping of the control, positive when trailing edge down
λ	Taper ratio (chord at tip/chord at root)
μ	Relative density, $\mu = \frac{m}{\pi \rho b^2}$
ρ	Air density
ω	Frequency

SUBSCRIPTS

f	Value of a parameter at flutter
r	Value of parameter at reference station of surface which for this report was taken at the 75% spanwise station from inboard edge.
1,2	First and second coupled vibration modes
h_1	First uncoupled bending vibration mode
α_1	First uncoupled torsion vibration mode
α_N	Reference first torsion vibration frequency (see Appendix III)
β	Uncoupled control surface flapping frequency
o	Root station
w	wing
a	aileron

SECTION I

INTRODUCTION

With the advent of thin lifting surfaces and flight at high dynamic pressure the prevention of flutter is becoming more and more a primary design consideration. In the subsonic flight regime, the aircraft designer could with the help of calculations and a small number of experimental tests obtain the information needed to prevent primary surface flutter. In the supersonic flight regime, the quantitative correlation between theoretical calculations and experimental results has so far not been good. Reference 1, for example, shows that there are large differences between the test and the calculated flutter boundaries, except in a very narrow band of Mach number around 1.35.

Until more satisfactory theoretical methods are available, the aircraft designer will probably rely heavily on experimental flutter test results in the supersonic flight regime. Fortunately, quite a large body of experimental data on primary surface flutter is available. Reference 1, for example, presents experimental data for a series of low-aspect-ratio straight, swept, and delta wing planforms. This data is compared with other supersonic results and transonic data, so that flutter boundaries over the Mach number range of 0.6 to 2.0 can be drawn for cantilever models with parameters similar to those tested.

Some serious flutter problems associated with supersonic flight for which little or no experimental data are available are the effects of external stores and control surfaces on flutter boundaries. In Ref. 1 some tests have been made to determine the effect of tip tanks on the flutter characteristics of straight and swept wing configurations. A few preliminary tests on wings with trailing edge control surfaces were also made. Reported here are the results of an extension and expansion of the tests described in Ref. 1 on the effects of control surface rotational restraint and mass balance on flutter boundaries. An attempt is made to define the minimum allowable control surface frequency for the same series of low-aspect-ratio planforms used in Ref. 1. The results of simple supersonic flutter calculations conducted for the straight wing planform are compared with the experimental results.

Manuscript released by the authors December 1957 for publication as a WADC Technical Report.

No basic changes were required in the model design and testing techniques from those described in Ref. 2. Static tests and vibration tests were carried out for each model; the vibration tests were made before each flutter test whereas the static tests were repeated only after major structural damage had occurred. The wind tunnel test procedure consisted of starting the tunnel at relatively high Mach number before injecting the semispan model quickly through the side wall. When the model was fully injected the Mach number was smoothly reduced over a predetermined range (see Ref. 3). The model was retracted immediately following flutter or just before the tunnel was stopped. The behavior of the model during the flutter test was recorded visually using a high-speed camera and on an oscillograph using signals generated by strain gages in the models.

The results of this series of tests on straight, swept and delta wings with control surface are presented in Section II and the straight wing data are compared with theoretical predictions. An outline of the prediction technique is presented in Appendix I. Section III contains conclusions and recommendations. A detailed tabulation of all the experimental data is in Appendix II. In order to aid in the correlation of the straight wing theoretical and experimental results it was helpful to calculate a reference torsional frequency for each model. This procedure is described in Appendix III.

SECTION II

DISCUSSION OF RESULTS

1. Introduction

The models of each of the three planforms were designed to have a specified margin of safety in flutter when not provided with a control surface. The margin of safety was defined as the ratio of the torsional stiffness to be built into the model to the minimum torsional stiffness necessary to prevent flutter over the Mach number range of 2.0 to 1.3. This minimum torsional stiffness was estimated from the test results of Ref. 1 presented in terms of the flutter parameter $(V_f/b\omega_\alpha)\,(1/\sqrt{\mu})$. For each planform the existence of a margin of safety was verified by the construction and testing of a model without control surface. When this basic model was demonstrated to be flutter free throughout the tunnel Mach number range, it was tested with both balanced and unbalanced control surface with a variety of hinge stiffnesses. In this way it was hoped to determine the variation of the flutter parameters with control surface frequency and mass balance.

Sketches of the model layouts are in Fig. 14 of Appendix II. Typical details of the control surface mounting so as to have an effective hinge line at its leading edge and a sealed gap are shown in Fig. 12 and discussed in the accompanying text. For the straight and swept planforms the semispan control surface was tapered to have at each station a chord of 20% of the local wing chord. For the delta planform the control surface extended over the entire span and was of constant chord equal to 14% of the wing root chord.

In the vibration tests a technique was developed to measure the control surface frequency with the body of the wing clamped to provide a nearly cantilever support condition ahead of the control surface hinge line (see Appendix II). This measured uncoupled control surface flapping frequency ω_β was used as a basic parameter for describing the stiffness of the hinge mounting.

2. Straight Wing Results

a. Theoretical Results

A considerable body of calculations was made for the straight wing planform models with ailerons. The most extensive calculations utilized three

degrees of freedom, wing first bending, wing first torsion, and aileron flapping. Two dimensional linearized supersonic aerodynamic forces were used. Some calculations were made for a single-degree-of-freedom aileron flapping, where the aileron was considered as a wing free to pitch about its leading edge. These calculations were made on the basis of a representative section at the aileron midspan and also used two-dimensional linearized supersonic aerodynamic coefficients. The calculations are discussed in some detail in Appendix I.

Figures 1 and 2 show the results for mass unbalanced and mass balanced ailerons respectively from the three-degree-of-freedom calculations at four values of Mach number, 5/4, 10/7, 5/3 and 2.0. Above M = 10/7 the points of Figs. 1 and 2 can be faired smoothly, and somewhat surprisingly indicate that the mass balanced ailerons have slightly larger regions of instability than unbalanced ailerons. The rather large spread between the two-degree-of-freedom curve $(\omega_\beta/\omega_{\alpha_1}) = \infty$ and the three-degree-of-freedom curves may result from the apparently critical combination of μ and $(\omega_h/\omega_{\alpha_1})^2$ for this wing as shown in Fig. 3.1 of Ref. 1. The region of greatest interest on Figs. 1 and 2 lies below M = 10/7 because the calculated flutter points at M = 5/4 are sharply lower and because all of the experimental flutter points for the straight wing models were obtained in this Mach number regime. It should also be noted that all the experimental swept wing flutter points also occurred at cross flow Mach numbers based on the sweep of the hinge line in this Mach number regime. Below M = 10/7, supersonic aerodynamic coefficients are available for the aileron only at M = 5/4. Therefore, only one point can be calculated in the range of interest, and the fairing of the boundries between M = 5/4 and M = 10/7, the next point calculated, is somewhat arbitrary.

In Figs. 1 and 2 the abscissa of the $V_f/b_{o_w}\ \omega_{\alpha_1}$ plot is shown as a boundary of instability at Mach numbers below M $=\sqrt{2}$ for $(\omega_\beta/\omega_{\alpha_1}) = 0$. In Appendix I, it is shown that this case, which corresponds to a completely rigid wing, $\omega_{h_1} = \omega_{\alpha_1} = \infty$, arises from the possibility of single-degree-of-freedom flutter below M = $1/\sqrt{2}$. For higher $\omega_\beta/\omega_{\alpha_1}$, Figs. 10 and 11 in Appendix I, which are the plots of $V_f/b_{o_w}\ \omega_{\alpha_1}$ versus $(\omega_\beta/\omega_{\alpha_1})$ for the Mach numbers used in the calculation show that the rapid increases in the regions of instability below

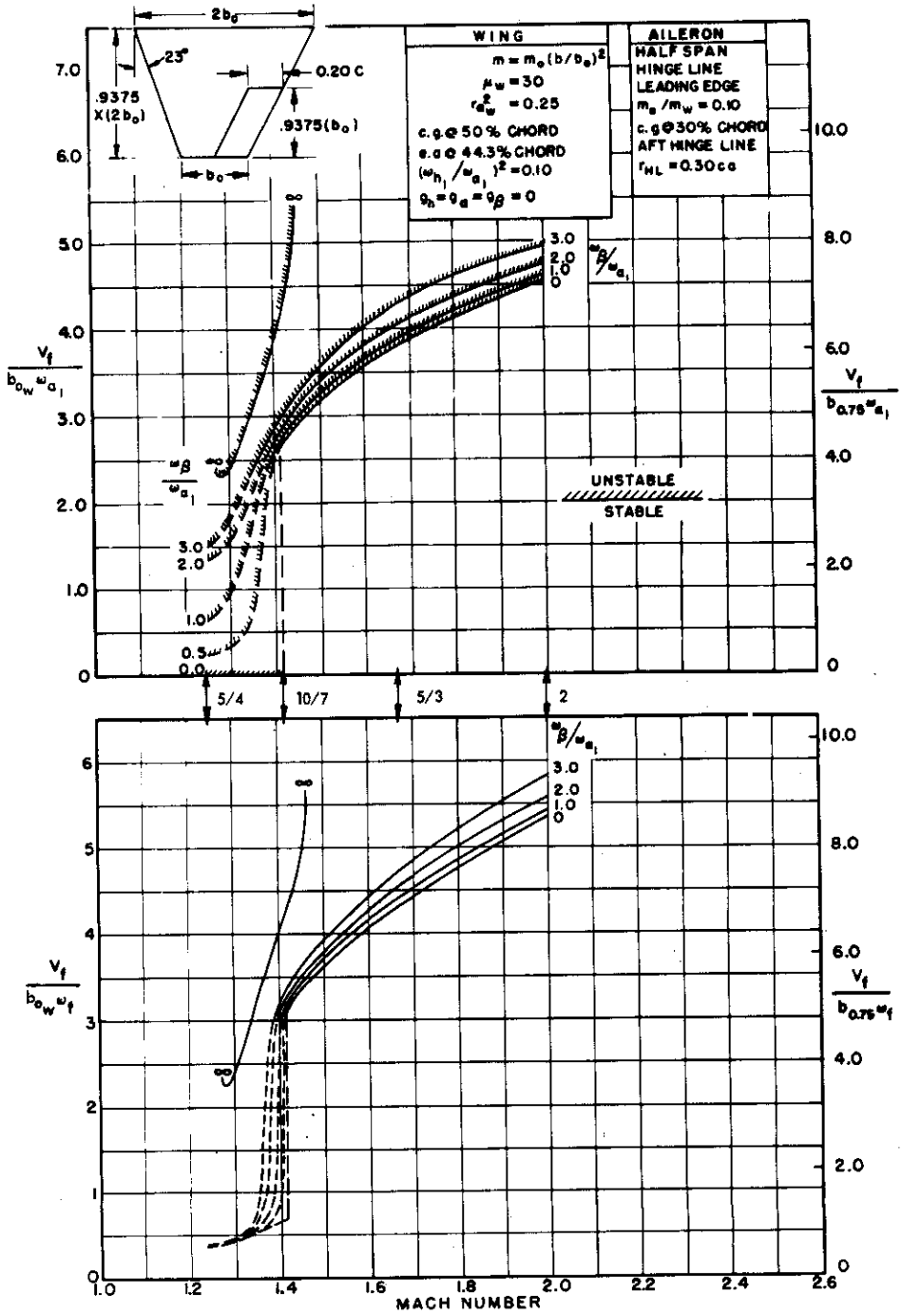

Fig. 1. Flutter parameters $V_f/b_{o_w}\omega_{\alpha_1}$ and $V_f/b_{o_w}\omega_f$ versus Mach number for straight wings with mass unbalanced ailerons from three-degree-of-freedom calculations.

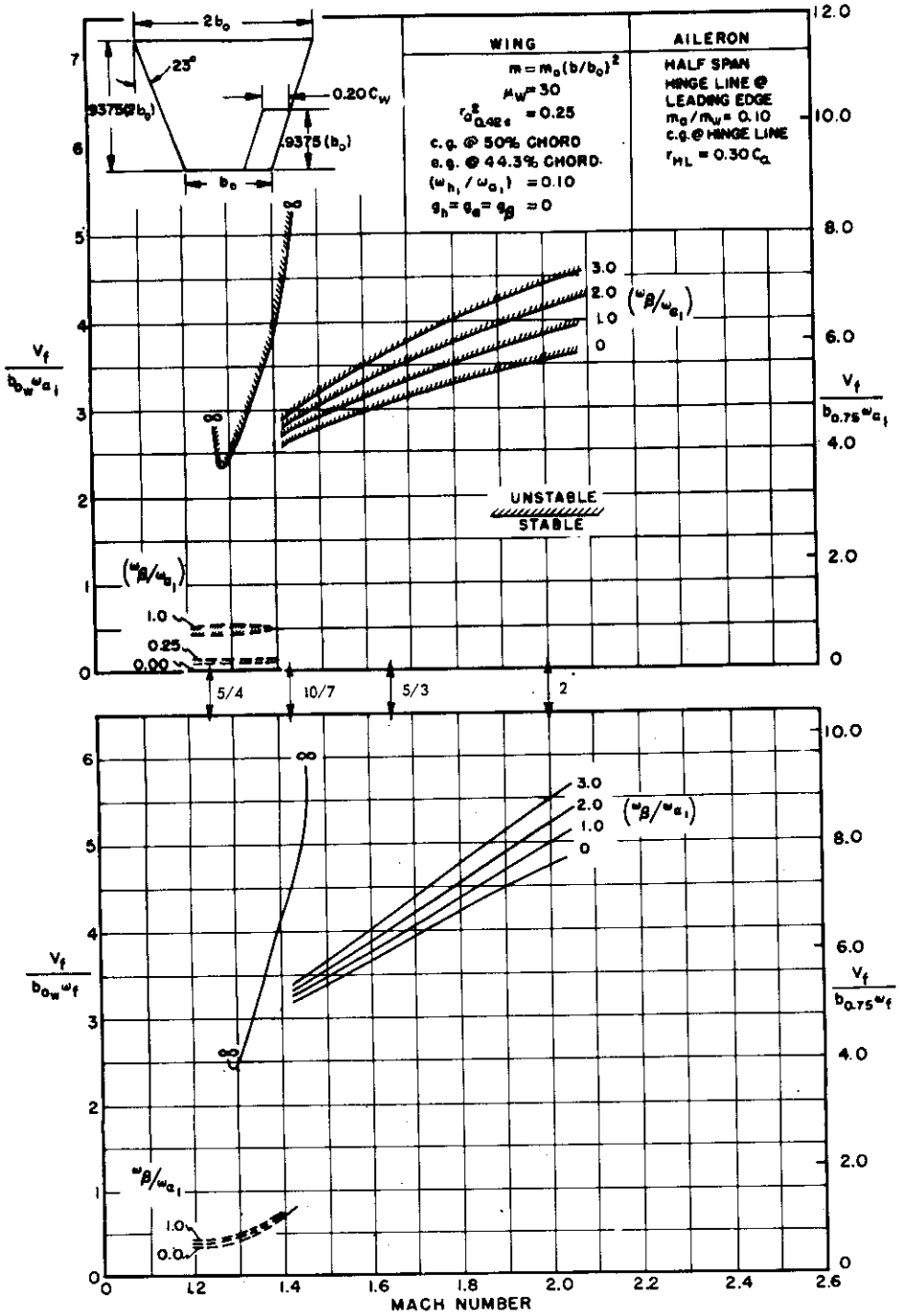

Fig. 2. Flutter parameters $V_f/b_{o_w}\omega_{a_1}$ and $V_f/b_{o_w}\omega_f$ versus Mach number for straight wings with mass balanced ailerons from three-degree-of-freedom calculations.

M = 10/7 are probably caused by changes in the critical flutter mode shape from one involving primarily bending, torsion, and aileron motions to one involving mainly aileron motion. This change in mode shape is accompanied by a sharp increase in the flutter frequency as shown by the curves of $V_f/b_{o_w}\,\omega_f$ on Figs. 1 and 2. As lower and lower values of $(\omega_\beta/\omega_{\alpha_1})$ are taken, the change in mode shape is more rapid and the drop in frequency more violent. In the limiting case when $(\omega_\beta/\omega_{\alpha_1}) = 0$, the boundary for $M > \sqrt{2}$ represents the bending-torsion-aileron mode and corresponds to the case of a free-aileron, $\omega_\beta = 0$. Below $M = \sqrt{2}$ the boundary, now the abscissa of Figs. 1 and 2, corresponds to the rigid wing case $\omega_{\alpha_1} = \infty$, or single-degree-of-freedom flutter. Further interpretation of this limiting case can be made from the curves in Appendix I.

Even a casual glance shows that there are marked differences between the boundaries for unbalanced and balanced ailerons. If the boundary for $(\omega_\beta/\omega_{\alpha_1}) = 1.0$ is considered, two separate branches are found for the balanced case. The upper branch is similar to that found in the unbalanced cases of Fig. 1 and probably represents a flutter mode in which wing bending and torsion modes and aileron flapping modes all figure importantly. No solutions were found for this branch at M = 5/4, so it may be assumed that this mode is not unstable at this Mach number. Below $M = \sqrt{2}$ a second branch of the $(\omega_\beta/\omega_{\alpha_1}) = 1.0$ boundary appears as discussed in Appendix I. This branch, which represents a high-frequency flutter in which aileron motion predominates, forms a small closed region of instability. As ω_β is increased to values of $(\omega_\beta/\omega_{\alpha_1})$ slightly greater than 1.0, the lower branch disappears entirely. As $(\omega_\beta/\omega_{\alpha_1})$ is decreased, the second branch which forms the closed region of instability below $M = \sqrt{2}$ moves closer to the abscissa, until, in the limit at $(\omega_\beta/\omega_{\alpha_1}) = 0$, it lies on the abscissa itself. For $(\omega_\beta/\omega_{\alpha_1}) = 0$ the interpretation of this region is the same as it was in the unbalanced case. It represents single-degree-of-freedom flutter of the aileron. The upper $(\omega_\beta/\omega_{\alpha_1}) = 0$ branch represents the bending-torsion-aileron flutter of a free aileron, $\omega_\beta = 0$. Comparison of the flutter boundaries between the balanced and unbalanced cases shows that below $M = \sqrt{2}$, the balanced aileron is, theoretically at least, much less susceptible to flutter.

The results of the single-degree-of-freedom analysis are shown in Fig. 3, which presents plots of the parameters $V_f/b_{r_a}\,\omega_\beta$ and $V_f/b_{r_a}\,\omega_f$ versus Mach

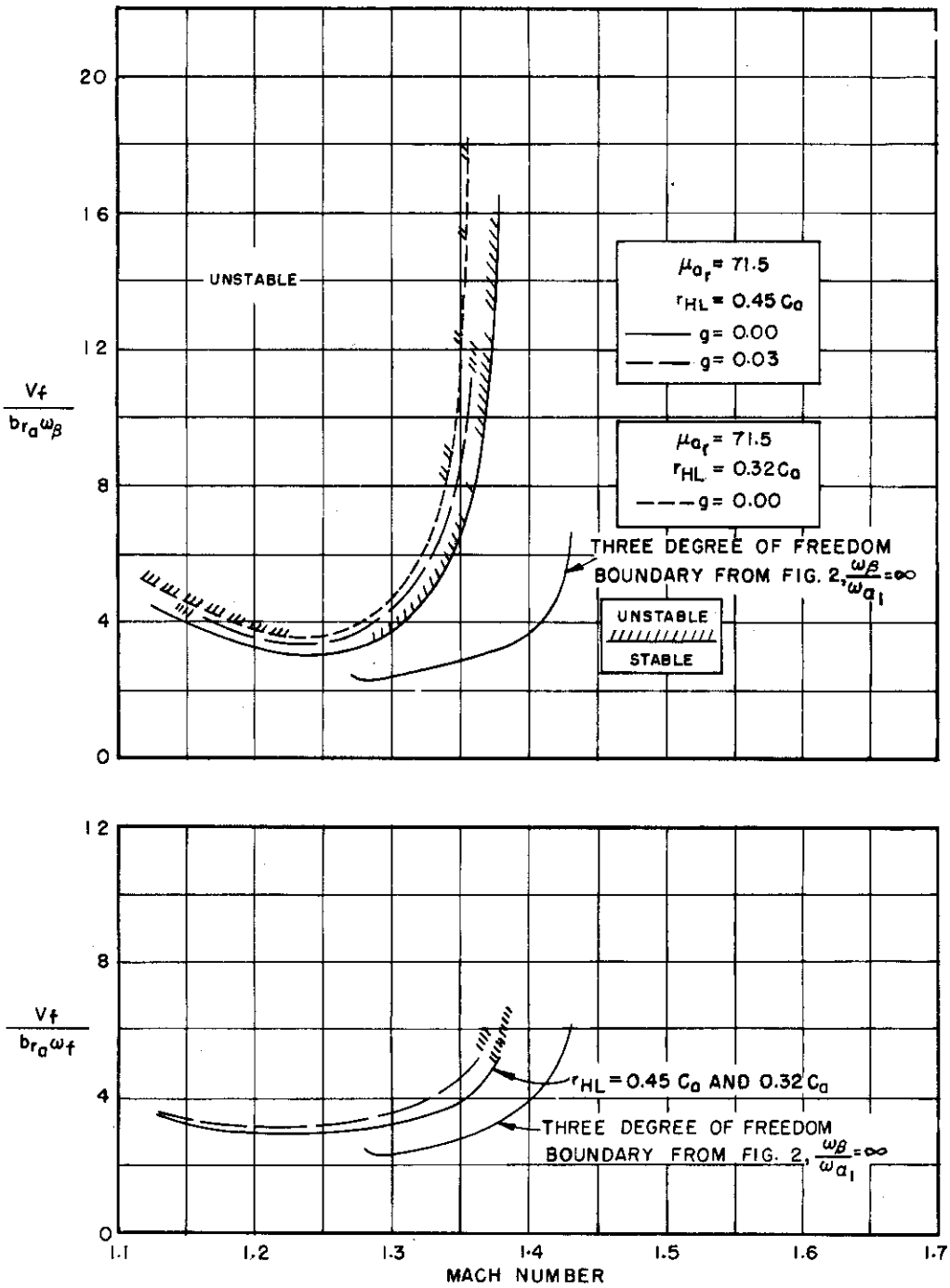

Fig. 3. Flutter parameters $V_f/b_{r_a}\omega_\beta$ and $V_f/b_{r_a}\omega_f$ versus Mach number for straight wing ailerons from single-degree-of-freedom calculations. Calculations made at M = 1.1, 1.2, 1.3, 1.4 and 1.5.

number. Below M = $\sqrt{2}$ the strong tendency of the aileron toward instability is very apparent and correlates closely with the sudden shifts in Figs. 1 and 2. Three single-degree-of-freedom cases were studied. For no structural damping, g = 0, two aileron radii of gyration, r_{HL}, were studied; $r_{HL} = 0.45\ c_a$ corresponding to the unbalanced ailerons and $r_{HL} = 0.32\ c_a$ corresponding to the balanced ailerons. The curves of Fig. 3 show that decreasing the radius of gyration decreases the region of instability slightly. For a radius of gyration $r_{HL} = 0.45\ c_a$, the effects of structural damping were shown to decrease the region of instability slightly.

The most important theoretical results presented in this section may be summarized as follows:

1) Both three-degree-of-freedom and single-degree-of-freedom calculations predict that high-frequency flutter will occur in the Mach number range below M = $\sqrt{2}$.

2) Three-degree-of-freedom calculations predict that there are large differences in the flutter boundaries for the balanced and unbalanced aileron cases. Below M ≅ 1.4 the mass balanced aileron cases have much smaller regions of instability than the balanced cases. Above M ≅ 1.4 the balanced cases show a slightly larger region of instability.

b) Experimental Results

The basic straight wing model without aileron designated ST-13, was designed to have a relative density μ of 30 and a margin of safety in flutter of 27% in torsional stiffness over that necessary to just prevent flutter over the Mach number range 2.0 to 1.3. Since the distributions of mass, external shape and stiffness were the same as the straight wing models of Ref. 1, the flutter data presented there in the form of $(V_f/b\omega_\alpha)(1/\sqrt{\mu})$ was used as the basis for calculating the margin of safety. After the ST-13 model was demonstrated by test to be flutter free it was redesigned to include an aileron without any change in its over-all properties.

The semispan, 20 percent chord ailerons had a running mass ten percent of the total wing running mass ($m_a/m_w = 0.10$) and were of two types, unbalanced and balanced. The unbalanced ailerons (ST-13A series) were designed to have their center of gravity at 30% of their chord and a radius of gyration r_{HL} about their hinge line of 45% of their chord. The balanced ailerons (ST-13AB series) had their center of gravity on the hinge line and a radius of gyration r_{HL} of 30% of their chord. (It should be noted that in all of the three-degree-of-freedom calculations r_{HL} was taken as $0.30\ c_a$, a figure which proved

[redacted]

unattainable in the design of the unbalanced ailerons.) The mass and stiffness data for these straight wing models are in Tables 2, 5, and 8. Vibration modes and frequencies are in Table 9.

The plan of the test program was to try models with successively softer aileron restraining springs in order to define a minimum allowable control surface frequency for both the unbalanced and balanced cases. Unexpectedly the first unbalanced aileron tests indicated a high frequency (above 600 cps) flutter involving predominatly aileron flapping at Mach numbers less than 1.4. As a result the single-degree-of-freedom calculations were carried out and the three-degree-of-freedom calculations were re-examined. In order to search for combined bending-torsion-aileron flutter without losing the model in the predominately aileron mode, models ST-13-A4, ST-13-A5, ST-13-AB, ST-13-AB1 and ST-13-AB2 were not tested below M = 1.4. At the same time two new model series were started to investigate further the low Mach number high-frequency aileron flutter. These two new series, ST-14 with unbalanced and ST-15 with balanced ailerons, were machined out of solid aluminum but had lightweight ailerons similar to those of the ST-13 series. These models were designed to emphasize the high-frequency aileron flutter by raising sharply their torsional frequency and relative density μ above those of the basic ST-13 model. It was hoped that the much higher margin of safety of these solid wings would preclude combined bending-torsion-aileron flutter. The mass, stiffness and vibration properties of these wings are also listed in Tables 2, 5, 8, and 9.

The experimental flutter data for the straight wings are listed in Table 12 and are plotted in Figs. 4 and 5. Of the twenty models tested, seven fluttered in the high-frequency aileron mode and thirteen did not flutter. Of the seven that fluttered, two exhibited flutter in both the aileron mode and at the same time a bending-torsion-aileron mode. The results are plotted as $V_f/b_{r_a}\ \omega_\beta$ and $V_f/b_{r_a}\ \omega_f$ versus M in Fig. 4 to examine the importance of ω_β as a parameter and to afford a comparison with an average single-degree-of-freedom theoretical curve (see Fig. 3). They are also plotted as $\left(V_f/b_{o_w}\ \omega_{\alpha_N}\right)(1/\sqrt{\mu_f})$ versus M in Figs. 5a and 5b to examine the importance of torsional frequency as a parameter and to permit comparison with both three-degree-of-freedom theory (Figs. 1 and 2) and the experimental data on the same planform without aileron from Ref. 1. The reference torsional frequency, ω_{α_N}, is the torsional frequency estimated for the model with aileron locked rigidly to the wing and compares closely with ω_{α_1} used in the theory. The technique for determining ω_{α_N} is the subject of Appendix III.

[redacted]

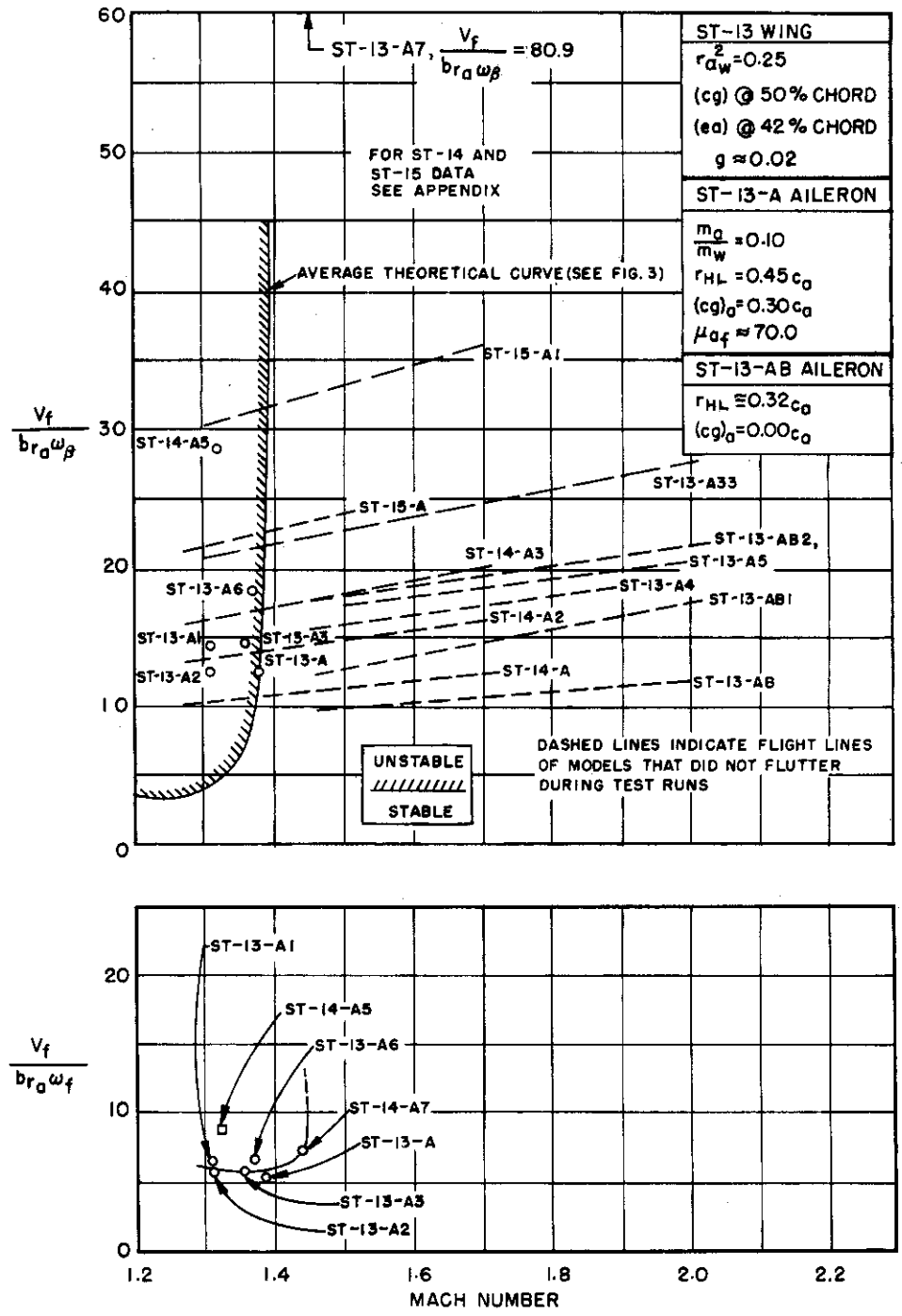

Fig. 4. Flutter parameters $V_f/b_{r_\alpha}\omega_\beta$ and $V_f/b_{r_\alpha}\omega_f$ versus Mach number for straight wings with ailerons.

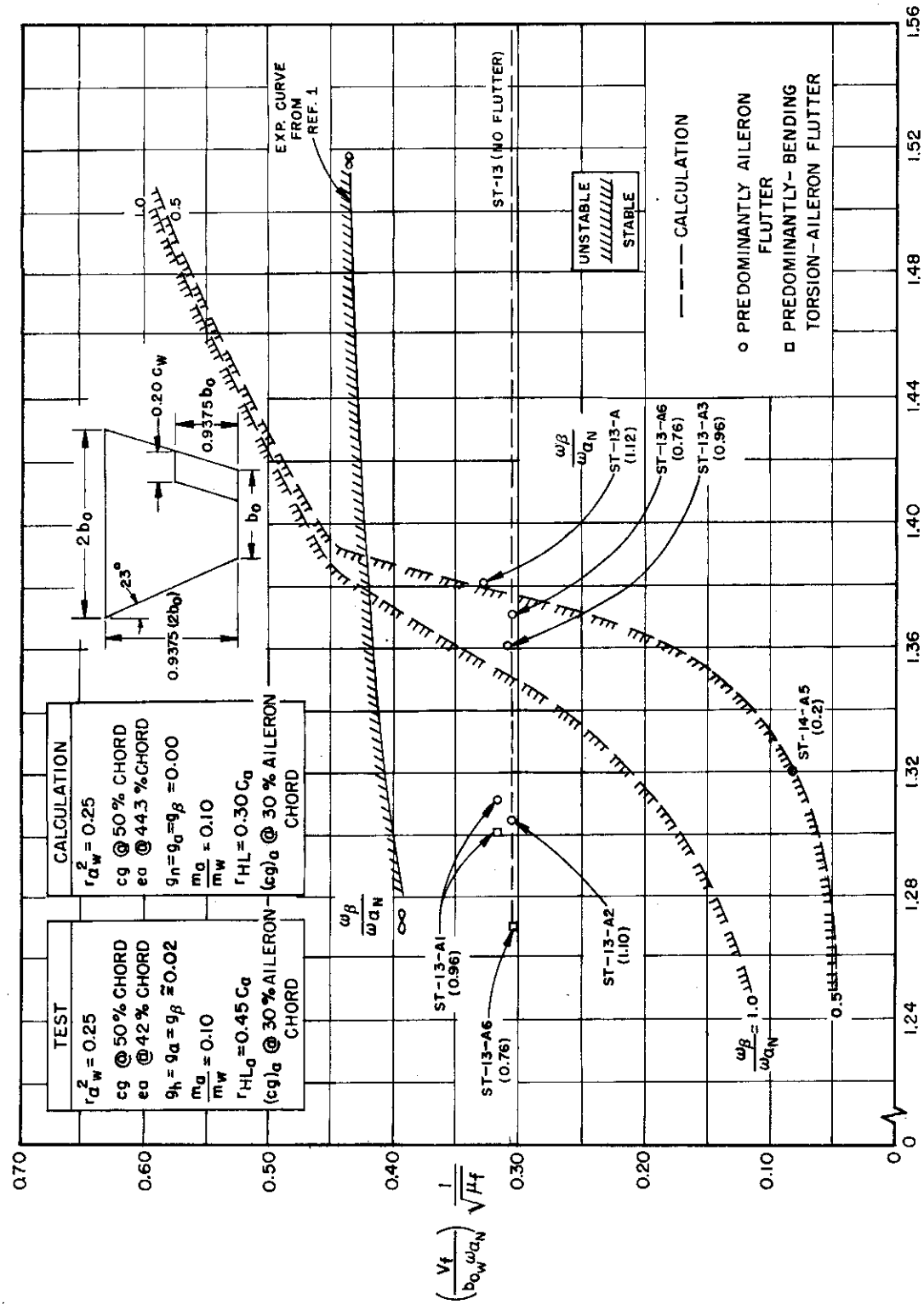

Fig. 5a. Flutter parameter $(V_f/b_{o_w}\omega_{\alpha_N})(1/\sqrt{\mu_f})$ versus Mach number for straight wings with unbalanced ailerons.

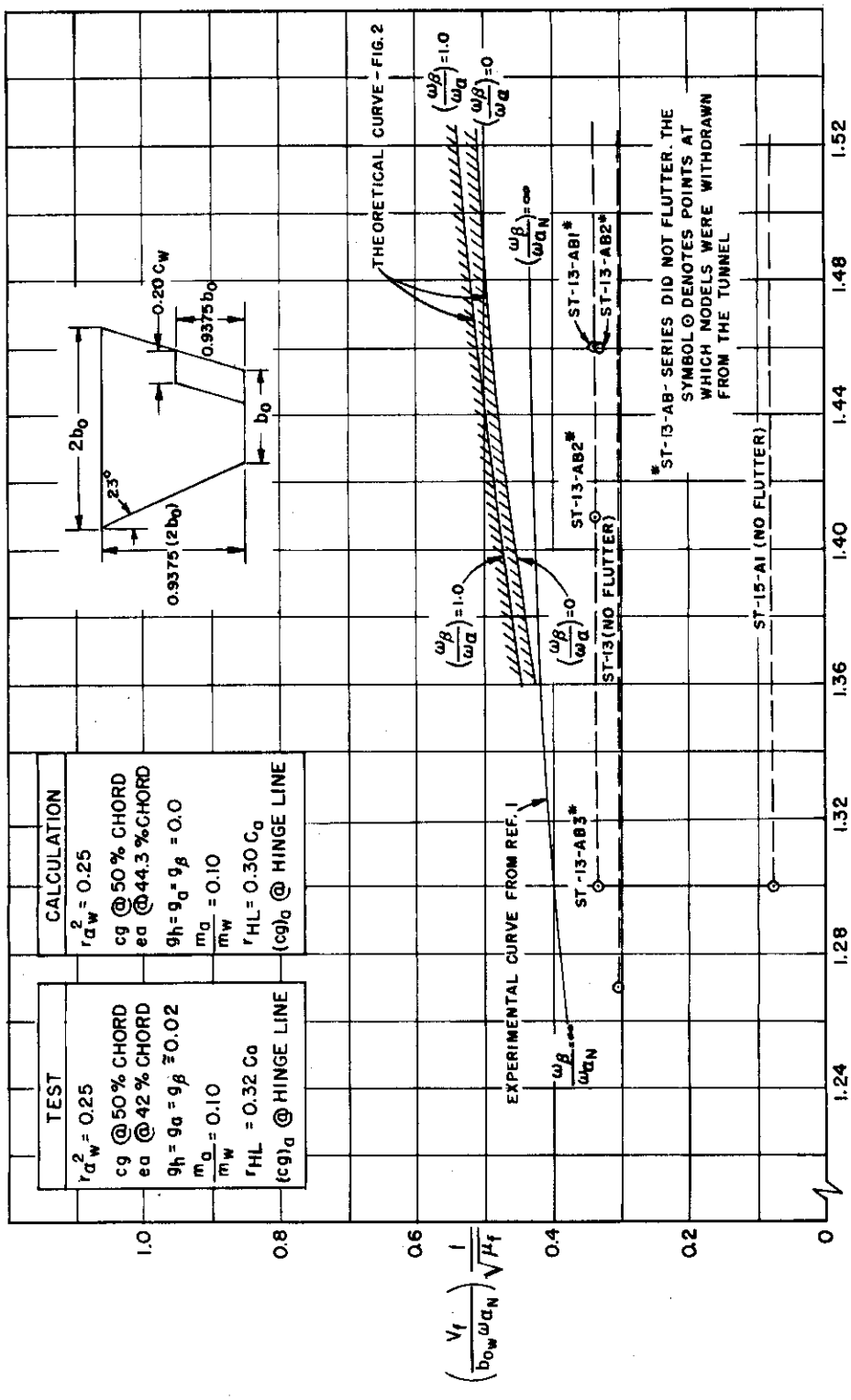

Fig. 5b. Flutter parameter $(V_F/b_{o_w}\omega\alpha_N)(1/\sqrt{\mu_f})$ versus Mach number for straight wings with balanced ailerons.

Looking first at Fig. 4 and particularly the unbalanced ST-13A series of models an encouraging correlation between simple theory and experiment is evident. The scatter of the flutter points can be explained at least in part by differences in the structural damping of the aileron flapping mode (see Table 9). Models with higher g_β flutter at a lower Mach number implying a smaller region of instability and checking the trend indicated by theory in Fig. 3. Notice this effect particularly for two pairs of nearly identical models, ST-13-A and -A2 and ST-13-A1 and -A3. The scatter may also arise from the effects of the higher vibration modes of the wing aileron combination. Examination of the high-speed movies shows definite evidence of structural deformation of the aileron trailing edge, and vertical translation of the tip accompanies the aileron flapping. These deformations are too small to be measured for the straight wing models and cannot be clearly seen in the enlargements of the flutter of the ST-13-A1 movies as shown in Fig. 16. Nevertheless there is no doubt that the flutter includes some of the characteristics of higher vibration modes. For example, Table 9 shows that the fifth mode for the ST-13-A series has, when it could be excited clearly, a frequency of about 600 cps and a node line on the aileron that could easily be associated with the type of deformation noticeable in the high-speed movies.

Looking next at the balanced aileron data in Fig. 4, no flutter was encountered on the first three of this series ST-13-AB, ST-13-AB1 and ST-13-AB2. Actually no high-frequency aileron flutter was expected because the test Mach number for these models was not allowed to go below 1.4. Model ST-13-AB3 was tested down to M = 1.30 to see if high-frequency aileron flutter would occur and it did not. This may be explained partly on the basis that both the single- and three-degree-of-freedom calculations show that at low M a decrease in unbalance indicates less susceptibility to flutter. Another partial explanation notes that the higher vibration modes had slightly different node lines for the AB series. In particular the fifth mode for the ST-13-AB models had a different node line on the aileron than did the ST-13-A models.

Looking lastly at the data for the ST-14 and ST-15 series which were designed to emphasize the high-frequency aileron flutter, five of the six models tested did not flutter down to M = 1.27, the minimum Mach number of the wind tunnel. Model ST-14-A5, which did exhibit a high frequency flutter at M = 1.32, had the lowest ω_β of the unbalanced ST-14 series. A balanced case, ST-15-A1, had an even lower ω_β but still did not flutter above M = 1.27. Although it seems probable that the ST-14 models would have all fluttered if the Mach number could have been lowered a little more, it can only be said that again the balanced ailerons seem less prone to flutter and that the effects of higher

frequency modes may be of considerable importance. For example, the third vibration mode (Table 9) for the ST-14 and ST-15 models shows node lines on the aileron that are similar to those of the fifth mode of the ST-13 models although the frequency is somewhat higher.

A different view of the flutter data is shown in Figs. 5a and 5b for the unbalanced and balanced cases respectively. Notice that the Mach number scale in Fig. 5a has been expanded considerably to emphasize the lower end of the range. In each case theoretical curves from Figs. 1 and 2 have been superimposed and the experimental flutter curve for straight wings without ailerons from Ref. 1 has been included. The basic ST-13 wing without aileron and with a margin of safety of 27% was tested as shown without fluttering. Since all of the other ST-13 series models had the same semichord and reference torsional frequency as ST-13 itself, their operating lines and flutter points will lie almost on top of that for ST-13. The main factor shifting them up slightly is the variation in relative density μ.

The main information to be gleaned from Fig. 5a is the manner in which decreasing frequency ratio ($\omega_\beta / \omega_{\alpha_N}$) is associated with slightly increasing flutter Mach number. Note that the two lowest Mach number points correspond to relatively low frequency bending-torsion-aileron flutter. The strain gage traces for the ST-13-A1 model are shown in Fig. 20. The high-frequency aileron instability starts first in the aileron trace at about 600 cps and does not show appreciably on the root bending trace. (The root torsion gage was inoperative and is not shown.) At a slightly lower Mach number a low frequency signal starts in the root bending trace and the aileron trace shows signs of beating between the high and low frequency signals. Careful examination of the high speed movie in Fig. 16 reveals the high frequency oscillations of the aileron. Detailed analysis of the wing tip motion in the movies of Fig. 16 resulted in the time histories of Fig. 18. Similar results were obtained for the ST-13-A6 model. In both cases the high-frequency flutter occurred at a higher Mach number and was therefore the critical one. Note the ST-14-A5 flutter point near the bottom of the figure which was included for completeness. In interpreting the high frequency flutter points notice again the stabilizing effect of structural damping for the model pairs ST-13-A and -A2 and ST-13-A1 and -A3.

A simple interpretation of Fig. 5b is that flutter was not predicted theoretically and did not occur. Apparently balancing of the aileron is stabilizing in the critical lower end of the wind tunnel Mach number range.

A tabulation of flutter data and flutter calculations such as in Table 1 gives an impression of unusually good correlation especially with the three-degree-of-

Table 1. Comparison of theoretical and test values of flutter Mach numbers and frequencies for straight wings.

Model	Test		Three-Degree-of-Freedom Calculation		Single-Degree-of-Freedom Calculation $g\beta = 0$	
	M_f	$\frac{V_f}{b_{o_w}\omega_f}$	M_f	$\frac{V_f}{b_{o_w}\omega_f}$	M_f	$\frac{V_f}{b_{o_w}\omega_f}$
ST-13-A	1.38	0.651	1.35	0.59	1.37	0.575
ST-13-A1	1.31	0.800	1.35	0.59	1.37	0.575
ST-13-A2	1.31	0.735	1.35	0.59	1.37	0.575
ST-13-A3	1.36	0.730	1.35	0.59	1.37	0.575
ST-13-A4	No flutter to M = 1.46*		1.36	0.61	1.37	0.575
ST-13-A5	No flutter to M = 1.50		1.36	0.61	1.38	0.650
ST-13-A6	1.37	0.788	1.36	0.61	1.38	0.650
ST-13-A7	1.44	0.898	1.40	0.76	1.40	0.825
ST-13-AB	No flutter to M = 1.46		No flutter		1.34	0.462
ST-13-AB1	No flutter to M = 1.46		No flutter		1.35	0.488
ST-13-AB2	No flutter to M = 1.41		No flutter		1.35	0.488
ST-13-AB3	No flutter to M = 1.30		No flutter		1.36	0.525
ST-14-A5	No flutter to M = 1.27				1.37	0.575
ST-14-A1	No flutter to M = 1.27				1.37	0.575
ST-14-A2	No flutter to M = 1.27				1.38	0.650
ST-14-A3	No flutter to M = 1.27				1.38	0.650
ST-14-A5	1.32	1.17			1.38	0.650
ST-15-A	No flutter to M = 1.27				1.38	0.650
ST-15-A1	No flutter to M = 1.30				1.38	0.650

* Due to the characteristics of the wing models and the wind tunnel, the models were injected into the tunnel at a high Mach number and then the Mach number was reduced as the run proceeded. Thus the phrase "no flutter to $M = M_1$" means that no flutter was encountered as the Mach number was reduced from $M \cong 2.10$ to $M = M_1$.

freedom theory. A look at the plots of Figs. 4 and 5a however indicates that the apparent good correlation may be a result of a fortuitous intersection of theory and experiment in the neighborhood of M = 1.3 to 1.4.

The results of the experiments and their comparison with theory may be summarized as follows:

1) For a wing with a margin of safety in bending-torsion flutter of about 27% over the Mach number range 1.27 to 2.10, a high-frequency flutter involving mainly the aileron was obtained when mass unbalanced ailerons were fitted to the ST-13 wing. This mode of flutter occurred for all values of ω_β tested and appears to be the critical flutter mode for the wing-aileron combination tested. Extrapolation of the data indicates that flutter will not occur over the Mach range 1.27-2.10 at values of $(\omega_\beta / \omega_{\alpha_N})$ greater than 1.2.

2) For the same basic wing with mass balanced ailerons no flutter occurred over the range of Mach numbers and ω_β's tested.

3) A model which has had its margin of safety in bending-torsion flutter sharply increased by raising μ and torsional stiffness may still flutter in the high-frequency aileron mode.

4) A mode of flutter resembling classical bending-torsion-aileron flutter was also encountered for two of the mass unbalanced aileron cases. This mode of flutter does not appear to be critical for the models tested in this report since it occurs in a region that is already unstable for the high-frequency aileron flutter mode.

5) Good correlation was apparently attained both qualitatively and quantitatively between the results of three-degree-of-freedom calculations using wing bending, wing torsion, and aileron flapping modes and the results of test made on the ST-13 series straight wing models with unbalanced ailerons in the limited range M = 1.3 to 1.4.

6) Single-degree-of-freedom calculations illustrate the basic instability of the aileron flapping mode below M = $\sqrt{2}$.

7) The addition of the higher vibration modes of the wing-aileron combination in the theoretical studies might aid the understanding of the changes in the flutter Mach number and frequency that occurred for the various models tested.

8) Trends in the experimental flutter results with changes in the radius of gyration and structural damping coefficient are predicted correctly by single-degree-of-freedom calculations.

3. Swept Wing Results

The basic swept wing model without aileron, designated SW-9, was designed to have a relative density μ of 30 and a margin of safety in flutter of 30% in torsional stiffness over that necessary to just prevent flutter over the Mach number range 2.0 to 1.3. Since the SW-9 was very similar to the swept wings of Ref. 1, the flutter data presented there and reproduced in Fig. 7 was used as the basis for calculating the margin of safety. After the SW-9 model was demonstrated by test to be free of flutter it was redesigned to include an aileron. Since the SW-9 model had a first bending frequency somewhat lower than desired, the aileron models, designated SW-10, incorporated some design changes to raise the bending frequency without significantly changing the basic torsion frequency. It was not felt necessary to retest the modified wing without aileron to demonstrate its freedom from flutter.

The aileron preperties were designed to be the same as for the straight wings; that is, the aileron chord was twenty percent of the local wing chord and the local aileron to wing mass ratio was 0.10. The unbalanced ailerons (SW-10A series) were designed to have their center of gravity at 30% of their chord and a radius of gyration r_{HL} about their hinge line of 45% of their chord. The balanced ailerons (SW-10AB series) had their center of gravity on the hinge line and a radius of gyration r_{HL} of 30% of their chord. The mass and stiffness data are in Tables 3, 6, and 8. The vibration modes and frequencies are in Table 10.

As in the straight wing program the plan of the tests was to try successively lower aileron frequencies in order to define a minimum allowable control surface frequency for both the unbalanced and balanced cases. Once again high-frequency flutter in a dominantly aileron mode occurred, this time for both aileron types. Since no theoretical studies were made for the swept wings with ailerons, the method of investigating further the high-frequency flutter by means of models with a higher margin of safety was employed. Two new model series were designed, SW-11 with unbalanced and SW-12 with balanced ailerons. Like their straight wing counter parts they were machined from solid aluminum in order to increase both the relative density μ and torsional frequency above those of the basic SW-10 model. The mass, stiffness and vibration data for these models are also listed in Tables 3, 6, 8, and 10.

The experimental flutter data for the swept wings are listed in Table 13 and plotted on Figs. 6 and 7. Of the twenty-two models tested eight fluttered,

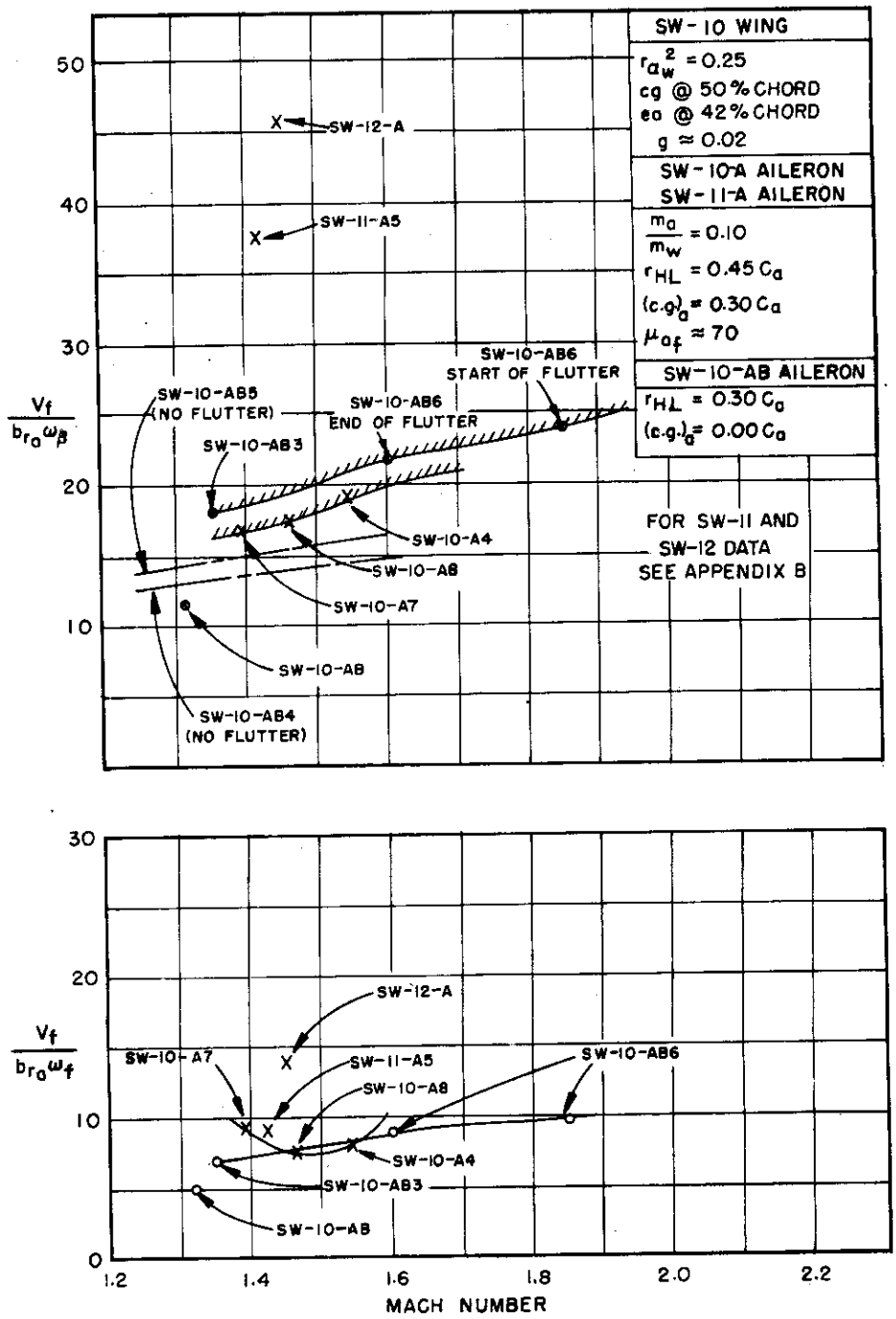

Fig. 6. Flutter parameters $V_f/b_{r_a}\omega_\beta$ and $V_f/b_{r_a}\omega_f$ versus Mach number for swept wings with ailerons from test.

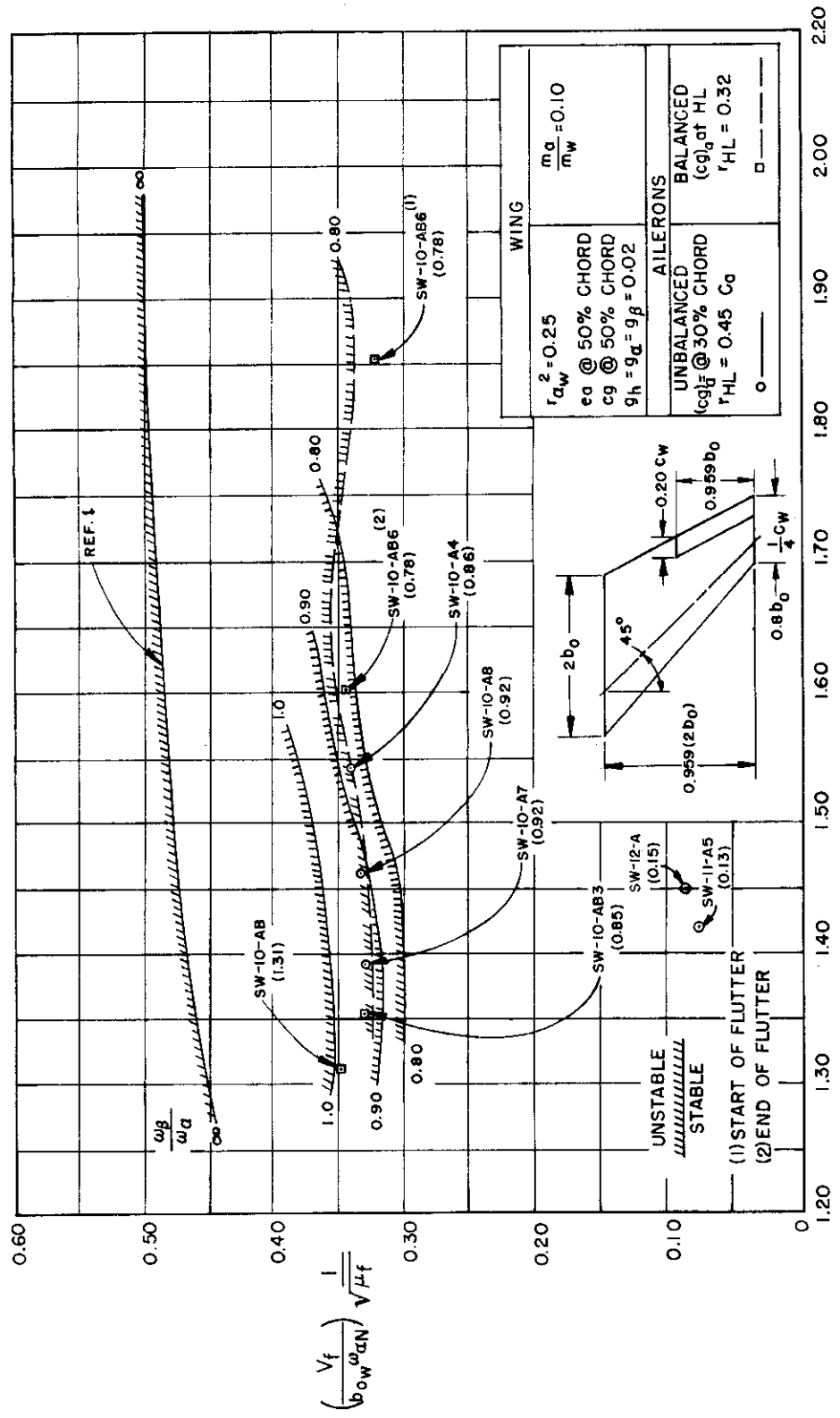

Fig. 7. Flutter parameter $(V_f/b_{o_w}\omega_{\alpha_N})(1/\sqrt{\mu_f})$ versus Mach number for swept wings with ailerons from test.

all in the high-frequency mode, and two failed on injection. It is interesting to note that in each flutter case the cross-flow Mach number based on the sweep of the hinge line was about $\sqrt{2}$ or less. The results are plotted as $V_f/b_{r_a}\,\omega_\beta$ and $V_f/b_{r_a}\,\omega_f$ versus M in Fig. 6 and as $(V_f/b_{o_w}\,\omega_{\alpha_N})\,(1/\sqrt{\mu_f})$ versus M in Fig. 7. The reference torsional frequency is estimated as in the straight wing case (see Appendix III).

The first four tests of the higher ω_β's with unbalanced ailerons, the SW-10-A through SW-10-A3 models, were made without flutter. The first flutter occurred with the SW-10-A4 model at fairly low ω_β. Flutter was also encountered for the SW-10-A7 and SW-10-A8 models. The characteristics of the flutter encountered for these three models are similar to those found for the straight wing models with the flutter frequency high and the motion mainly confined to the aileron. Examination of the high-speed movies shows that higher structural vibration modes of the wing-aileron combination are involved in the flutter mode and there is some evidence that the higher modes are more important for the swept wings than they are for the straight

For the swept wing with balanced ailerons, the SW-10-AB series, high-frequency flutter was also obtained and in general was precipitated by lowering the aileron frequency sufficiently. (The flutter point for the SW-10-AB model is an exception to this rule and will be discussed in detail in a later portion of this section.) The flutter occurred at high frequency in a mode in which the motion was confined mainly to the aileron, and higher structural vibration modes were evident. It can be seen in Fig. 6 that the SW-10-A4, -A7, and -A8 data form a reasonable flutter boundary for the SW-10 models with unbalanced ailerons. The SW-10-AB3 and SW-10-AB6 data form a reasonable boundary for the models with mass balanced ailerons. The balanced models show a slightly smaller region of instability than the unbalanced ones, and the effect of balance is seen to be generally stabilizing.

One of the balanced aileron wings, the SW-10-AB, does not fit well on the boundary. It fluttered, as can be seen by its low value of $V_f/b_{r_a}\,\omega_f$, at much higher frequency than the other models with balanced ailerons. Furthermore, the shape of this flutter mode is different from the rest of the swept wing aileron flutter modes. Since the configuration of the swept wing allows examination of only the tip of the aileron in the high-speed movies, no motion except that at the tip can be studied. The SW-10-AB model shows little of the tip vertical translation motion evident in the other balanced aileron flutter modes. The motion of the tip is confined mainly to aileron flapping. This change in mode shape is probably responsible for the large differences between this SW-10-AB point and the

points for the other SW-10 models with balanced ailerons. It should also be noted that the SW-10-AB4 and SW-10-AB5 models have ω_β's between that of the SW-10-AB and SW-10-AB3, but show no sign of flutter. Operating lines for these two models are shown on Fig. 6. The occurrence of flutter for the SW-10-AB model is disturbing since it represents flutter at a relatively high value of $\omega_\beta/\omega_{\alpha_N}$; higher than that of any of the other of the swept wings with balanced ailerons. It may represent the start of a new region of instability at these higher values of $\omega_\beta/\omega_{\alpha_N}$. Further investigation should probably be made at lower Mach numbers than can be attained in the presently used facility.

The importance of the higher vibration modes is further demonstrated by the results of the solid aluminum SW-11 and SW-12 model tests. High-frequency aileron flutter occurred for both of these models when the aileron flapping frequency was lowered sufficiently. Lower aileron frequencies were necessary to produce flutter than for the SW-10 series models. The SW-11-A5, with an aileron identical to that of the SW-10-A, fluttered at a value of $V_f/b_{r_a}\,\omega_\beta$ almost twice as great as those of the SW-10-A series models. Examination of the vibration data of Table 9 shows that there are important changes in the vibration mode shapes and frequencies between the SW-10 series models and the SW-11 series models which may account for the significant shift in the flutter points. Since there is little difference in the vibration mode shapes and frequencies between the SW-11-A5 and SW-12-A models, the difference in flutter Mach number and frequency for these models is probably due to the change in balance of the SW-12-A model. While not enough data has been obtained to establish a flutter boundary definitely, it does appear that balancing the aileron reduces the chances of high-frequency aileron flutter just as it did in the straight wing case.

Turning to Fig. 7 the SW-10 flutter points all fall near the nearly horizontal operating line for this basic model. The models were injected at about M = 1.9 and the Mach number was reduced until flutter occurred or until the low end of the tunnel range was reached. Note that as in the straight wing tests, reducing $(\omega_\beta/\omega_{\alpha_N})$ moves the flutter point to higher Mach number. Some tentative boundaries for both unbalanced and balanced aileron models have been sketched. Their nearly horizontal slope was indicated by the large Mach number range of flutter for the SW-10-AB6 model and the horizontal separation of the nearly identical models SW-10-A7 and SW-10-A8. In general the balanced cases seem to show a slightly smaller region of instability. Note that the Mach number range over which flutter occurred for swept wings is larger than that for straight (see Fig. 5a) unless cross-flow Mach number is used as a parameter.

Some general conclusions may be drawn from the swept wing data:

1) For a model with a 30% margin of safety against bending-torsion flutter, high-frequency flutter modes resulted when the aileron flapping frequency was reduced sufficiently. This occurred with both balanced and unbalanced ailerons.

2) A model with a much higher margin of safety in bending-torsion flutter also fluttered in an aileron mode when the flapping frequency was reduced sufficiently. This flutter Mach number and frequency differed from the values obtained for the lightweight lower frequency models to a greater extent than for the similar straight wing situation. The more drastic changes for the swept wing were probably due to the relatively larger effect of high-frequency wing-aileron vibration modes. The importance of the higher vibration modes was also demonstrated by the results of the SW-10-AB tests which showed flutter in an aileron mode apparently quite different from the flutter at lower values of $(\omega_\beta/\omega_{\alpha_N})$.

3) Balancing the aileron decreased the chance of high-frequency aileron flutter just as it did for the straight wing case.

4. Delta Wing Results

The planform for the delta wings with elevon is shown in Fig. 14 and the mass, static and vibration test data are in Tables 4, 7, 8 and 11. All of the delta wing models flown were designed to have a relative density at flutter of 30. No solid aluminum models with lightweight elevons were built for this planform since each instance flutter encountered had mode shapes with large amounts of wing bending and torsion motion as well as elevon motion. No cases of high-frequency elevon flutter were encountered.

Two different series of models with mass unbalanced ailerons were tested. The De-3k-A1 through -A5 models had a 5% thickness ratio and had a reference torsional frequency of 680 cps. These models had a margin of safety in flutter of about 120% referred as before to the corresponding data of Ref. 1 which is plotted in Fig. 9. No flutter was encountered for any value of $(\omega_\beta/\omega_{\alpha_N})$ from 0.956 down to 0.441.

A second series of basic wings De-3k-A6 through -A15, was then tested with much lower margin of safety in flutter. These models had a 4% thickness ratio and a margin of safety in flutter of about 7%. The De-3k-A15 has a somewhat higher

ω_{α_N} than the rest of this group but was tested at lower values of μ and so has an apparent margin of safety based on Fig. 9 of only 7%. Flutter occurred for the models with mass unbalanced elevons when the elevon flapping frequency was lowered sufficiently.

The basic delta wing model De-3k-AB with mass balanced elevon also has a 4% thickness ratio. Its reference frequency is somewhat higher than that for the 4% model with unbalanced elevon, and so it has a margin of safety in flutter of about 20%. Flutter was produced in this case also when the elevon frequency was lowered sufficiently.

Figures 8 and 9 and Table 14 show the flutter data for the delta wing models. From Fig. 9 one of the basic difficulties encountered in testing the delta wings is immediately apparent. A tunnel operating curve is very nearly a horizontal line on Fig. 9, and since the flutter boundary is very nearly horizontal also, it can be seen that it is difficult to avoid injection and retraction flutter. All of the delta models that fluttered, did so either on injection or retraction. For the wings with unbalanced elevons, three such flutter points, covering the Mach number range from 1.27 to 2.10, were obtained with the higher aileron frequencies corresponding to the lower Mach numbers.

For the balanced elevons flutter does not occur for the De-3k-AB model with $(\omega_\beta/\omega_{\alpha_N}) = 0.95$. Injection flutter occurs at approximately M = 2.0 for $(\omega_\beta/\omega_{\alpha_N}) = 0.74$ for the De-3k-AB1 model, and for $(\omega_\beta/\omega_{\alpha_N}) = 0.53$ for the De-3k-AB2 model.

The general conclusions that can be drawn from the delta wing results are given below:

1) Delta wing models with both balanced and unbalanced elevons encountered flutter which involved wing bending, wing torsion, and elevon flapping modes when the elevon flapping frequency was lowered sufficiently.

2) For a delta wing with a margin of safety in flutter of about 7%, flutter will not occur in the Mach number range of 1.27 to 2.10 if the ratio $(\omega_\beta/\omega_{\alpha_N})$ is slightly greater than 0.77 for mass unbalanced elevons.

3) For a delta wing with mass balanced aileron and a margin of safety in flutter of about 20%, flutter occurs in the Mach number range of 1.27 to 2.10 if the ratio $(\omega_\beta/\omega_{\alpha_N})$ is 0.74 and does not occur if $(\omega_\beta/\omega_{\alpha_N})$ is 0.95.

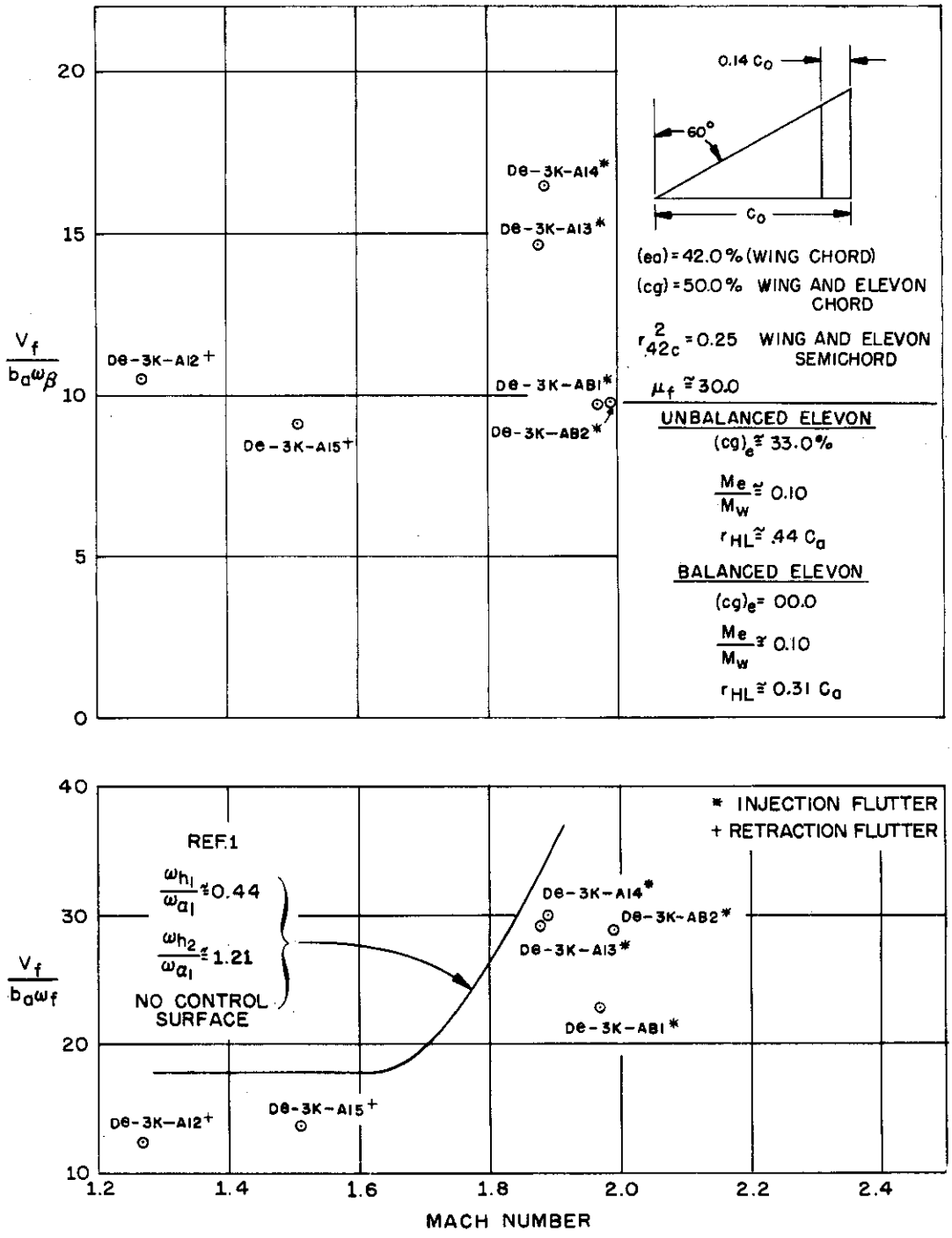

Fig. 8. Flutter parameters $V_f/b_a\omega_\beta$ and $V_f/b_a\omega_f$ versus Mach number for delta wings with elevons from test.

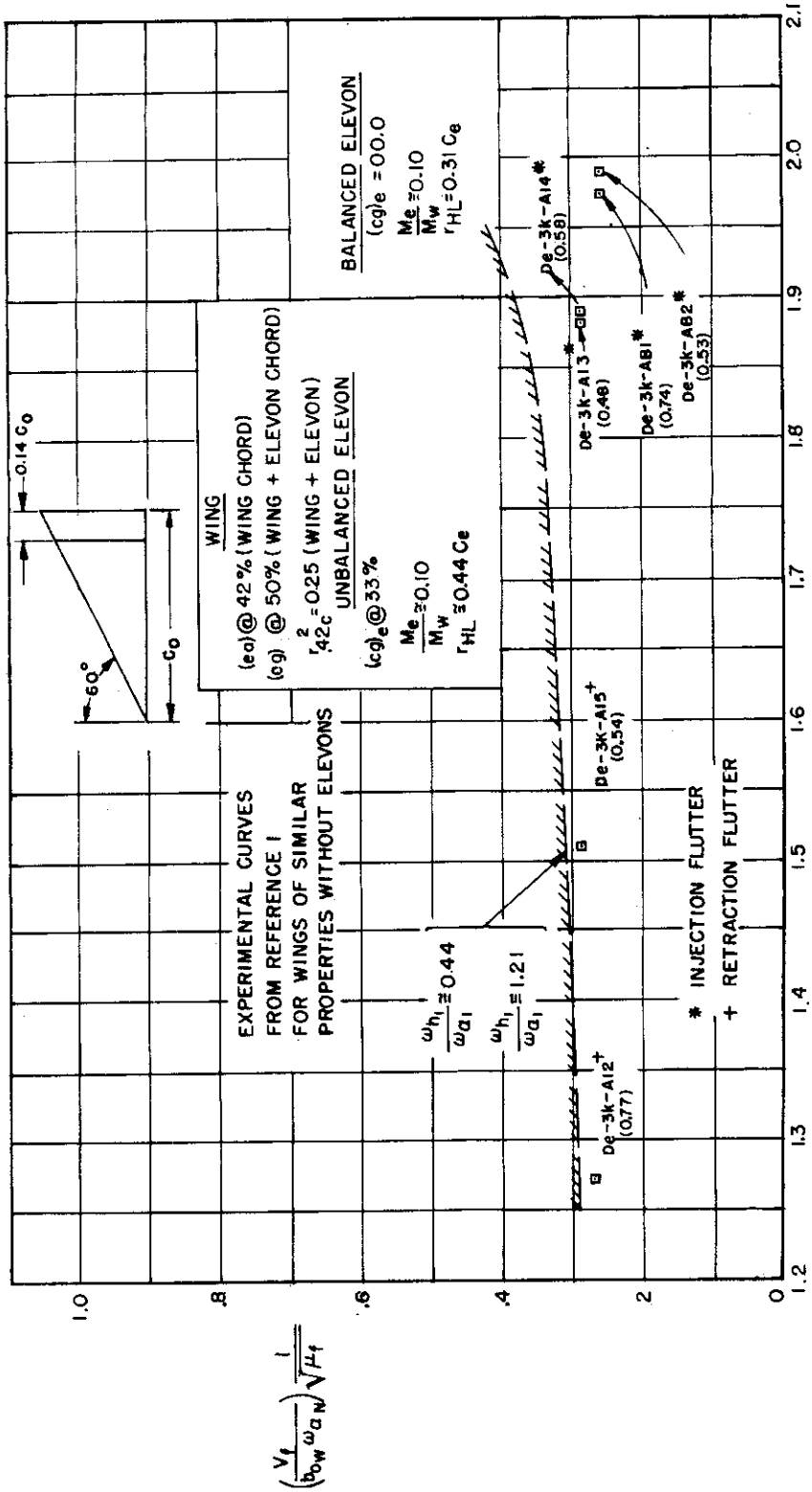

Fig. 9. Flutter parameter $(V_f/b_{o_w}\omega_{a_N})(1/\sqrt{\mu_f})$ versus Mach number for delta wings with elevons from test.

SECTION III

CONCLUSIONS AND RECOMMENDATIONS

The planned testing program had to be modified considerably when the unexpected high-frequency flutter in a predominantly aileron flapping mode occurred for both the straight and swept wings. Particularly for the swept wings the flutter seemed to be somewhat influenced by the character of relatively high-frequency vibration modes. In general the balanced ailerons seemed less likely to flutter than the unbalanced ones although an insufficient number of tests were made to permit sweeping conclusions. The auxiliary series of models with much higher margins of safety but filled with normal lightweight ailerons also exhibited the high-frequency aileron flutter somewhat affected by high-frequency natural vibration characteristics. All the flutter data for straight and swept wings with ailerons occurred at a cross-flow Mach number based on hinge line sweep of about $\sqrt{2}$ or less. The delta wing models exhibited flutter boundaries nearly tangent to the wind tunnel operating curve and so flutter occurred only on injection or retraction.

Specific conclusions for the various planforms are listed below:

Straight Wing

1) For a wing with a margin of safety in bending-torsion flutter of about 27% over the Mach number range 1.27 to 2.10, a high-frequency flutter involving mainly the aileron was obtained when mass unbalanced ailerons were fitted to the ST-13 wing. This mode of flutter occurred for all values of ω_β tested and appears to be the critical flutter mode for the wing-aileron combination tested. Extrapolation of the data indicates that flutter will not occur over the Mach range 1.27-2.10 at values of $(\omega_\beta / \omega_{\alpha_N})$ greater than 1.2.

2) For the same basic wing with mass balanced ailerons no flutter occurred over the range of Mach numbers and ω_β's tested.

3) A model which has had its margin of safety in bending-torsion flutter sharply increased by raising μ and torsional stiffness may still flutter in the high-frequency aileron mode.

4) A mode of flutter resembling classical bending-torsion-aileron flutter was also encountered for two of the mass unbalanced aileron cases. This mode of flutter does not appear to be critical for the models tested in this report since it occurs in a region that is already unstable for the high-frequency aileron flutter mode.

5) Good correlation was apparently attained both qualitatively and quantitatively between the results of three-degree-of-freedom calculations using wing bending, wing torsion, and aileron flapping modes and the results of tests made on the ST-13 series straight wing models with unbalanced ailerons in the limited range M = 1.3 to 1.4.

6) Single-degree-of-freedom calculations illustrate the basic instability of the aileron flapping mode below $M = \sqrt{2}$.

7) The addition of the higher vibration modes of the wing-aileron combination in the theoretical studies might aid the understanding of the changes in the flutter Mach number and frequency that occurred for the various models tested.

8) Trends in the experimental flutter results with changes in the radius of gyration and structural damping coefficient are predicted correctly by single-degree-of-freedom calculations.

Swept Wing

1) For a model with a 30% margin of safety against bending-torsion flutter, high-frequency flutter modes resulted when the aileron flapping frequency was reduced sufficiently. This occurred with both balanced and unbalanced ailerons.

2) A model with a much higher margin of safety in bending-torsion flutter also fluttered in an aileron mode when the flapping frequency was reduced sufficiently. This flutter Mach number and frequency differed from the values obtained for the lightweight lower frequency models to a greater extent than for the similar straight wing situation. The more drastic changes for the swept wing were probably due to the relatively larger effect of high-frequency wing-aileron vibration modes. The importance of the higher vibration modes was also demonstrated by the results of the SW-10-AB tests which showed flutter in an aileron mode apparently quite different from the flutter at lower values of $(\omega_\beta/\omega_{\alpha_N})$.

3) Balancing the aileron decreased the chance of high-frequency aileron flutter just as it did for the straight wing case.

Delta Wing

1) Delta wing models with both balanced and unbalanced elevons encountered flutter which involved wing bending, wing torsion, and elevon flapping modes when the elevon flapping frequency was lowered sufficiently.

2) For a delta wing with a margin of safety in flutter of about 7%, flutter will not occur in the Mach number range of 1.27 to 2.10 if the ratio $(\omega_\beta/\omega_{\alpha_N})$ is slightly greater than 0.77 for mass unbalanced elevons.

3) For a delta wing with mass balanced aileron and a margin of safety in flutter of about 20%, flutter occurs in the Mach number range of 1.27 to 2.10 if the ratio $(\omega_\beta/\omega_{\alpha_N})$ is 0.74 and does not occur if $(\omega_\beta/\omega_{\alpha_N})$ is 0.95.

It is recommended that further tests be carried out in the low supersonic range to permit a better understanding of the high-frequency aileron type of flutter. Some type of instrumentation to permit the determination of the modal content of the flutter would probably be of great help in evaluating the tests.

BIBLIOGRAPHY

1. McCarthy, J. F., Jr., Zartarian, G., Martuccelli, J. R., and Asher, G. W., (UNCLASSIFIED TITLE) Three-Dimensional Supersonic Flutter Model Tests Near Mach Number 1.5, Part II Experimental and Theoretical Data for Bare Wings and Wings with Tip Tanks, WADC Technical Report 54-113 Part II, December 1955. (CONFIDENTIAL)

2. McCarthy, J. F., Jr., Asher, G. W., Prigge, J. S., Jr., and Levey, G. M., Three-Dimensional Supersonic Flutter Model Tests Near Mach Number 1.5, Part I Model Design and Testing Techniques, WADC Technical Report 54-113, December 1955.

3. Halfman, R. L., McCarthy, J. F., Jr., Prigge, J. S., Jr., and Wood, G. A., Jr., A Variable Mach Number Supersonic Test Section for Flutter Research, WADC Technical Report 54-114, December 1954,

4. Garrick, I. E., and Rubinow, S. I., Flutter and Oscillating Air Force Calculations for an Airfoil in Two-Dimensional Supersonic Flow, NACA Technical Report 846, May 1946.

5. Huckel, V., and Durling, B. J., Tables of Wing-Aileron Coefficients of Oscillating Air Forces for Two-Dimensional Supersonic Flow, NACA T. N. 2055, March 1950.

6. Smilg, B., and Wasserman, L. S., Application of Three-Dimensional Flutter Theory to Aircraft Structures, Air Corps Technical Report No. 4798, July 1942.

7. Navy Department, Bureau of Ordnance, Handbook of Supersonic Aerodynamics, Vol. 4, NaVord Report 1488, January 1952.

APPENDIX I

THEORETICAL RESULTS

1. Introduction

Since a straightforward method of theoretical flutter calculation existed only for the straight wing configuration, the considerable amount of flutter analysis carried out in this program is limited to this case. In Ref. 1 the analysis was set up for the straight wing without aileron. The extension to the straight wing with aileron follows closely the procedures detailed in Appendices A and C of Ref. 1 and will only be outlined here.

Although most of the calculations included three degrees of freedom, it was found useful to look also at the simple subcase involving only rotation of the aileron about its hinge line. This single-degree-of-freedom case is developed in Section 3 of this appendix.

2. Three-Degree-of-Freedom Calculations

These calculations were based on the uncoupled modes of wing first bending, wing first torsion and aileron rotation about the hinge line. They were carried out for mass-balanced as well as unbalanced ailerons for the wing and aileron properties listed on Figs. 10 and 11. These properties describe the actual light weight models quite well except for the aileron radius of gyration about its hinge line. The value used in the calculations was 30% of the aileron chord. The values achieved on the models were 32% for the balanced case and 45% for the unbalanced case. This inconsistency is probably not serious enough to distort markedly the comparisons between theory and experiment.

For the three-degree-of-freedom calculations, four Mach numbers were picked for analysis, 5/4, 10/7, 5/3, and 2, corresponding to the tabulated values of aerodynamic coefficients given in Refs. 4 and 5. For the three higher Mach numbers, the calculations presented no difficulties. At M = 5/4, however, no real solutions were found during the preliminary analyses at values of the reduced frequency parameter $\bar{\omega}$, ($\bar{\omega} = 2kM^2/(M^2 - 1)$) corresponding to those for the higher Mach numbers. The presence in the test data of high-frequency flutter

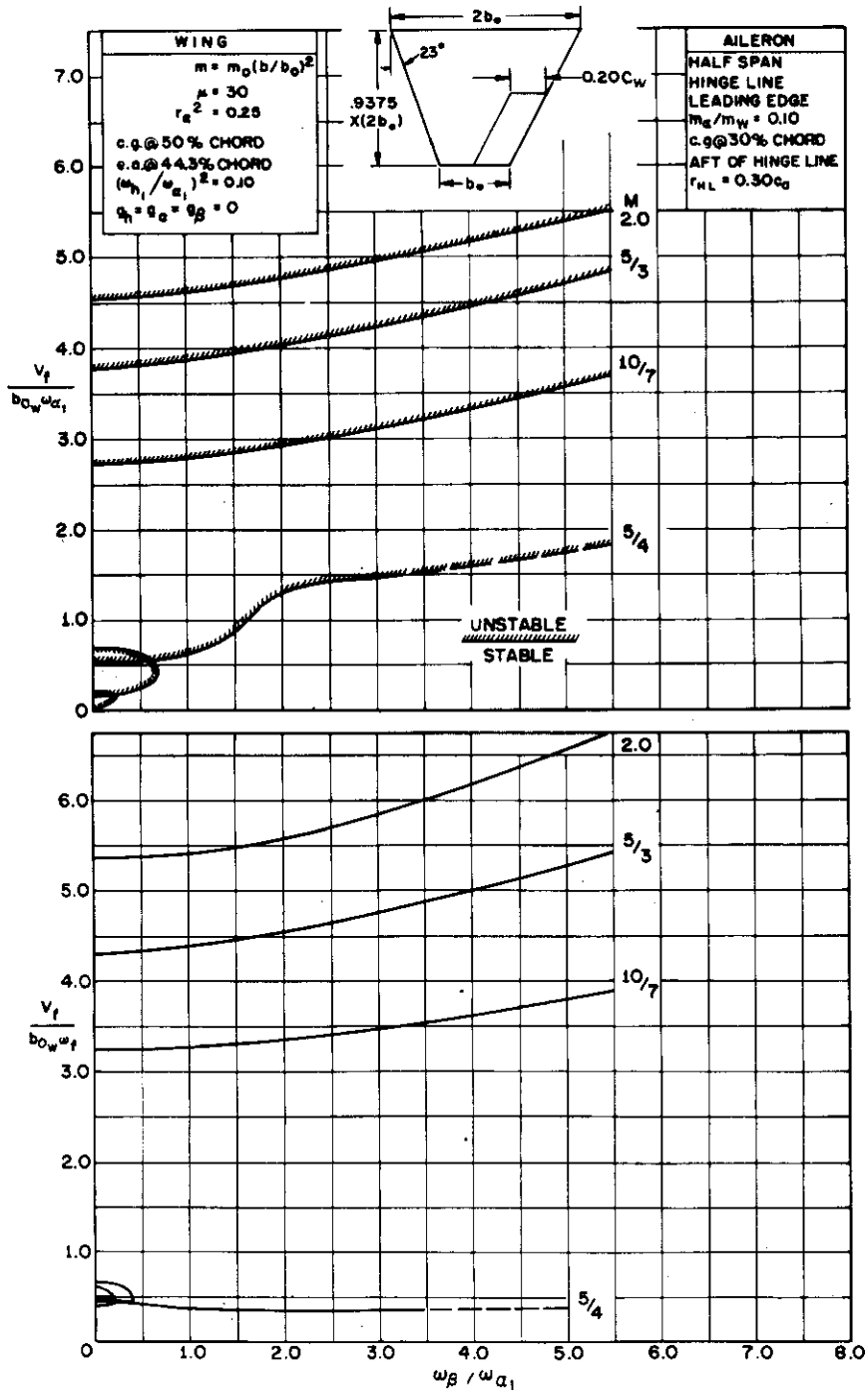

Fig. 10. Flutter parameters $V_f/b_{o_w}\omega_{\alpha_1}$ and $V_f/b_{o_w}\omega_f$ versus $\omega_\beta/\omega_{\alpha_1}$ for straight wings with mass unbalanced ailerons from three-degree-of-freedom calculations.

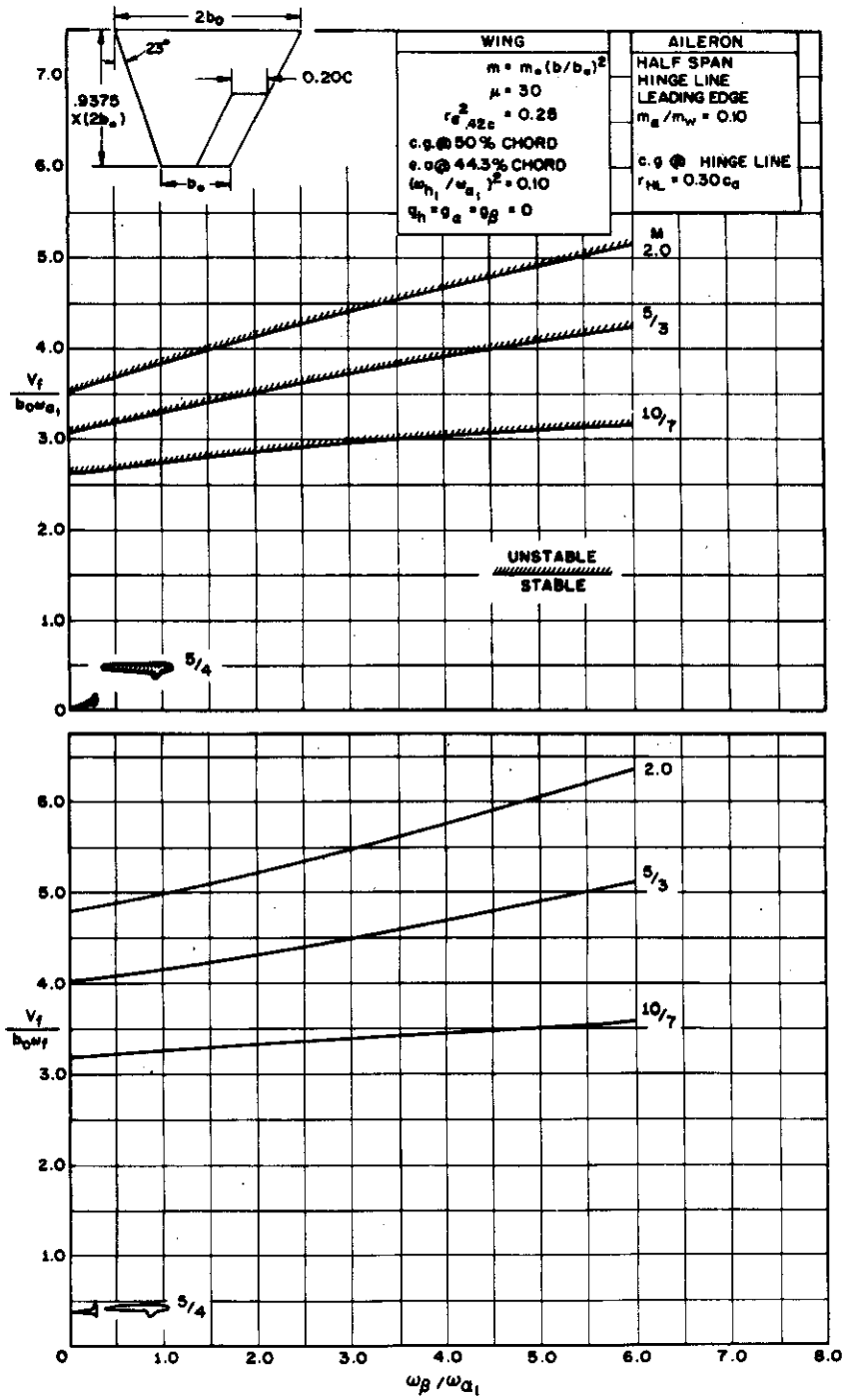

Fig. 11. Flutter parameters $V_f/b_{o_w}\omega_{\alpha_1}$ and $V_f/b_{o_w}\omega_f$ versus $\omega\beta/\omega_{\alpha_1}$ for straight wings with mass balanced ailerons from three-degree-of-freedom calculations.

indicated that perhaps there should be solutions at high values of $\bar{\omega}$. Such solutions were found and are discussed in some detail below. The major difficulty involved in the solutions was that the aileron aerodynamic coefficients are not completely tabulated in the range of $\bar{\omega}$'s desired, so it was necessary to calculate some of the aerodynamic coefficients.

The results of the three-degree-of-freedom calculations are shown in Figs. 10, 11, and 12 of this appendix, and Figs. 1 and 2 of Section II. Figures 10 and 11 show that the calculated results for Mach numbers 10/7, 5/3, and 2.0 are smooth for both the balanced and unbalanced cases. The balanced cases show an increase in the region of instability in this range of Mach numbers. Below Mach numbers of 10/7, however, drastic changes take place in the curves of Figs. 10 and 11, and hence in Figs. 1 and 2 of Section II. Apparently, these drastic changes occur because below a Mach number of $\sqrt{2}$, a single-degree-of-freedom aileron instability is possible, as noted in Ref. 4. Figure 12, which is a sketch of the eigenvalues $(\omega_\beta/\omega_{\alpha_1})^2$ and $(\omega_{\alpha_1}/\omega_f)^2$ used in the solution of the flutter determinant, (see Appendix III, Section III-3, Ref. 1), shows a number of interesting phenomena. The frequencies ω_β and ω_{α_1} are the uncoupled aileron and first torsion frequencies respectively, and ω_f is the flutter frequency. At several points along the curves, values of the reduced frequency parameter $\bar{\omega}$ are given. These values are much higher than those for which real positive solutions were found for the cases with M = 10/7 or greater. The high values of $\bar{\omega}$ indicate that the instability occurs at high frequency. Also , of great interest, is the root which is found for both balanced and unbalanced cases at $\bar{\omega} \approx 9.15$ where $(\omega_{\alpha_1}/\omega_f)^2$ approaches infinity and $(\omega_\beta/\omega_{\alpha_1})^2$ approaches zero. This root is interesting because in this case, where $\bar{\omega}$ and hence ω_f are finite, the implication is that $(\omega_{\alpha_1}/\omega_f)^2$ approaches infinity because ω_{α_1} does. If ω_{α_1} approaches infinity, when ω_{h_1} the uncoupled first bending frequency, must also approach infinity since the ratio of $(\omega_{\alpha_1}/\omega_{h_1})$ is fixed for the wing, and the wing itself can be considered infinitely stiff or rigid. Instability is, however, still possible at this point, and this instability must then be the single-degree-of-freedom instability discussed in Ref. 4 and in Section 3 of this appendix. Examination of the term in the flutter determinant, Eq. (A. 38) of Appendix A of Ref. 1, shows that the imaginary part of this term does go to zero at $\bar{\omega} \approx 9.15$ which corresponds to the condition given by Eq. (8) of this appendix for single-degree-of-freedom flutter. This point at $(\omega_{\alpha_1}/\omega_f)^2 = \infty$, $(\omega_\beta/\omega_{\alpha_1})^2 = 0$ occurs at the origin of the $V_f/b_{o_w}\omega_{\alpha_1}$ versus $(\omega_\beta/\omega_{\alpha_1})$ curves, Figs. 10 and 11. For the

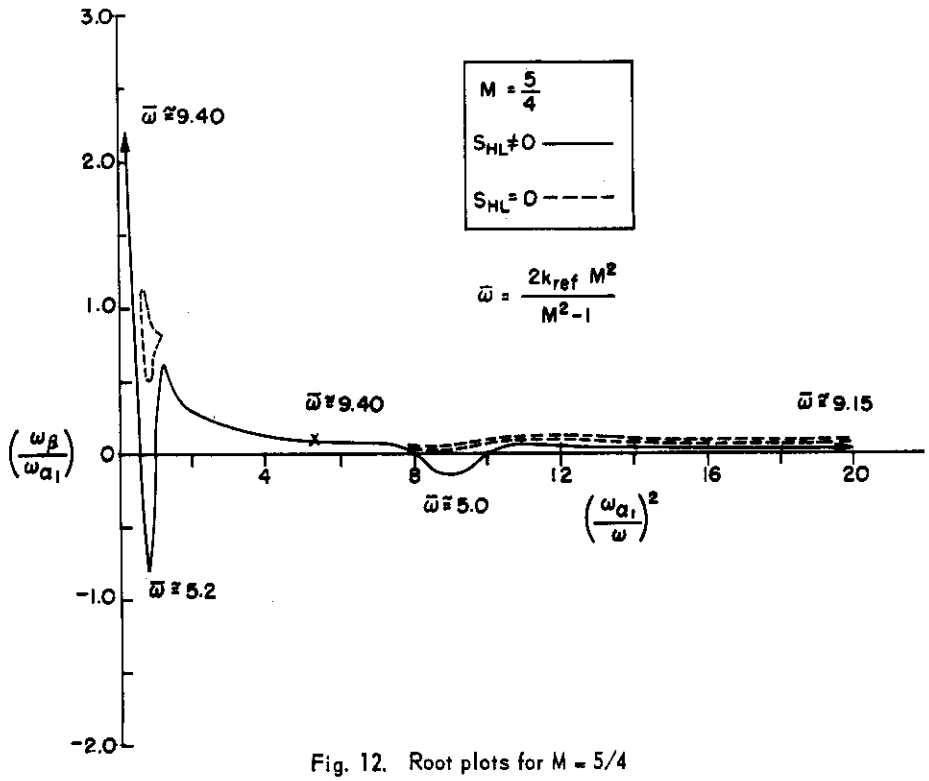

Fig. 12. Root plots for M = 5/4

unbalanced case ($S_{HL} \neq 0$) a single branch approaches infinity. In the balanced case ($S_{HL} = 0$) the point at infinity forms part of a closed loop as can be seen from Figs. 10, 11, and 12. Thus in Fig. 10, the unbalanced case, the region of instability near the origin is larger than for the balanced case. Furthermore, in Fig. 12 it can be seen that real solutions do not exist for all values of $(\omega_\beta/\omega_{\alpha_1})$ in the balanced case as they do in the unbalanced case, where a branch of the roots goes to $(\omega_\beta/\omega_{\alpha_1})$ equal to infinity. Hence in Fig. 11, the balanced case, only small enclosed regions of instability occur at values of $(\omega_\beta/\omega_{\alpha_1})$ of about 1.0 or less for M = 5/4 while on Fig. 10, the unbalanced case, the region of instability extends over the complete range of $(\omega_\beta/\omega_{\alpha_1})$ values. When these results are plotted versus Mach number in Figs. 1 and 2 portion of the curves must be dashed to indicate that insufficient data was available below M of 10/7 to completely determine the curves.

3. Single-Degree-of-Freedom Calculations

Following the idea that the drastic shifts in Figs. 1, 2, 10 and 11 at low Mach number are connected with a high-frequency flutter involving predominantly aileron motion, a simple single-degree-of-freedom analysis was carried out. The wing

was assumed to remain motionless at zero angle of attack during flutter and the aileron was considered as a wing which can pitch about its leading edge. These assumptions allow the use of the more extensively tabulated two-dimensional wing supersonic aerodynamic coefficients rather than the less well tabulated supersonic aileron coefficients. A representative station at the 50 percent span of the aileron was chosen for analysis.

The equation of motion for the representative section can be written as:

$$\ddot{\beta}\ I_{HL} + K_\beta \beta = M_\beta \qquad (1)$$

where β is the flapping angle of the aileron, I_{HL} the mass moment about the hinge line, K_β the restraining spring constant, and M_β the aerodynamic moment about the hinge line. Equation (1) is valid for both mass balanced and unbalanced ailerons of the type tested in this program.

If simple harmonic motion is introduced into Eq. (1) by taking

$$\beta = \bar{\beta}\, e^{i\omega_f t} \qquad (2)$$

where β is the complex amplitude of the angle of attack, and if the usual nondimensionalizing procedures are used, Eq. (1) becomes

$$\left\{ \bar{r}_{HL}^2 \left[1 - (1 + ig_\beta) \left(\frac{\omega_\beta}{\omega_f} \right)^2 \right] - \frac{1}{\mu_a} (M_3' + iM_4') \right\} \bar{\beta} = 0 \qquad (3)$$

where

$\bar{r}_{HL}$ is nondimensional radius of gyration about the hinge line,

$$\bar{r}_{HL}^2 = \frac{I_{HL}}{m_a b_{r_a}^2}$$

ω_β is the still air vibration frequency, $\omega_\beta^2 = \dfrac{K_\beta}{I_{HL}}$

μ_a is the relative density, $\mu_a = \dfrac{m_a}{4\rho\, b_{r_a}^2}$

g_β is the structural damping coefficient as defined in Ref. 6

m_a is the aileron mass per unit length

b_{r_a} is the aileron semichord at the reference station

M_3' and M_4' are the aerodynamic moment coefficients defined below

In terms of the notation of Ref. 7 the aerodynamic moments M'_3 and M'_4 are written as:

$$M'_3 + iM'_4 = - \frac{\pi}{4} \left(C_{M\alpha} + \frac{1}{4} C_{Lh} + \frac{1}{2} C_{L\alpha} + \frac{1}{2} C_{Mh}\right) \qquad (4)$$

and are functions of the Mach number M and the reduced frequency $\overline{\omega}_{r_a}$ defined as:

$$\overline{\omega}_{r_a} = \frac{2 k_{r_a} M^2}{M^2 - 1} \qquad (5)$$

The flutter condition is obtained by satisfying simultaneously the real and imaginary parts of Eq. (3).

$$\mu_a \bar{r}^2_{HL} \, g_\beta \left(\frac{\omega_\beta}{\omega_f}\right)^2 + M'_4 = 0 \qquad \text{imaginary} \qquad (6)$$

$$\mu_a \bar{r}^2_{HL} \left[1 - \left(\frac{\omega_\beta}{\omega_f}\right)^2\right] - M'_3 = 0 \qquad \text{real} \qquad (7)$$

When the structural damping, g_β, is taken as zero, Eq. (6) reduces to

$$M'_4 = 0 \qquad (8)$$

and the solution is particularly simple.

Flutter solutions for Eqs. (6) and (7) are presented in Fig. 3 for the two values of radius of gyration corresponding to the balanced and unbalanced ailerons of the models of this program and for values of g_β of zero and 0.03. The boundary is asymptotic to $M = \sqrt{2}$ as predicted in Ref. 4 and the effect of damping appears to be small. Figure 3 also shows that decreases in the radius of gyration may decrease the region of instability slightly. It is also of some interest to note from Eqs. (6) and (7) that a change in μ_a will have the same effect as a change in radius of gyration and that this is the opposite of the μ effect for simple bending-torsion flutter.

APPENDIX II

DETAILED TABULATION OF DATA FOR MODELS TESTED

In this appendix a detailed tabulation of data is presented for all the models tested.

A discussion of the testing techniques is given in Ref. 2. Dangerous aileron buffeting was encountered in injecting aileron models with low values of ω_β. In an attempt to solve this problem, an aileron restraint appearing very much like a clothes pin was put over the aileron before the start of each run. This restraint reduced the aileron oscillations until the wing was completely in the test section where the action of the air stream slipped the restraint off of the wing and carried it downstream. Despite the preceding precautions some of the wing-aileron models were damaged by buffeting during the process of injection.

Two types of construction were used in building the models tested during this program. The first type of model was similar to those of Refs. 1 and 2 in which an aluminum spar is used to carry the main loads, balsa wood to give the required aerodynamic shape, and lead weights to give the proper mass distribution. The second type of model was machined out of solid aluminum. Here, the ailerons were built, as before, of balsa wood with lead weights. This second series of wings was built in an attempt to isolate single-degree-of-freedom aileron flutter. Figure 1 shows a typical lightweight model during construction.

As in Refs. 1 and 2, the thickness ratio of the models is constant, and therefore all dimensions are tapered linearly in thickness and in width giving the following distributions of mass and stiffness:

$$m = m_o \left(\frac{b}{b_o}\right)^2$$

$$EI = EI_o \left(\frac{b}{b_o}\right)^4$$

$$GJ = GJ_o \left(\frac{b}{b_o}\right)^4$$

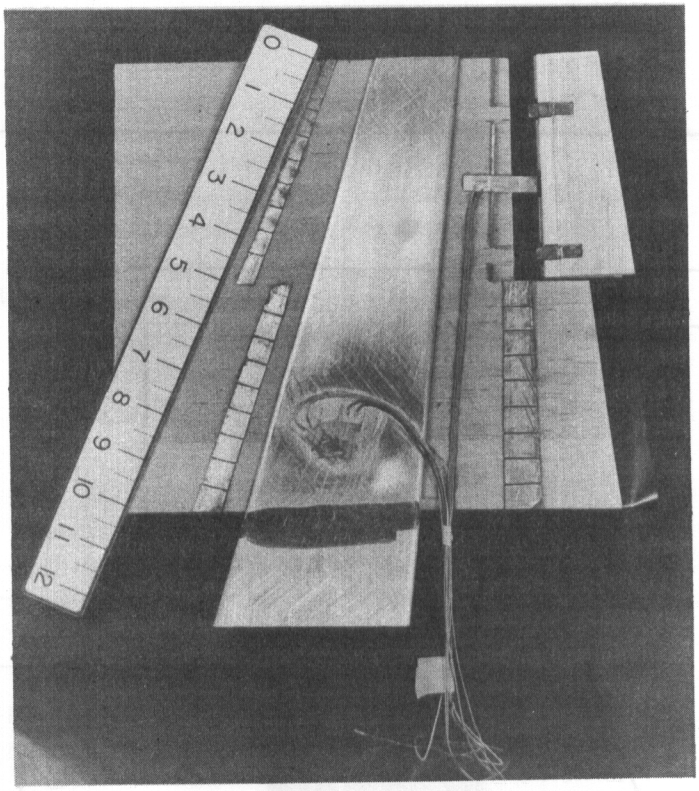

Fig. 13. Partially completed lightweight wing-aileron model.

where

$$\frac{b}{b_o} = 1 - (1 - \lambda)\frac{y}{\ell}$$

The planforms for the three different models tested are shown in Fig. 14. The basic mass and stiffness parameters for all wings and control surfaces are listed in Tables 2 through 7. Influence coefficient data are given in Table 8 and the stations at which influence coefficients were measured are shown in Fig. 15.

The ailerons were fastened to the wing models by two hinges as shown in Fig. 13. The hinges or more accurately flexures, were flat thin strips of steel, one end of which was fastened to the wing and the other end to the aileron. The hinge frequency could be lowered by decreasing the cross-sectional area of the hinge in a plane perpendicular to the surface of the wing in the gap between the wing and the leading edge of the aileron. This was done by decreasing either the width or the thickness of the part of the hinge in the gap. An air gap seal, a piece of silk span glued on one side of the model to both the wing and the leading edge of the aileron and pressed down in the gap to permit freedom of movement by the aileron, was used for all tests. The motion of the aileron was picked up by electric strain gages glued on a piece of 0.004 in. brass and mounted between the wing and the aileron about midspan of the aileron (see Fig. 13).

TAU1 = TAU2 = 2.0

K5 = 1

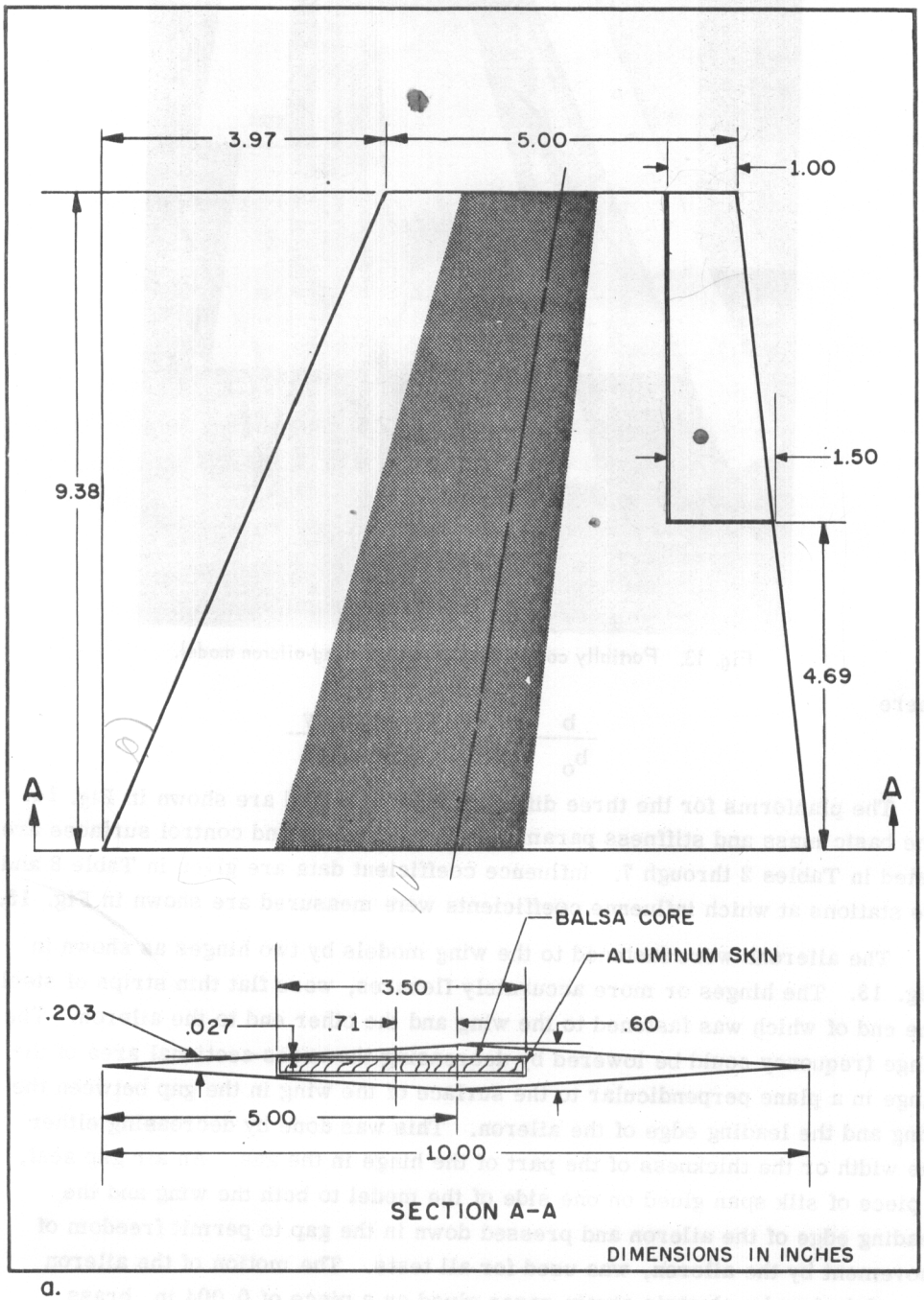

a.

Fig. 14. General layout of wing-aileron models.

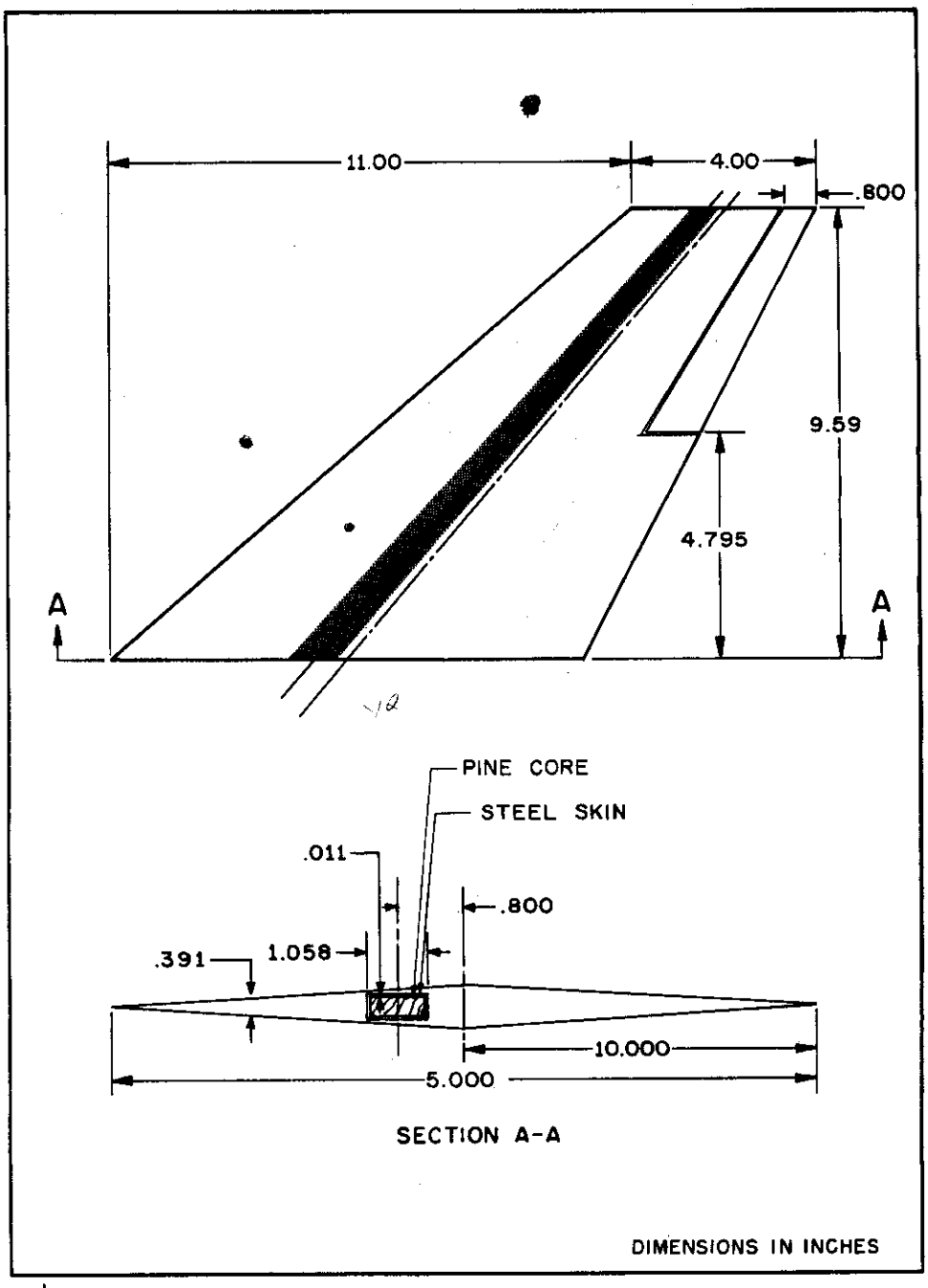

b.

Fig. 14. General layout of wing-aileron models. (cont.)

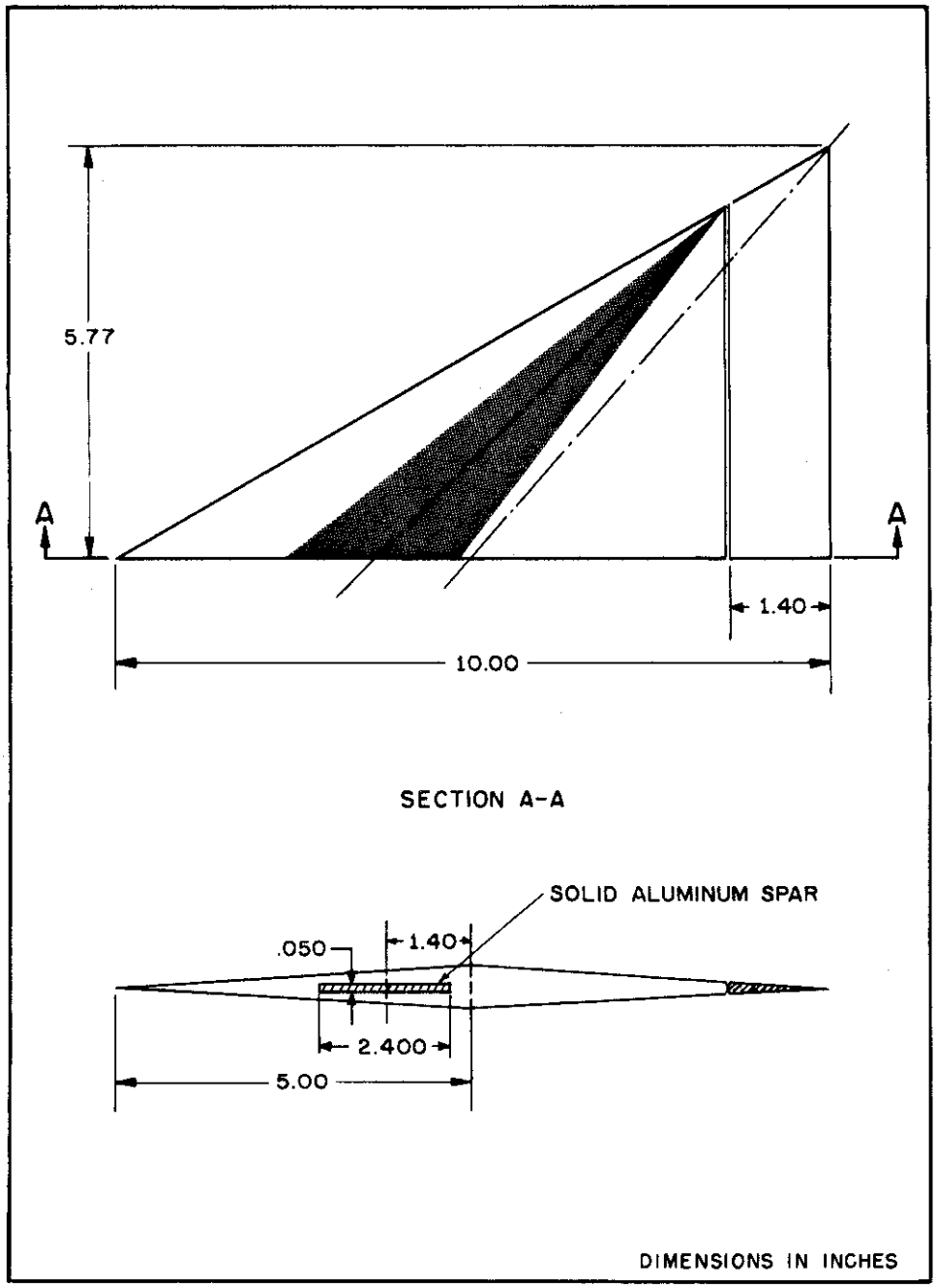

c.

Fig. 14. General layout of wing-aileron models. (cont.)

Table 2. Mass and stiffness data for straight wings.

Model	m_o (slug/in.)	Section cg % Chord	r_α^2 0.42c	$EI_o \times 10^{-6}$ lb-in.^{2}	$GJ_o \times 10^{-6}$ lb-in.^{2}	Calculated Locus of Shear Center % Chord	Measured ea % Chord	ρ_{BA} [1] (lbs/in^3)	E_{BA} [2] (lbs/in^2 $\times 10^{-6}$)	G_{BA} [2] (lbs/in^2 $\times 10^{-6}$)	Remarks
						Light weight wings with unbalanced ailerons					
ST-13	0.00215	50.0	0.250	0.0287	0.0505	42.0	45.2	0.0042	0.00836	0.0235	First no flutter straight wing. No aileron
ST-13-A	0.00250	50.0		0.0269	0.0493		46.8	0.0043	0.0142	0.0239	First wing with aileron
ST-13-A1	0.00250			0.0280	0.0381		49.8	0.0043	0.0142	0.0239	Repaired ST-13-A
ST-13-A2	0.00252			0.0334	0.0455		48.0	0.0046	0.00765	0.0218	Rebuilt ST-13-A1
ST-13-A3	0.00252										Repaired ST-13-A2
ST-13-A4	0.00252										Rebuilt ST-13-A3
ST-13-A5	0.00252										Same as ST-13-A4 but with lower aileron frequency
ST-13-A6	0.00252										Same as ST-13-A5 but with lower aileron frequency
ST-13-A7	0.00252										Same as ST-13-A6 but with lower aileron frequency
						Light weight wings with balanced ailerons					
ST-13-AB	0.00246	50.0	0.250	0.0281	0.0417	42.0	46.0	0.0042	0.0133	0.0246	Basic wing with balanced aileron
ST-13-AB1	0.00243								0.00632	0.0200	Rebuilt ST-13-AB
ST-13-AB2											Same as ST-13-AB1 but with lower aileron frequency
ST-13-AB3											Same as ST-13-AB2 but with lower aileron frequency
							Solid aluminum wings				
ST-14, ST-15	0.00942	50.0		0.472	0.695	50.0	—	—	—	—	All wing models identical with various ailerons

(1) Subscript BA signifies balsa wood.
(2) Estimated balsa properties for bending of and twisting about the wing center line.

Table 3. Mass and stiffness data for swept wings.

Model	m_o (slug/in.)	Section cg % Chord	r_a^2 0.42c	EI_o $\times 10^{-6}$ lb-in.^{2}	GJ_o $\times 10^{-6}$ lb-in.^{2}	Calculated Locus of Shear Center % Chord	Measured ea % Chord	ρ_{BA} [1] (lbs/in^3)	E_{BA} [2] (lbs/in^2 $\times 10^{-6}$)	G_{BA} [2] (lbs/in^2 $\times 10^{6}$)	Remarks
						Light weight wings with unbalanced ailerons					
SW-9	0.00248	50.0	0.250	0.0269	0.0336	42.0	38.6	0.0042	0.00697	0.0214	First no flutter swept wing. No aileron
SW-10-A	0.00228			0.0349	0.0302		47.0	0.0051	0.0101	0.0244	First swept wing with aileron
SW-10-A1											Same as SW-10-A but with lower aileron frequency
SW-10-A2											Same as SW-10-A1 but with lower aileron frequency
SW-10-A3				0.0365	0.0303		45.0				Repaired SW-10-A2
SW-10-A4				0.0341	0.0271						Repaired SW-10-A3
SW-10-A5											Repaired SW-10-A4
SW-10-A7											Repaired SW-10-A5
SW-10-A8											Same as SW-10-A7
						Light weight wings with balanced ailerons					
SW-10-AB	0.00229	50.0	0.250	0.0307	0.0250	42.0	46.0	0.0046	0.0104	0.0285	Basic wing with balanced ailerons
SW-10-AB1											Same as SW-10-AB but with lower aileron frequency
SW-10-AB3											Same as SW-10-AB1 but with lower aileron frequency
SW-10-AB4											Repaired SW-10-AB3 but with higher aileron frequency
SW-10-AB5											Same as SW-10-AB4 but with lower aileron frequency
SW-10-AB6											Same as SW-10-AB5 but with lower aileron frequency
							Solid aluminum wings				
SW-11 SW-12	0.00942	50.0	——	0.472	0.695	50.0	——	——	——	——	All wings identical with various ailerons

(1) Subscript BA signifies balsa wood.
(2) Estimated balsa properties for bending of and twisting about the wing center line.

Table 4. Mass and stiffness data for delta wings.

Model	m_o (slug/in.)	Section cg % Total Chord	r_α^2 0.42c	Calculated Locus of Shear Centers % Wing Chord	ρ_{BA}[1] (lbs/in^3)	E_{BA}*[2] (lbs/in^2 × 10^{-4})	G_{BA}*[2] (lbs/in^2 × 10^{-4})	r	Remarks
					Delta wings with unbalanced elevons				
Dc-3k-A1	0.00261	50.0	0.250	42.0	0.0047	0.715	2.23	0.05	5% thickness ratio wing with elevon
Dc-3k-A2	↓	↓	↓	↓	↓	↓	↓	↓	Same as Dc-3k-A1 but with lower elevon frequency
Dc-3k-A4	↓	↓	↓	↓	↓	↓	↓	↓	Same as Dc-3k-A2 but with lower elevon frequency
Dc-3k-A5	↓	↓	↓	↓	↓	↓	↓	↓	Same as Dc-3k-A4 but with lower elevon frequency
Dc-3k-A6	0.00262	↓	↓	↓	↓	↓	↓	0.04	4% thickness ratio wing with elevon locked out
Dc-3k-A8	↓	↓	↓	↓	↓	↓	↓	↓	Same as Dc-3k-A6 but with elevon
Dc-3k-A10	↓	↓	↓	↓	↓	↓	↓	↓	Same as Dc-3k-A8 but with lower elevon frequency
Dc-3k-A11	↓	↓	↓	↓	↓	↓	↓	↓	Same as Dc-3k-A10 but with lower elevon frequency
Dc-3k-A12	↓	↓	↓	↓	↓	↓	↓	↓	Same as Dc-3k-A11 but with lower elevon frequency
Dc-3k-A13	↓	↓	↓	↓	↓	↓	↓	↓	Repaired Dc-3k-A12 but with lower elevon frequency
Dc-3k-A14	↓	↓	↓	↓	↓	↓	↓	↓	Repaired Dc-3k-A13 but with higher elevon frequency
Dc-3k-A15	0.00235	↓	↓	↓	0.0039	0.516	1.81	↓	Rebuilt Dc-3k model
					Delta wings with balanced ailerons				
Dc-3k-AB	0.00245	50.0	0.250	42.0	0.0046	0.700	0.0229	0.04	4% delta wing with balanced elevon
Dc-3k-AB1	↓	↓	↓	↓	↓	↓	↓	↓	Same as Dc-3k-AB but with lower elevon frequency
Dc-3k-AB2	↓	↓	↓	↓	↓	↓	↓	↓	Same as Dc-3k-AB1 but with lower elevon frequency

(1)-Subscript BA signifies balsa wood.
(2) Estimated balsa properties for bending of and twisting about the wing center line.

Table 5. Mass parameters for straight wing ailerons.

Model	m_{a_o} (slugs/in.)	$\frac{m_a}{m_w}$	$(cg)_a$ % Aileron Chord Aft of Hinge Line	r_{HL} Fraction of Aileron Chord	Remarks
ST-13-A1 through ST-13-A7		0.10	30.0	0.45	Light-weight wing and aileron
ST-13-AB through ST-13-AB3		0.10	00.0	0.32	Light-weight wing and aileron
ST-14-A	0.000292	0.0310	30.0	0.45	Solid aluminum wing, light-weight ailerons differing in ω_β and r_{HL}
ST-14-A1	0.000292	0.0310	30.0	0.45	
ST-14-A2	0.000251	0.0266	30.0	0.45	
ST-14-A3	0.000251	0.0266	30.0	0.45	
ST-14-A4	0.000251	0.0266	30.0	0.45	
ST-14-A5	0.000251	0.0266	30.0	0.50	
ST-15-A	0.000188	0.0199	30.0	0.33	
ST-15-A1	0.000188	0.0199	30.0	0.33	

Table 6. Mass parameters for swept wing ailerons.

Model	m_{a_o} (slugs/in.)	$\frac{m_a}{m_w}$	$(cg)_a$ % Aileron Chord Aft of Hinge Line	r_{HL} Fraction of Aileron Chord	Remarks
SW-10-A through SW-10-A8		0.10	30.0	0.45	Light-weight wing and unbalanced aileron
SW-10-AB through SW-10-AB6		0.10	30.0	0.30	Light-weight wing and balanced aileron
SW-11-A	0.000237	0.0252	30.0	0.45	Solid aluminum model with light-weight ailerons differing in ω_β and r_{HL}
SW-11-A1	↓	↓	↓	↓	
SW-11-A2	↓	↓	↓	↓	
SW-11-A4	↓	↓	↓	↓	
SW-11-A5	↓	↓	↓	↓	
SW-12-A	0.000219	0.0233	30.0	0.33	

Table 7. Mass parameters for delta wing elevons.

Model	$\frac{m_e}{m_w}$	$(cg)_e$ % Elevon Chord Aft of Hinge Line	r_{HL}
De-3k-A1 through De-3k-A5	0.094	35.7	0.45 c_e
Dc-3k-A6 through Dc-3k-A15	0.10	30.8	0.42 c_e
Dc-3k-AB through Dc-3k-AB2	0.10	00.0	0.31 c_e

Table 8.

EXPERIMENTALLY DETERMINED FORCE-DEFLECTION INFLUENCE-COEFFICIENT MATRIX FOR MODEL ST-13-A

	(1)	(2)	(3)	(4)	(5)	(6)	(7)	(8)	(9)
(1)	0.0140	0.0156	0.0116	0.0052	0.0048	0.0054	0.0020	0.0002	0.0016
(2)	0.0140	0.0156	0.0152	0.0040	0.0066	0.0066	0.0016	0.0010	0.0016
(3)	0.0124	0.0168	0.0172	0.0036	0.0042	0.0070	0.0014	0	0.0022
(4)	0.0061	0.0064	0.0052	0.0033	0.0022	0.0025	0.0014	0	0.0007
(5)	0.0069	0.0075	0.0073	0.0028	0.0033	0.0041	0.0012	0.0009	0.0015
(6)	0.0065	0.0074	0.0085	0.0025	0.0025	0.0060	0.0009	0.0001	0.0021
(7)	0.0020	0.0016	0.0017	0.0014	0	0.0009	0.0011	0	0.0003
(8)	0.0019	0.0024	0.0021	0.0009	0.0011	0.0014	0.0006	0.0006	0.0008
(9)	0.0019	0.0025	0.0024	0.0009	0.0010	0.0020	0.0004	0.0003	0.0020

Units are inches/#

EXPERIMENTALLY DETERMINED FORCE-DEFLECTION INFLUENCE-COEFFICIENT MATRIX FOR MODEL ST-13-A1

	(1)	(2)	(3)	(4)	(5)	(6)	(7)	(8)	(9)
(1)	0.0171	0.0168	0.0162	0.0074	0.0096	0.0086	0.0016	0.0028	0.0028
(2)	0.0180	0.0180	0.0198	0.0080	0.0086	0.0100	0.0018	0.0028	0.0029
(3)	0.0162	0.0196	0.0230	0.0070	0.0088	0.0114	0.0015	0.0028	0.0038
(4)	0.0074	0.0077	0.0073	0.0052	0.0040	0.0044	0.0019	0.0014	0.0015
(5)	0.0083	0.0087	0.0090	0.0041	0.0054	0.0062	0.0016	0.0021	0.0020
(6)	0.0090	0.0100	0.0117	0.0043	0.0054	0.0084	0.0015	0.0019	0.0035
(7)	0.0018	0.0018	0.0015	0.0013	0.0006	0.0012	0.0010	0.0007	0.0005
(8)	0.0028	0.0027	0.0030	0.0018	0.0017	0.0021	0.0007	0.0009	0.0011
(9)	0.0027	0.0032	0.0039	0.0014	0.0019	0.0030	0.0006	0.0011	0.0024

Units are inches/#

Table 8 (cont.)

EXPERIMENTALLY DETERMINED FORCE-DEFLECTION INFLUENCE-COEFFICIENT MATRIX FOR MODEL ST-13-AB

	(1)	(2)	(3)	(4)	(5)	(6)	(7)	(8)	(9)
(1)	0.0134	0.0135	0.0141	0.0062	0.0071	0.0057	0.0015	0.0017	0.0017
(2)	0.0123	0.0150	0.0165	0.0055	0.0071	0.0079	0.0019	0.0017	0.0023
(3)	0.0137	0.0166	0.0209	0.0051	0.0078	0.0088	0.0014	0.0019	0.0030
(4)	0.0063	0.0064	0.0062	0.0038	0.0039	0.0026	0.0013	0.0009	0.0010
(5)	0.0063	0.0067	0.0085	0.0030	0.0043	0.0040	0.0007	0.0009	0.0013
(6)	0.0063	0.0081	0.0109	0.0027	0.0050	0.0072	0.0005	0.0018	0.0023
(7)	0.0013	0.0017	0.0017	0.0011	0.0013	0.0009	0.0017	0.0005	0.0003
(8)	0.0016	0.0023	0.0025	0.0010	0.0016	0.0017	0.0008	0.0006	0.0007
(9)	0.0020	0.0024	0.0030	0.0011	0.0017	0.0019	0.0003	0.0007	0.0020

Units are inches/#

EXPERIMENTALLY DETERMINED FORCE-DEFLECTION INFLUENCE-COEFFICIENT MATRIX FOR MODEL ST-13-AB-1

	(1)	(2)	(3)	(4)	(5)	(6)	(7)	(8)	(9)
(1)	0.0153	0.0150	0.0145	0.0064	0.0071	0.0069	0.0017	0.0022	0.0020
(2)	0.0147	0.0160	0.0172	0.0057	0.0077	0.0084	0.0014	0.0021	0.0023
(3)	0.0149	0.0174	0.0214	0.0060	0.0080	0.0099	0.0011	0.0022	0 0030
(4)	0.0069	0.0065	0.0061	0.0044	0.0037	0.0030	0.0012	0.0016	0.0009
(5)	0.0074	0.0075	0.0084	0.0033	0.0046	0.0047	0.0009	0.0014	0.0016
(6)	0.0074	0.0084	0.0099	0.0033	0.0051	0.0072	0.0006	0.0013	0.0021
(7)	0.0020	0.0017	0.0015	0.0012	0.0011	0.0008	0.0008	0.0004	0.0001
(8)	0.0022	0.0022	0.0024	0.0010	0.0014	0.0014	0.0003	0.0006	0.0008
(9)	0.0021	0.0023	0.0030	0:0010	0.0017	0.0022	0.0001	0.0006	0.0019

Units are inches/#

Table 8 (cont.)

EXPERIMENTALLY DETERMINED FORCE-DEFLECTION INFLUENCE-COEFFICIENT MATRIX FOR MODEL SW-9

	(1)	(2)	(3)	(4)	(5)	(6)	(7)	(8)	(9)
(1)	0.0448	0.0504	0.0530	0.0168	0.0214	0.0282	0.0026	0.0054	0.0090
(2)	0.0556	0.0666	0.0766	0.0200	0.0272	0.0376	0.0030	0.0068	0.0122
(3)	0.0596	0.0744	0.0960	0.0202	0.0290	0.0424	0.0026	0.0068	0.0126
(4)	0.0162	0.0170	0.0170	0.0092	0.0096	0.0111	0.0019	0.0036	0.0050
(5)	0.0232	0.0262	0.0282	0.0109	0.0139	0.0180	0.0021	0.0046	0.0081
(6)	0.0310	0.0374	0.0427	0.0124	0.0179	0.0276	0.0020	0.0049	0.0096
(7)	0.0018	0.0016	0.0011	0.0016	0.0010	0.0012	0.0011	0.0009	0.0006
(8)	0.0045	0.0049	0.0047	0.0030	0.0030	0.0040	0.0009	0.0018	0.0026
(9)	0.0089	0.0106	0.0115	0.0046	0.0065	0.0089	0.0010	0.0028	0.0066

Units are inches/#

EXPERIMENTALLY DETERMINED FORCE-DEFLECTION INFLUENCE-COEFFICIENT MATRIX FOR MODEL SW-10-A

	(1)	(2)	(3)	(4)	(5)	(6)	(7)	(8)	(9)
(1)	0.0299	0.0337	0.0279	0.0106	0.0150	0.0138	0.0020	0.0020	0.0063
(2)	0.0322	0.0380	0.0447	0.0116	0.0160	0.0214	0.0019	0.0030	0.0072
(3)	0.0362	0.0445	0.0560	0.0134	0.0182	0.0268	0.0018	0.0044	0.0088
(4)	0.0112	0.0119	0.0116	0.0070	0.0072	0.0075	0.0015	0.0023	0.0031
(5)	0.0148	0.0165	0.0178	0.0068	0.0091	0.0109	0.0016	0.0025	0.0046
(6)	0.0181	0.0217	0.0255	0.0074	0.0113	0.0174	0.0015	0.0033	0.0061
(7)	0.0023	0.0021	0.0010	0.0014	0.0016	0.0007	0.0009	0.0004	0.0007
(8)	0.0042	0.0045	0.0040	0.0023	0.0031	0.0031	0.0007	0.0011	0.0018
(9)	0.0058	0.0074	0.0083	0.0029	0.0047	0.0061	0.0004	0.0017	0.0040

Units are inches/#

Table 8 (cont.)

EXPERIMENTALLY DETERMINED FORCE-DEFLECTION INFLUENCE-COEFFICIENT MATRIX FOR MODEL SW-10-A3

	(1)	(2)	(3)	(4)	(5)	(6)	(7)	(8)	(9)
(1)	0.0314	0.0339	0.0356	0.0118	0.0152	0.0189	0.0030	0.0041	0.0064
(2)	0.0338	0.0379	0.0424	0.0119	0.0169	0.0223	0.0023	0.0044	0.0079
(3)	0.0354	0.0428	0.0608	0.0123	0.0192	0.0264	0.0024	0.0048	0.0093
(4)	0.0116	0.0120	0.0125	0.0064	0.0071	0.0075	0.0015	0.0025	0.0033
(5)	0.0152	0.0167	0.0193	0.0072	0.0095	0.0113	0.0017	0.0029	0.0052
(6)	0.0192	0.0223	0.0267	0.0078	0.0118	0.0218	0.0017	0.0035	0.0068
(7)	0.0025	0.0023	0.0021	0.0016	0.0015	0.0014	0.0011	0.0007	0.0008
(8)	0.0041	0.0047	0.0049	0.0025	0.0030	0.0033	0.0008	0.0013	0.0020
(9)	0.0067	0.0076	0.0093	0.0036	0.0048	0.0065	0.0008	0.0020	0.0045

Units are inches/#

EXPERIMENTALLY DETERMINED FORCE-DEFLECTION INFLUENCE-COEFFICIENT MATRIX FOR MODEL De-3k-A1

	(1)	(2)	(3)	(4)	(5)	(6)	(7)	(8)	(9)	(10)
(1)	0.0015	0.0015	0.0009	0.0012	0.0004	0	0.0002	0	0	0.0001
(2)	0.0015	0.0035	0.0045	0.0054	0.0007	0.0006	0.0010	0	0.0006	0
(3)	0.0013	0.0049	0.0093	0.0114	0.0010	0.0040	0.0042	0	0.0006	0.0001
(4)	0.0010	0.0053	0.0089	0.0189	0.0009	0.0043	0.0072	0	0.0015	0
(5)	0.0005	0.0009	0	0.0013	0.0004	0	0.0005	0	0.0001	0
(6)	0.0006	0.0021	0.0009	0.0043	0.0006	0.0007	0.0041	0	0.0019	0
(7)	0.0002	0.0020	0.0036	0.0075	0.0006	0.0024	0.0077	0	0.0025	0.0001
(8)	0.0001	0.0004	0	0.0005	0.0001	0	0.0006	0	0.0003	0.0001
(9)	0.0001	0.0005	0.0001	0.0019	0.0001	0	0.0021	0	0.0037	0
(10)	0	0	0	0.0001	0.0001	0.0001	0	0	0.0003	0.0015

Units are inches/#

Table 8 (cont.)

EXPERIMENTALLY DETERMINED FORCE-DEFLECTION
INFLUENCE-COEFFICIENT MATRIX FOR MODEL De-3k-A6

	(1)	(2)	(3)	(4)	(5)	(6)	(7)	(8)	(9)	(10)
(1)	0.0064	0.0060	0.0052	0.0040	0.0019	0.0017	0.0008	0	0	0.0001
(2)	0.0067	0.0147	0.0144	0.0161	0.0028	0.0077	0.0061	0.0005	0.0013	0
(3)	0.0044	0.0150	0.0209	0.0313	0.0029	0.0104	0.0119	0.0014	0.0022	0
(4)	0.0042	0.0163	0.0302	0.0523	0.0019	0.0138	0.0196	0.0015	0.0042	0
(5)	0.0016	0.0030	0.0032	0.0031	0.0006	0.0019	0.0009	0.0002	0	0
(6)	0.0021	0.0072	0.0103	0.0145	0.0012	0.0073	0.0079	0.0011	0.0025	0.0001
(7)	0.0010	0.0063	0.0116	0.0199	0	0.0079	0.0158	0.0008	0.0044	0
(8)	0.0002	0.0005	0.0011	0.0017	0.0001	0.0009	0.0011	-0.0003	0.0006	0.0001
(9)	0.0003	0.0012	0.0023	0.0050	0	0.0027	0.0045	0.0007	0.0062	0.0003
(10)	0	0	0	0	0	0.0001	0	0	0.0003	0.0021

Units are inches/#

EXPERIMENTALLY DETERMINED FORCE-DEFLECTION
INFLUENCE-COEFFICIENT MATRIX FOR MODEL De-3k-AB

	(1)	(2)	(3)	(4)	(5)	(6)	(7)	(8)	(9)	(10)
(1)	0.0024	0.0022	0.0020	0.0013	0.0002	0	0.0002	0	0	
(2)	0.0017	0.0080	0.0097	0.0093	0.0009	0.0028	0.0032	0	0.0002	
(3)	0.0012	0.0090	0.0174	0.0238	0.0011	0.0037	0.0084	0	0.0010	
(4)	0.0008	0.0093	0.0233	0.0520	0.0017	0.0073	0.0151	0	0.0023	
(5)	0.0002	0.0010	0.0014	0.0019	0.0003	0.0006	0.0008	0	0.0001	
(6)	0.0003	0.0027	0.0048	0.0074	0.0003	0.0023	0.0048	0	0.0010	
(7)	0	0.0033	0.0080	0.0158	0.0002	0.0051	0.0138	0	0.0032	
(8)	0	0.0002	0.0002	0.0006	0	0	0.0007	0	0.0004	
(9)	0	0.0006	0.0016	0.0030	0	0.0006	0.0038	0	0.0073	
(10)	0	0	0	0.0002	0	0	0	0	0.0001	0.0018

Units are inches/#

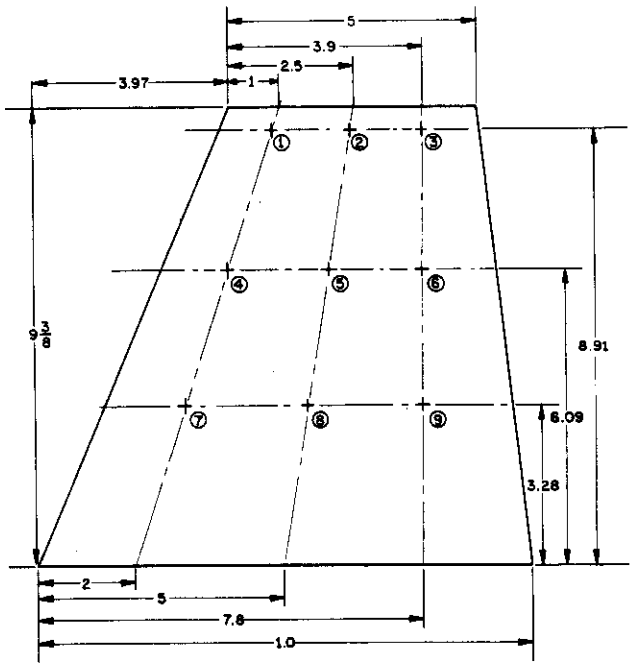

Straight Wing

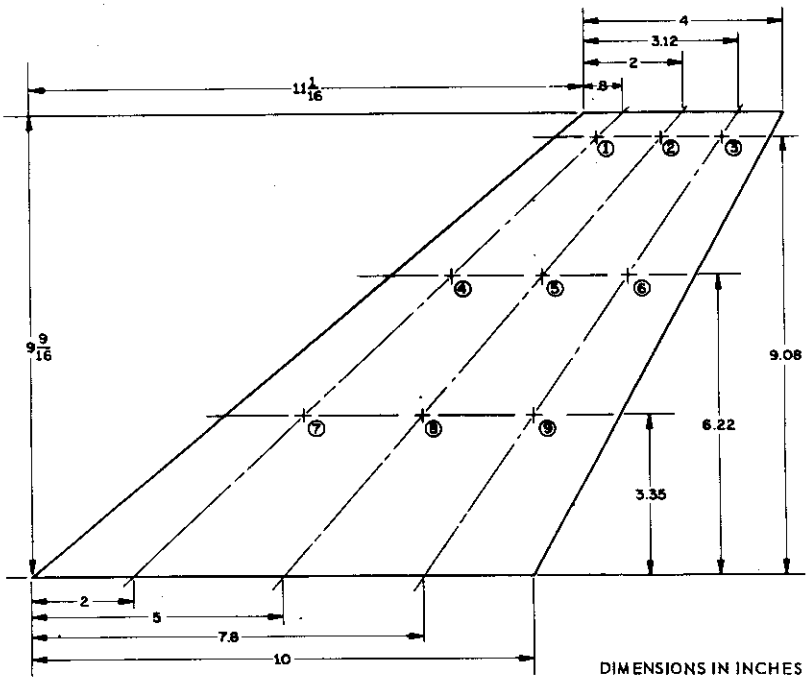

Swept Wing

Fig. 15. Influence coefficient stations for wing-aileron models.

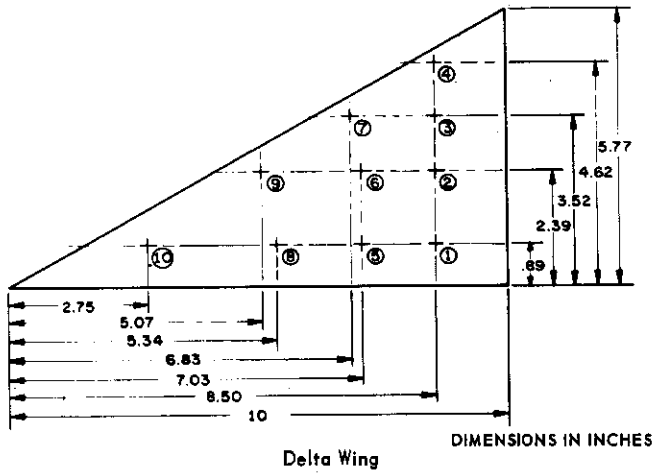

Fig. 15. Influence coefficient stations for wing-aileron models. (cont.)

Vibration data for all models tested are presented in Tables 9 through 11. Techniques used to obtain the data are described in Ref. 2. In an attempt to measure the uncoupled aileron modes for the lightweight wing models, pieces of balsa wood were clamped over the wing planform leaving only the aileron itself free to vibrate. This method of suppressing wing vibration modes was only partially successful, because it was not possible, by this means to completely suppress the higher frequency modes of the wing. However, the first bending and, more importantly, the first torsion modes of the various wing models were almost completely suppressed. The uncoupled aileron frequency given in Tables 9 through 11 was determined by this procedure.

It is also to be noted that certain blank spaces are left in the vibration spectrum data of Tables 9 through 11. The omissions are related to inadequacies of the shaking equipment rather than any pecularities of individual models. Although the excitation by electromagnetic shakers through the massive elastically supported root block of the models (see Ref. 2) was generally quite satisfactory certain modes on certain models could not be adequately excited. This situation could only have been remedied by moving the attachment points of the shakers or by increasing their size. For example, no second bending mode could be clearly excited for the ST-13-A, ST-13-A1 and ST-13-A7 models. Certain of the higher frequency vibration modes were also difficult to excite. For example, the mode which occurs at about 600 cps for most of the straight wing models with unbalanced ailerons could not be clearly excited for the ST-13-A2 and ST-13-A3 models.

Also missing from the vibration data of the De-3k-A series models is the second mode which is composed mainly of wing torsion and aileron flapping

Table 9. Vibration data for straight wings.

MODEL \ MODE	FIRST		SECOND		THIRD		FOURTH		FIFTH		AILERON WING CLAMPED	
	ω (cps)	g	ω	g	ω	g	ω	g	ω	g	ω	g
ST-13	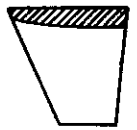				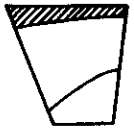		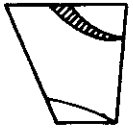					
	93.3	0.016	292	0.009	350	0.010	583	0.008				
ST-13-A	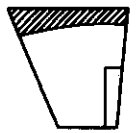		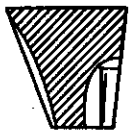				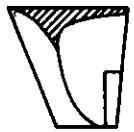		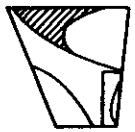		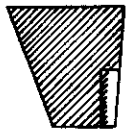	
	93.1	0.018	258	0.015			356	0.014	616	0.014	325	0.031
ST-13-A1	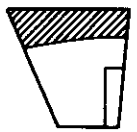		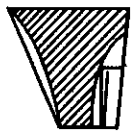				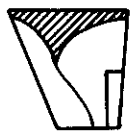		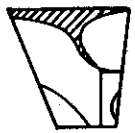		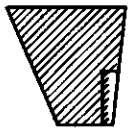	
	91.6	0.020	238	0.021			346	0.026	620	0.021	280	0.03
ST-13-A2	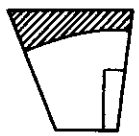				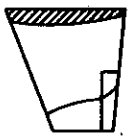		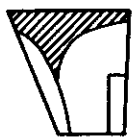				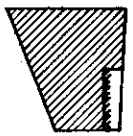	
	91.0	0.015	264	0.027	330	0.018	370	0.027			319	0.044

NOTE: FREQUENCIES, ω, ARE GIVEN IN CPS.

Table 9. Vibration data for straight wings. (cont.)

MODEL \ MODE	FIRST		SECOND		THIRD		FOURTH		FIFTH		AILERON WING CLAMPED	
	ω (CPS)	g	ω	g	ω	g	ω	g	ω	g	ω	g
ST-13-A3					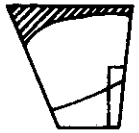				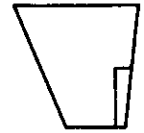		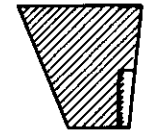	
	88.5	0.016	252	0.017	321	0.026	360	0.018	450	0.026	278	0.018
ST-13-A4	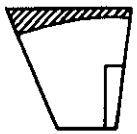				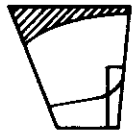				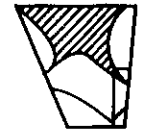		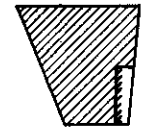	
	88	0.02	244	0.026	314	0.024	350	0.028	571	0.07	271	0.04
ST-13-A5	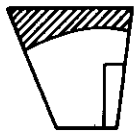				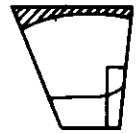				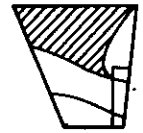		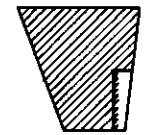	
	87.5	0.020	225	0.022	310	0.022	329	0.015	600	—	250	—
ST-13-A6	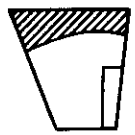		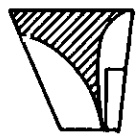		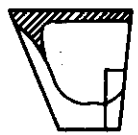		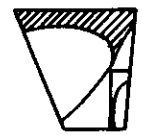		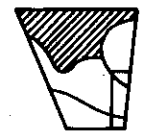		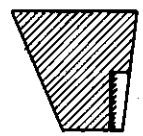	
	90	—	215	—	306	0.024	394	0.044	542	0.044	222	—
ST-13-A7	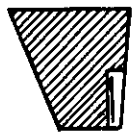		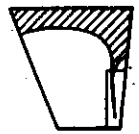						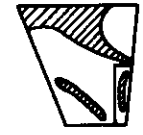		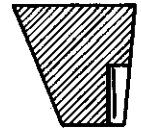	
	43.5	—	93.3	0.018	304	0.012.			570	0.018	51	—

NOTE: FREQUENCIES, ω, ARE GIVEN IN CPS.

Table 9. Vibration data for straight wings. (cont.)

MODEL \ MODE	FIRST		SECOND		THIRD		FOURTH		FIFTH		SIXTH		AILERON WING CLAMPED	
	ω(cps)	g	ω	g	ω	g	ω	g	ω	g	ω	g	ω	g
ST-13-AB	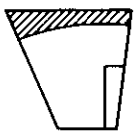		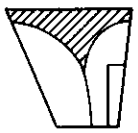		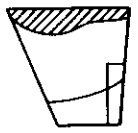				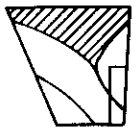				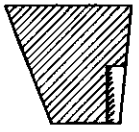	
	95.7	0.012	286	0.024	375	0.03	480	—	595	0.03			443	0.03
ST-13-AB1	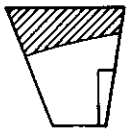						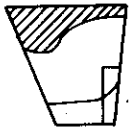		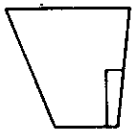		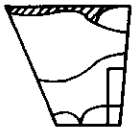		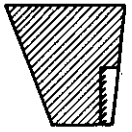	
	97.0	0.013	270	0.008	307	0.022	320	0.031	600	—	1000	0.014	300	0.040
ST-13-AB2	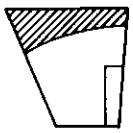		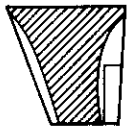		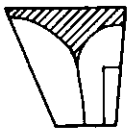		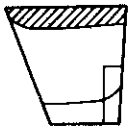				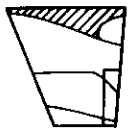		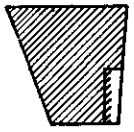	
	97.5	0.015	222	0.018	300	0.013	330	—			850	0.026	240	0.031
ST-13-AB3	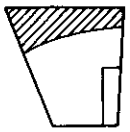		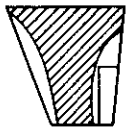		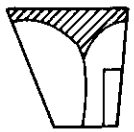		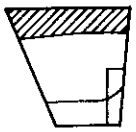		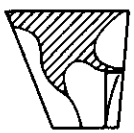		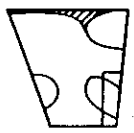		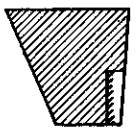	
	97.0		166	0.044	296	0.015	330	—	550	0.02	900	0.01	188	0.04

NOTE: FREQUENCIES, ω, ARE GIVEN IN CPS.

Table 9. Vibration data for straight wings. (cont.)

MODEL \ MODE	FIRST		SECOND		THIRD		AILERON	
	ω (cps)	g	ω	g	ω	g	ω	g
ST-14-A	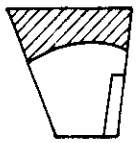 185	—					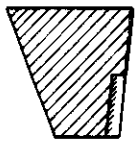 380	—
ST-14-A2	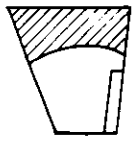 200	0.006			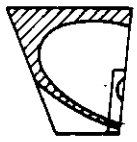 800	0.022	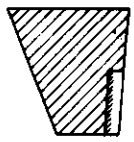 290	0.023
ST-14-A3	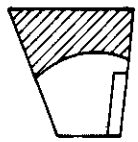 200	0.005	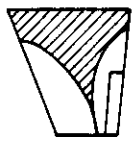 700	0.006	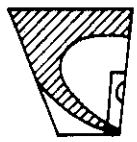 813	0.025	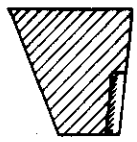 236	0.023

NOTE: FREQUENCIES, ω, ARE GIVEN IN CPS.

Table 9. Vibration data for straight wings. (cont.)

MODE / MODEL	FIRST		SECOND		THIRD		AILERON	
	ω(cps)	g	ω	g	ω	g	ω	g
ST-14-A4	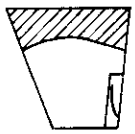		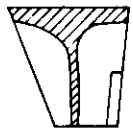		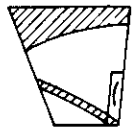		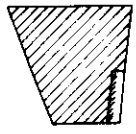	
	207	0.008	700	0.017	825	—	167	0.014
ST-14-A5	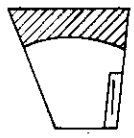		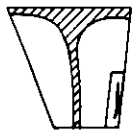		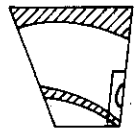		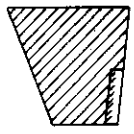	
	210	0.010	700	0.028	850	0.037	138	0.055
ST-15-A	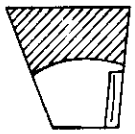		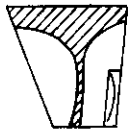		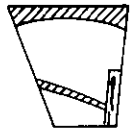		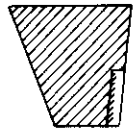	
	216	0.012	725	0.024	850	0.024	181	0.030
ST-15-A1	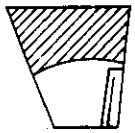		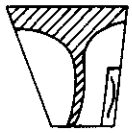		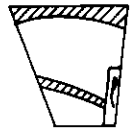		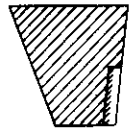	
	212	0.007	712	0.028	834	0.011	129	0.034

NOTE: FREQUENCIES, ω, ARE GIVEN IN CPS.

Table 10. Vibration data for swept wings.

MODEL \ MODE	FIRST		SECOND		THIRD		FOURTH		FIFTH		AILERON WING CLAMPED	
	ω (cps)	g	ω	g	ω	g	ω	g	ω	g	ω	g
SW-9	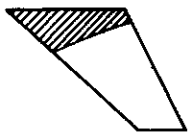 57.5	0.015	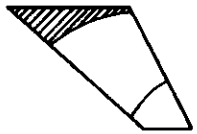 210	0.014	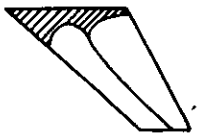 280	0.015	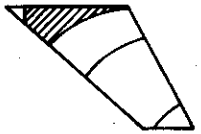 450	0.028				
SW-10-A	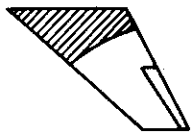 74.8	0.018	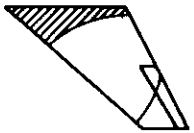 248	0.017	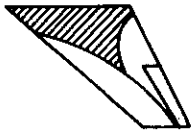 309	0.017	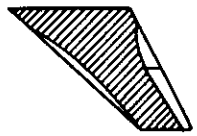 390	0.037	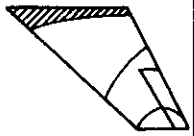 613	0.034	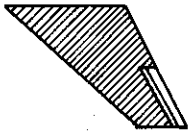 424	0.09
SW-10-A1	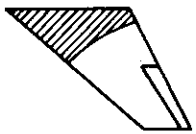 73.8	0.014	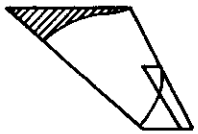 249	—	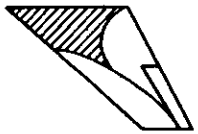 300	—			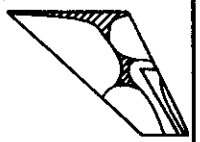 725	0.019	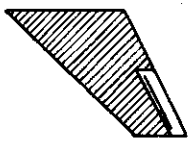 364	—
SW-10-A2	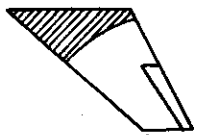 729	0.015	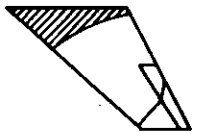 246	—	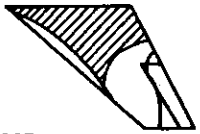 293	—			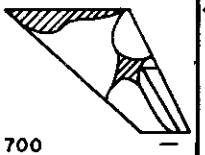 700	—	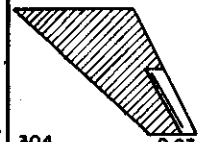 304	0.03

NOTE: FREQUENCIES, ω, ARE GIVEN IN CPS.

Table 10. Vibration data for swept wings. (cont.)

MODEL \ MODE	FIRST		SECOND		THIRD		FOURTH		FIFTH		SIXTH		AILERON WING CLAMPED	
	ω	g	ω	g	ω	g	ω	g	ω	g	ω	g	ω	g
SW-10-A3	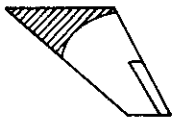 73.8	0.012	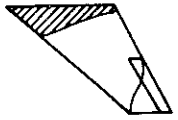 224	0.031	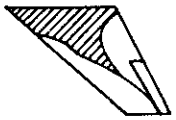 280	0.028	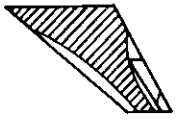 310	0.028	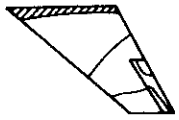 600	0.022			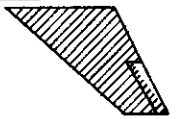 320	0.049
SW-10-A4	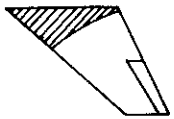 72.4	0.016	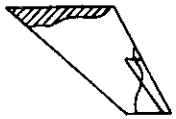 228	0.032	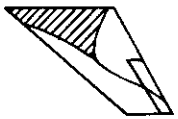 257	0.028			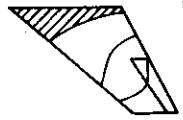 583	0.026			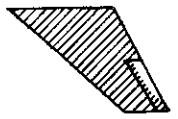 259	0.026
SW-10-A5	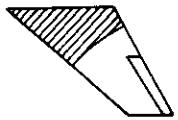 76.9	0.01	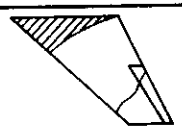 271	0.012	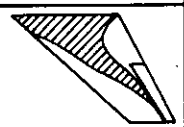 275	0.036			 625	0.017			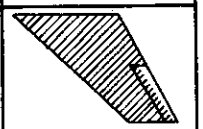 271	0.031
SW-10-A7	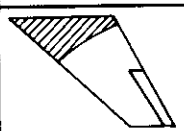 72.7	0.018	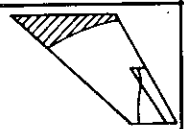 225	0.022	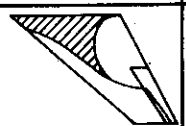 264	0.022	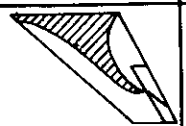 333	0.023			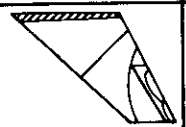 900	0.031	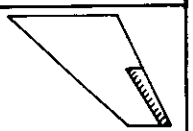 275	0.017
SW-10-A8	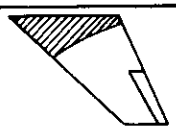 73.7	0.02	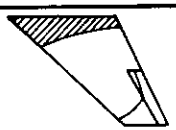 239	0.03	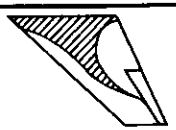 270	0.03			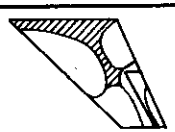 700	—	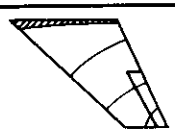 800	—	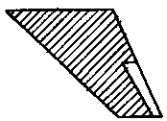 275	0.03

NOTE: FREQUENCIES, ω, ARE GIVEN IN CPS.

Table 10. Vibration data for swept wings. (cont.)

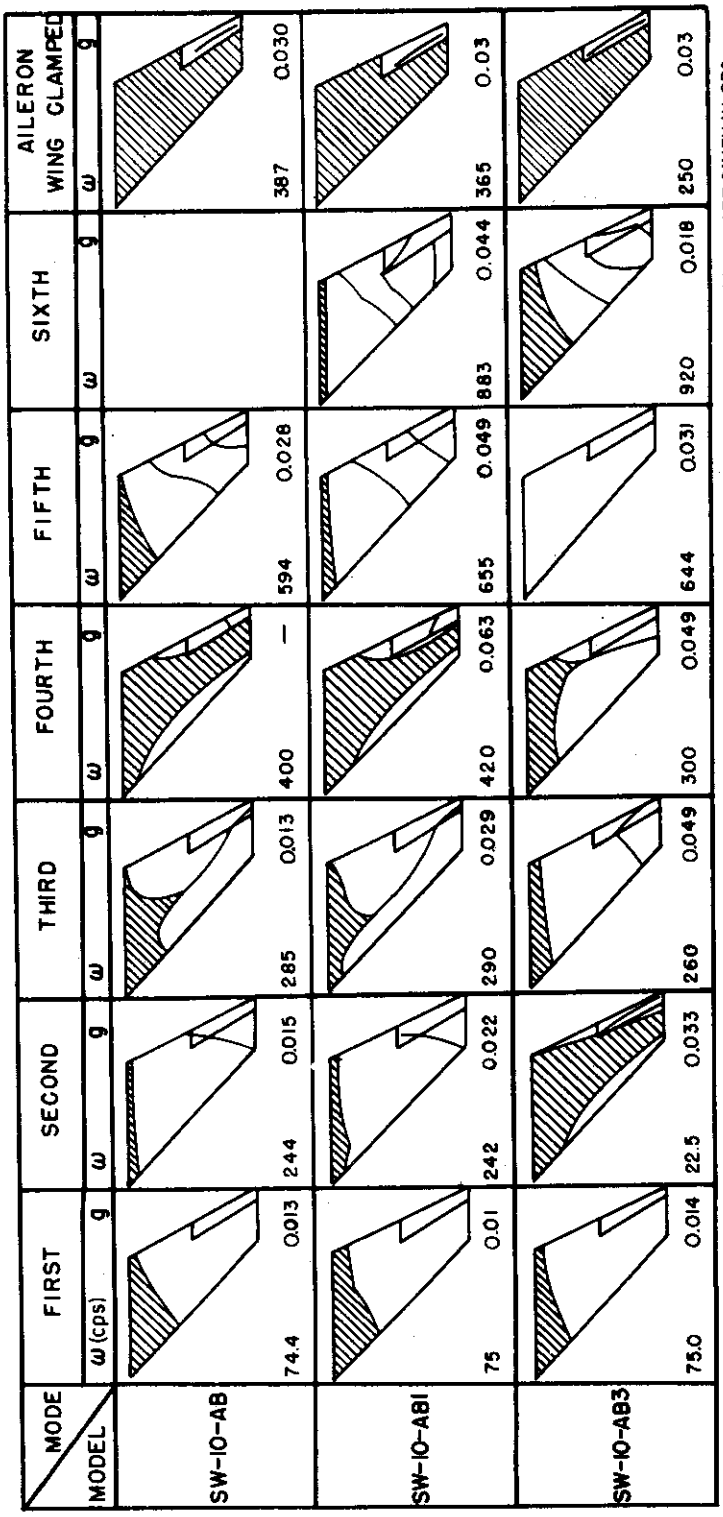

NOTE: FREQUENCIES, ω, ARE GIVEN IN CPS.

Table 10. Vibration data for swept wings. (cont.)

MODEL \ MODE	FIRST		SECOND		THIRD		FOURTH		FIFTH		SIXTH		AILERON WING CLAMPED	
	ω (cps)	g	ω	g	ω	g	ω	g	ω	g	ω	g	ω	g
SW-10-AB4	73.9	0.011	260	0.016	300	0.017							300	
SW-10-AB5	73.7	0.012	257	0.016	292	0.011	320	—					304	
SW-10-AB6	73.1	0.011	225	0.019	250		270		—	—			230	—

NOTE: FREQUENCIES, ω, ARE GIVEN IN CPS.

Table 10. Vibration data for swept wings. (cont.)

MODE / MODEL	FIRST		SECOND		THIRD		FOURTH		AILERON	
	ω(cps)	g	ω	g	ω	g	ω	g	ω	g
SW-II-A	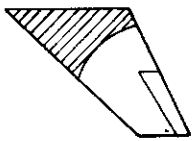 ~140	—			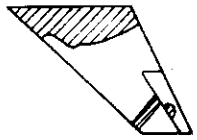 ~500	—	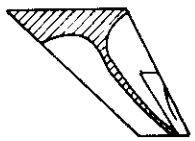 783	0.004	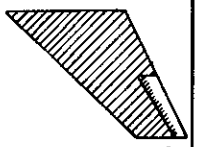 492	0.030
SW-II-A1	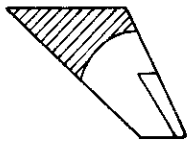 141	0.023			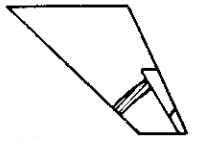 500	—	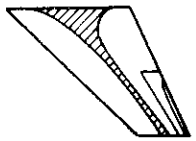 800	0.014	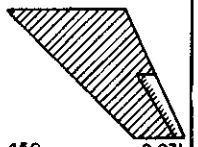 450	0.031
SW-II-A2	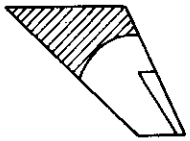 141	0.006			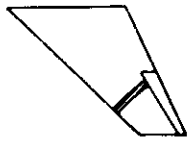 500	—	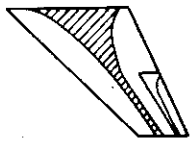 800	0.014	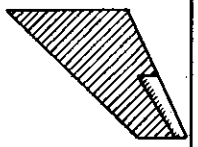 286	0.031
SW-II-A3	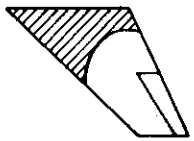 142	0.005				—	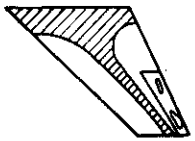 ~800	—	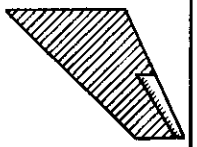 267	0.022

NOTE: FREQUENCIES, ω, ARE GIVEN IN CPS.

Table 10. Vibration data for swept wings. (cont.)

MODE / MODEL	FIRST		SECOND		THIRD		FOURTH		AILERON	
	ω(cps)	g	ω	g	ω	g	ω	g	ω	g
SW-11-A4	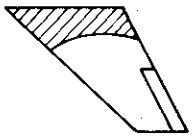 144.5	~0	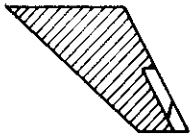 300	0.028	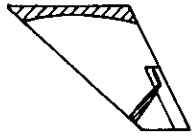 550	—	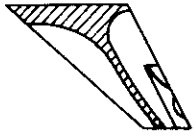 775	~0.004	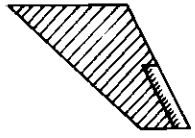 225	0.012
SW-11-A5	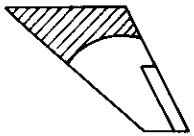 150	0.008	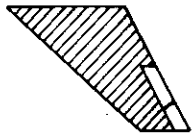 262	—	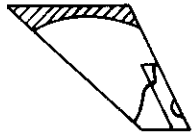 521	0.009	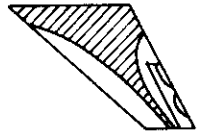 800	0.018	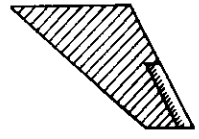 126	0.03
SW-12-A	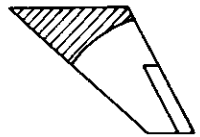 147	0.004			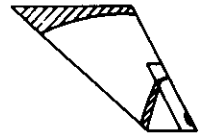 517	0.007	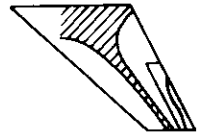 775	—	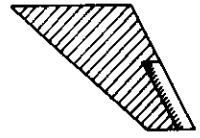 105	—

NOTE: FREQUENCIES, ω, ARE GIVEN IN CPS.

Table 11. Vibration data for delta wings.

MODEL \ MODE	FIRST		SECOND		THIRD		FOURTH		AILERON WING CLAMPED	
	ω(cps)	g	ω	g	ω	g	ω	g	ω	g
De — 3K — A1	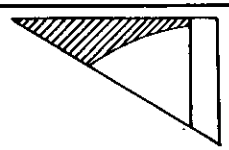 204	—	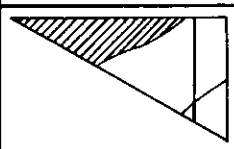 483	—	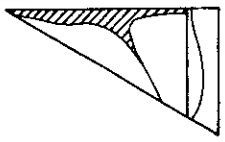 671	0.031	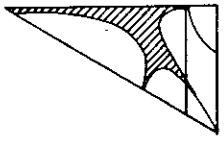 875	0.049	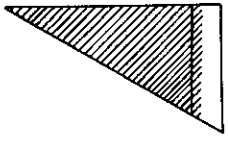 650	—
De — 3K — A2	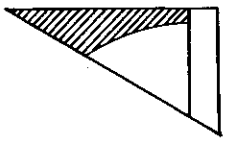 197	0.03	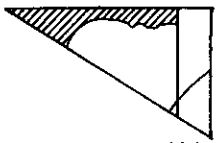 488	0.04	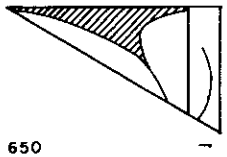 650	—	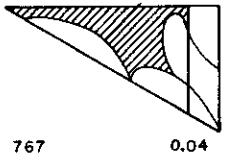 767	0.04	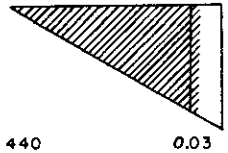 440	0.03
De — 3K — A4	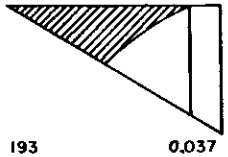 193	0.037	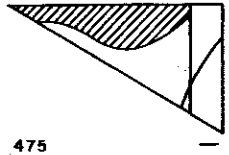 475	—	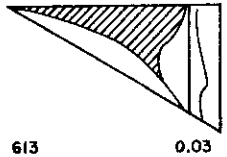 613	0.03	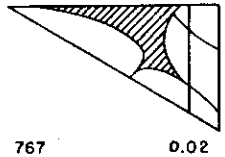 767	0.02	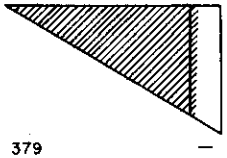 379	—
De — 3K — A5	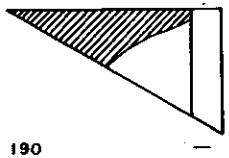 190	—	475	—	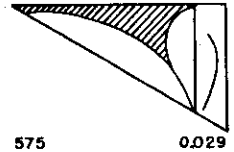 575	0.029	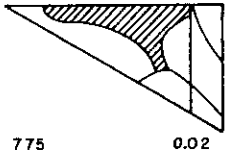 775	0.02	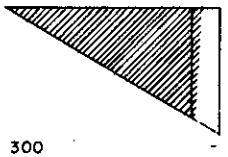 300	-

NOTE: FREQUENCIES, ω, ARE GIVEN IN CPS.

Table 11. Vibration data for delta wings. (cont.)

MODEL \ MODE	FIRST ω (cps)	FIRST g	SECOND ω	SECOND g	THIRD ω	THIRD g	FOURTH ω	FOURTH g	AILERON WING CLAMPED ω	AILERON WING CLAMPED g
De – 3K – A6	144	0.031	333	0.055	406	0.034	540	–		
De – 3K – A8	138	–	283	0.037	350	0.055	595	0.027	455	0.015
De – 3K – A10	130	0.05	264	0.03	350	–	558	0.04	313	–
De – 3K – A11	128	0.05	256	0.03	343	–	545	–	282	–

NOTE: FREQUENCIES, ω, ARE GIVEN IN CPS.

Table 11. Vibration data for delta wings. (cont.)

MODEL / MODE	FIRST		SECOND		THIRD		FOURTH		AILERON WING CLAMPED	
	ω (cps)	g	ω	g	ω	g	ω	g	ω	g
De-3K-A12	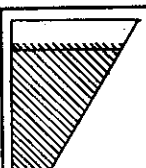 127	0.04	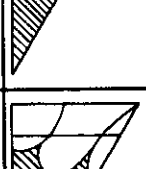 250	0.005	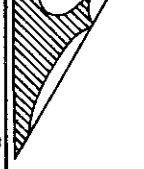 330	0.05	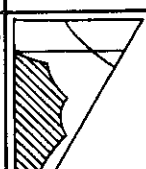 565	0.03	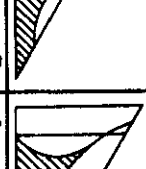 254	0.04
De-3K-A13	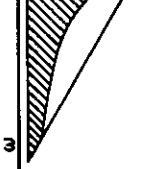 117	0.04	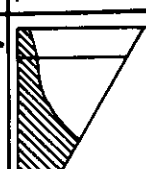 230	—	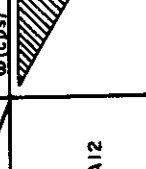 310	—	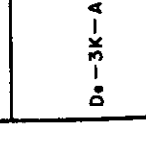 550	—	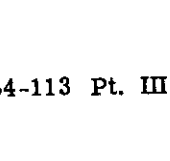 160	—
De-3K-A14	128	—	200	—	277	—	563	—	190	—
De-3K-A15	158	0.018	231	—	321	0.023	425	0.020	193	—

NOTE: FREQUENCIES, ω, ARE GIVEN IN CPS.

Table 11. Vibration data for delta wings. (cont.)

MODEL \ MODE	FIRST	SECOND	THIRD	FOURTH	FIFTH	AILERON WING CLAMPED
	ω (cps) g	ω g	ω g	ω g	ω g	ω g
De-3K-AB	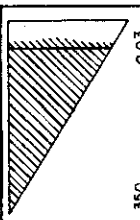 170 0.021	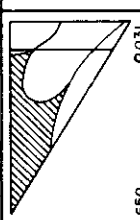 350 0.005	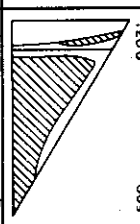 400 0.031	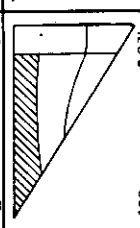 500 0.031	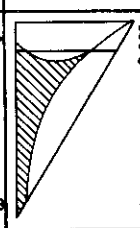 650 0.031	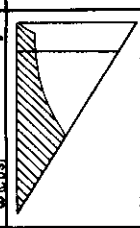 350 0.03
De-3K-AB1	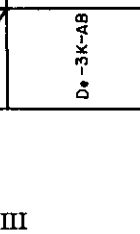 175 0.029	333 0.04	 400 0.022	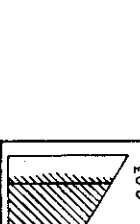 475 0.040	650 —	275 —
De-3K-AB2	165 0.026	310 0.022	383 0.022	478 —	675 0.011	195 —

NOTE: FREQUENCIES, ω, ARE GIVEN IN CPS.

motions. This mode exists for these models, but its significance was not fully recognized at the time these vibration tests were made. The lower, more important, vibration mode involving torsion and aileron flapping motions is included. The vibration data for the De-3k-AB series models includes both of these modes. Some peculiarities exist in the vibration data for these models.

Flutter data from all of the successful tests are included in Tables 12 through 14. Enough information is given so that if the reader wants particular parameters which are not included in this report, he should be able to calculate them easily. (See Section D. 4 of Ref. 1.)

Excerpts from the high-speed movies of the test run of the ST-13-A1 model are presented in Fig. 16. The portions showing the beginning of the bending-torsion-aileron flutter and the portion just before model descrimination are presented. Analyses of wing tip and aileron tip motion at the start of the tunnel test and during model failure for the ST-13-A1 model based on the high-speed movies are presented in Figs. 17 and 18. Careful examination of the pictures shows that the high-frequency aileron flutter exists along with the bending-torsion-aileron flutter.

Tracings of strain gages records during flutter for the ST-13-A, ST-13-A1, and ST-13-A2 models are given in Fig. 19 through Fig. 21. Figures 19 and 21 show typical traces obtained from the high-frequency aileron flutter encountered. Figure 20 again shows the combination of bending-torsion-aileron mode and high-frequency aileron mode that exists for the ST-13-A1 model flutter.

Finally a picture of the SW-10-AB3 model after destructive flutter has taken place is shown in Fig. 22. This type of model failure is typical of the high-frequency aileron flutter encountered during the present test program.

Table 12. Flutter data for straight wings.

Model	M_f	f_f cps	V_f fps	μ_f	$\frac{V_f}{b_{o_w}\omega_f}$	$\frac{V_f}{b_{o_w}\omega_{a_N}}$	$\frac{V_f}{b_{r_\alpha}\omega_\beta}$	$\frac{V_f}{b_{r_\alpha}\omega_f}$	$\frac{V_f}{b_{o_w}\omega_{a_N}}\frac{1}{\sqrt{\mu}}$	f_{a_N} cps	$\frac{f_{h_1}}{f_{a_N}}$	$\frac{f_{a_1}}{f_{a_N}}$	$\frac{f_{h_2}}{f_{a_N}}$	$\frac{f_\beta}{f_{a_N}}$	Remarks
Light weight wings with unbalanced ailerons															
ST-13	1.80 − 1.27		1451 − 1220	39.4 − 27.3		1.90 1.60	0		0.303 0.306	292	0.320	1.00	1.20	∞	No flutter
ST-13-A	1.38	780	1330	28.6	0.651	1.75	12.5	5.21	0.327	290	0.321	0.890		1.12	High frequency aileron flutter
ST-13-A1	1.31	620	1300	29.4	0.800	1.71	14.2	6.40	0.315	290	0.316	0.821		0.965	High frequency aileron flutter
	1.30	120	1290	28.9	4.10	1.70			0.316	290	0.316	0.821		0.965	Bending − torsion − aileron flutter
ST-13-A2	1.31	670	1290	31.1	0.735	1.70	12.3	5.88	0.305	290	0.314	0.910	1.14	1.10	High frequency aileron flutter
ST-13-A3	1.36	690	1320	31.7	0.730	1.74	14.5	5.84	0.309	290	0.305	0.869	1.11	0.959	High frequency aileron flutter
ST-13-A4	1.82 − 1.45		1600 − 1375	39.6 − 28.0		2.11 1.81	18.03 − 15.5		0.322 − 0.329	290	0.303	0.841	1.08	0.934	No flutter
ST-13-A5	1.98 − 1.50		1670 − 1410	48.0 30.3		2.20 1.86	20.4 − 17.2		0.310 − 0.322	290	0.302	0.776	1.07	0.862	No flutter
ST-13-A6	1.37	640	1320	31.9	0.787	1.74	18.2	6.30	0.303	290	0.310	0.741	1.06	0.765	High frequency aileron flutter
	1.27	110	1250	29.2	4.34	1.64			0.303	290	0.310	0.741	1.06	0.765	Bending − torsion − aileron flutter
ST-13-A7	1.44	575	1351	24.95	0.897	1.78	80.92	7.18	0.36	290	0.322	1.048		0.176	High frequency aileron flutter
Light weight wings with balanced ailerons															
ST-13-AB	1.98 − 1.46		1685 1385	47.5 − 29.0		2.22 1.82	11.6 9.51		0.323 0.332	290	0.330	0.986	1.29	1.53	No flutter
ST-13-AB1	1.97 − 1.46		1685 1390	46.9 − 29.2		2.22 1.83	17.2 14.2		0.324 0.339	290	0.334	0.931	1.10	1.03	No flutter
ST-13-AB2	1.97 − 1.41		1685 1350	46.9 − 28.0		2.22 1.78	21.4 17.2		0.324 0.338	290	0.336	0.765	1.14	0.828	No flutter
ST-13-AB3	1.98 − 1.30		1685 1270	47.3 − 25.2		2.22 1.67	27.4 20.6		0.323 0.334	290	0.334	0.572	1.14	0.648	No flutter

Model	M_f	f_f cps	V_f fps	μ_{a_f}	$\frac{V_f}{b_{r_\alpha}\omega_\beta}$	$\frac{V_f}{b_{r_\alpha}\omega_f}$	f_β cps	f_{h_1} cps	f_α cps	f_{h_2} cps	Remarks
Solid wings with unbalanced aileron											
ST-14-A	1.70 − 1.27		1525 − 1245	103 − 68.2	12.30 − 10.00		380	185			No flutter
ST-14-A2	1.70 − 1.27		1525 1240	101.2 − 71.5	16.08 − 13.01		290	200			No flutter
ST-14-A3	1.70 − 1.27		1550 1230	104.1 − 66.9	20.00 − 15.9		236	200	700	813	No flutter
ST-14-A4							167	207	700	825	Model failed on injection
ST-14-A5	1.32	450	1290	75.0	28.5	8.75	138	210	700	850	High frequency aileron flutter
ST-15-A	1.51 1.27		1425 1250		24.00 − 21.05		181	217	725	850	No flutter
ST-15-A1	1.68 − 1.30		1510 1270	95.0 − 74.4	35.8 − 30.1		129	212	713	833	No flutter, model failed during retraction

Table 13. Flutter data for swept wings.

Model	M_f	f_f cps	V_f fps	μ_{f_w}	$\frac{V_f}{b_{o_w}\omega_f}$	$\frac{V_f}{b_{o_w}\omega_{\alpha_N}}$	$\frac{V_f}{b_{r_\alpha}\omega_\beta}$	$\frac{V_f}{b_{r_\alpha}\omega_f}$	$\left(\frac{V_f}{b_{o_w}\omega_{\alpha_N}}\right)\left(\frac{1}{\sqrt{\mu}}\right)$	f_{α_N} cps	$\frac{f_{h_1}}{f_{\alpha_N}}$	$\frac{f_{\alpha_1}}{f_{\alpha_N}}$	$\frac{f_{h_2}}{f_{\alpha_N}}$	$\frac{f_\beta}{f_{\alpha_N}}$	Remarks
						Light weight wing with unbalanced ailerons									
SW-9	1.89 – 1.26		1625 – 1215	35.5 – 23.0		2.22 – 1.66			0.382 0.372	280	0.205	1.00	0.750	∞	No flutter
SW-10-A	1.90 – 1.27		1630 – 1245	42.8 24.0		2.09 – 1.60	13.4 10.2		0.318 0.324	300	0.249	1.03	0.827	1.41	No flutter
SW-10-A1	1.89 – 1.26		1640 – 1230	43.0 – 23.6		2.10 – 1.58	15.7 11.8		0.318 0.322	300	0.246	1.00	0.830	1.21	No flutter
SW-10-A2	1.89 – 1.26		1650 1245	43.8 – 24.5		2.12 – 1.60	18.9 14.3		0.318 0.322	300	0.243	0.977	0.820	1.01	No flutter Aileron lost on retraction
SW-10-A3	1.89 – 1.26		1665 1260	41.4 – 26.7		2.14 – 1.62	18.0 13.6		0.328 0.342	300	0.246	0.933	0.747	1.07	No flutter
SW-10-A4	1.54	620	1450	28.7	0.893	1.84	19.4	8.11	0.343	300	0.241	0.857	0.760	0.863	High frequency aileron flutter
SW-10-A5	1.70		1546	38.7		1.967	19.8		0.316	300	0.256	0.933	0.907	0.907	Model destroyed by buffeting on injection
SW-10-A7	1.39	493	1340	26.0	1.04	1.70	16.9	9.42	0.333	300	0.242	0.880	0.750	0.917	High frequency aileron flutter
SW-10-A8	1.46	650	1380	27.9	0.810	1.76	17.4	7.36	0.333	300	0.246	0.900	0.797	0.917	High frequency aileron flutter
						Light weight wings with balanced ailerons									
SW-10-AB	1.31	930	1290	22.8	0.529	1.67	11.6	4.81	0.350	295	0.252	0.969	0.827	1.31	High frequency aileron flutter
SW-10-AB1	1.98 – 1.45		1675 1365	45.2 – 27.5		2.17 1.77	15.9 12.9		0.322 0.339	295	0.254	0.983	0.820	1.24	No flutter
SW-10-AB3	1.35	650	1310	25.4	0.769	1.69	18.2	6.99	0.335	295	0.254	0.763	0.881	0.847	High frequency aileron flutter
SW-10-AB4	1.99 – 1.26		1665 1225	43.4 – 21.9		2.16 1.59	17.5 – 12.9		0.328 0.339	295	0.250	1.02	0.881	1.12	No flutter
SW-10-AB5	1.99 – 1.25		1670 1220	43.6 – 21.4		2.16 – 1.58	19.1 – 13.90		0.326 0.342	295	0.249	0.99	0.872	1.03	No flutter
SW-10-AB6	1.85 1.60	580 580	1600 1465	38.7 30.7	1.053 0.984	2.07 1.90	24.2 22.1	9.59 8.78	0.326 0.343	295 295	0.248 0.248	0.763 0.763	0.847 0.847	0.78 0.78	Start of flutter End of flutter

Model	M_f	f_f cps	V_f fps	μ_{α_f}	$\frac{V_f}{b_{r_\alpha}\omega_\beta}$	$\frac{V_f}{b_{r_\alpha}\omega_f}$	f_β cps	f_{h_1} cps	f_α cps	f_{h_2} cps	Remarks
					Solid wing with unbalanced aileron						
SW-11-A	1.86 – 1.27		1610 1240	112.3 63.1	11.3 8.74		492	160	783		No flutter
SW-11-A1	1.86 – 1.27		1630 1235	122.6 65.1	12.6 9.55		450	141	800	532	No flutter
SW-11-A2	1.86 – 1.27		1620 1250	105.3 63.7	19.6 15.2		286	141	800	500	No flutter
SW-11-A3	1.87 – 1.27		1630 1265	113.7 65.3	21.2 16.4		267	141	800		No flutter
SW-11-A4							225	144.5	775	550	Model failed on injection
SW-11-A5	1.42	510	1365	77.2	37.6	9.29	126	150	800	521	High frequency aileron flutter
SW-12-A	1.45	365	1385	69.6	45.8	13.8	105	147	775	517	High frequency aileron flutter

Table 14. Flutter data for delta wings.

Model	M_f	f_f cps	V_f fps	μ_f	$\frac{V_f}{b_{o_w}\omega_f}$	$\frac{V_f}{b_{e_w}\omega_{a_N}}$	$\frac{V_f}{b_{o_w}\omega_{a_N}}\frac{1}{\sqrt{\mu}}$	f_{a_N} cps	$\frac{f_{h_1}}{f_{a_N}}$	$\frac{f_{a_1}}{f_{a_N}}$	$\frac{f_{h_2}}{f_{a_N}}$	$\frac{f_\beta}{f_{a_N}}$	Remarks
						Delta wings with unbalanced elevons							
De-3k-A1	1.95 – 1.27		1965 – 1249	50.1 – 27.3		1.109 – 0.704	0.156 – 0.135	680	0.300	0.987	0.710	0.956	No flutter
De-3k-A2	1.90 – 1.27		1632 – 1248	47.6 – 30.4		0.919 0.701	0.133 0.127	680	0.290	0.956	0.718	0.647	No flutter – seal destroyed during injection
De-3k-A4	1.93 – 1.26		1680 1248	50.0 – 27.2		0.946 0.701	0.134 0.132	680	0.284	0.901	0.698	0.557	No flutter
De-3k-A5	1.89 – 1.26		1650 1248	49.0 – 27.6		0.926 0.700	0.137 0.132	680	0.279	0.846	0.698	0.441	No flutter
De-3k-A6 (locked)	1.88 – 1.27		1654 1138	45.0 – 29.1		1.900 1.301	0.283 0.242	333	0.432	1.00	1.220		No flutter
De-3k-A8	1.62 – 1.25		1498 996	36.5 – 25.6		1.731 1.153	0.284 0.228	330	0.418	0.858	1.06	1.38	No flutter
De-3k-A10	1.89 – 1.27		1668 1168	46.5 – 30.2		1.928 1.350	0.282 0.246	330	0.394	0.800	1.06	0.948	No flutter
De-3k-A11	1.88 – 1.27		1652 1269	45.8 – 29.5		1.914 1.468	0.283 0.272	330	0.388	0.776	1.04	0.855	No flutter
De-3k-A12	1.27	280	1270	29.8	1.73	1.47	0.269	330	0.385	0.758	1.00	0.770	Retraction flutter
De-3k-A13	1.88	156	1660	46.2	4.06	1.92	0.282	330	0.355	0.697	0.939	0.485	Injection flutter
De-3k-A14	1.89	150	1650	45.3	4.20	1.91	0.284	330	0.388	0.606	0.839	0.576	Injection flutter
De-3k-A15	1.51	280	1405	27.04	1.92	1.49	0.287	360	0.439	0.892	1.180	0.536	Retraction flutter
						Delta wings with balanced elevons							
De-3k-AB	1.88 – 1.30		1642 1256	43.7 – 25.4		1.698 1.296	0.256 0.257	370	0.459	0.946	1.08	0.946	No flutter
De-3k-AB1	1.97	200	1670	46.8	3.19	1.72	0.251	370	0.473	0.900	1.28	0.743	Injection flutter
De-3k-AB2	1.99	160	1690	48.0	4.03	1.74	0.251	370	0.441	0.838	1.29	0.527	Injection flutter

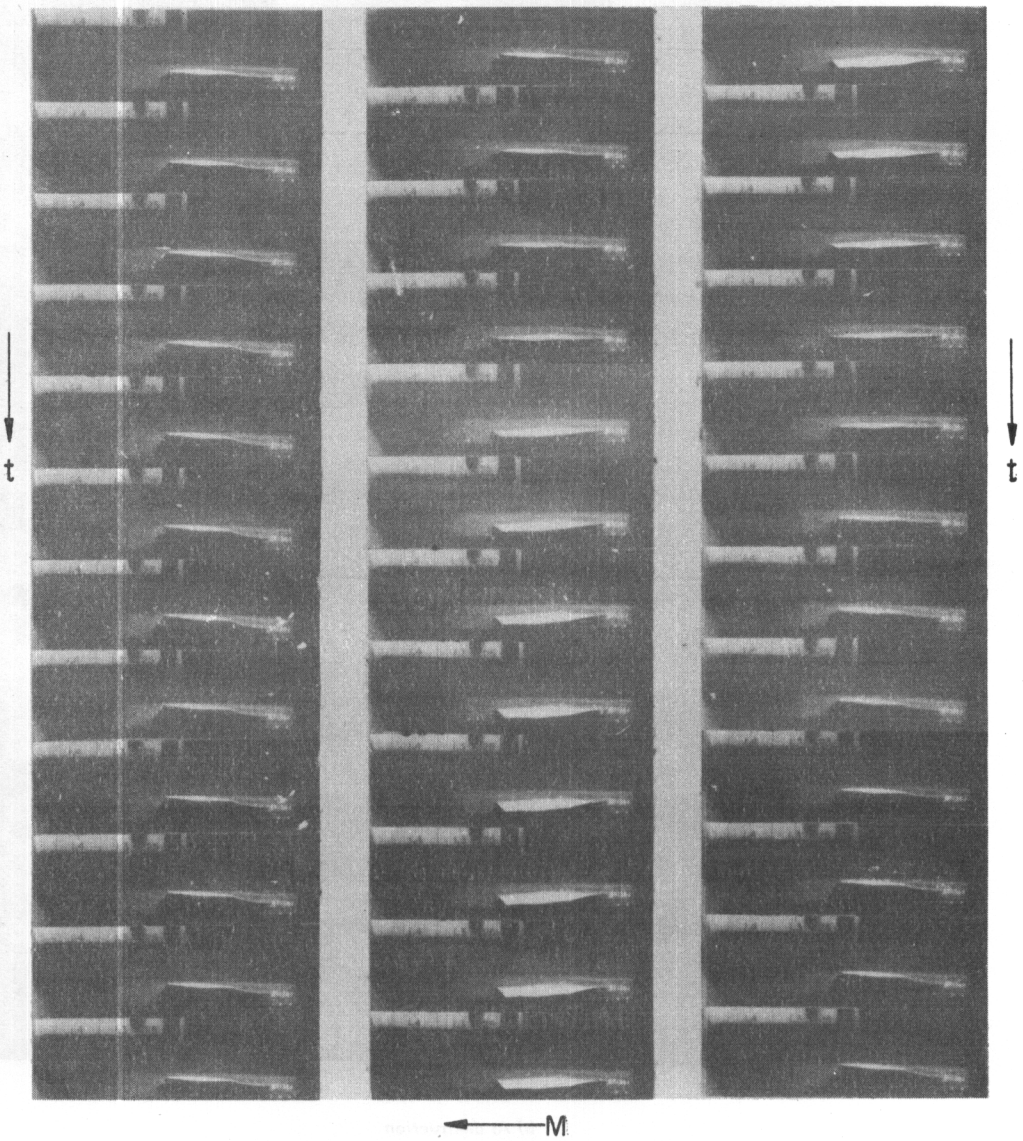

a) Near start of flutter

Fig. 16. High-speed movies of ST-13-A1 model during flutter.

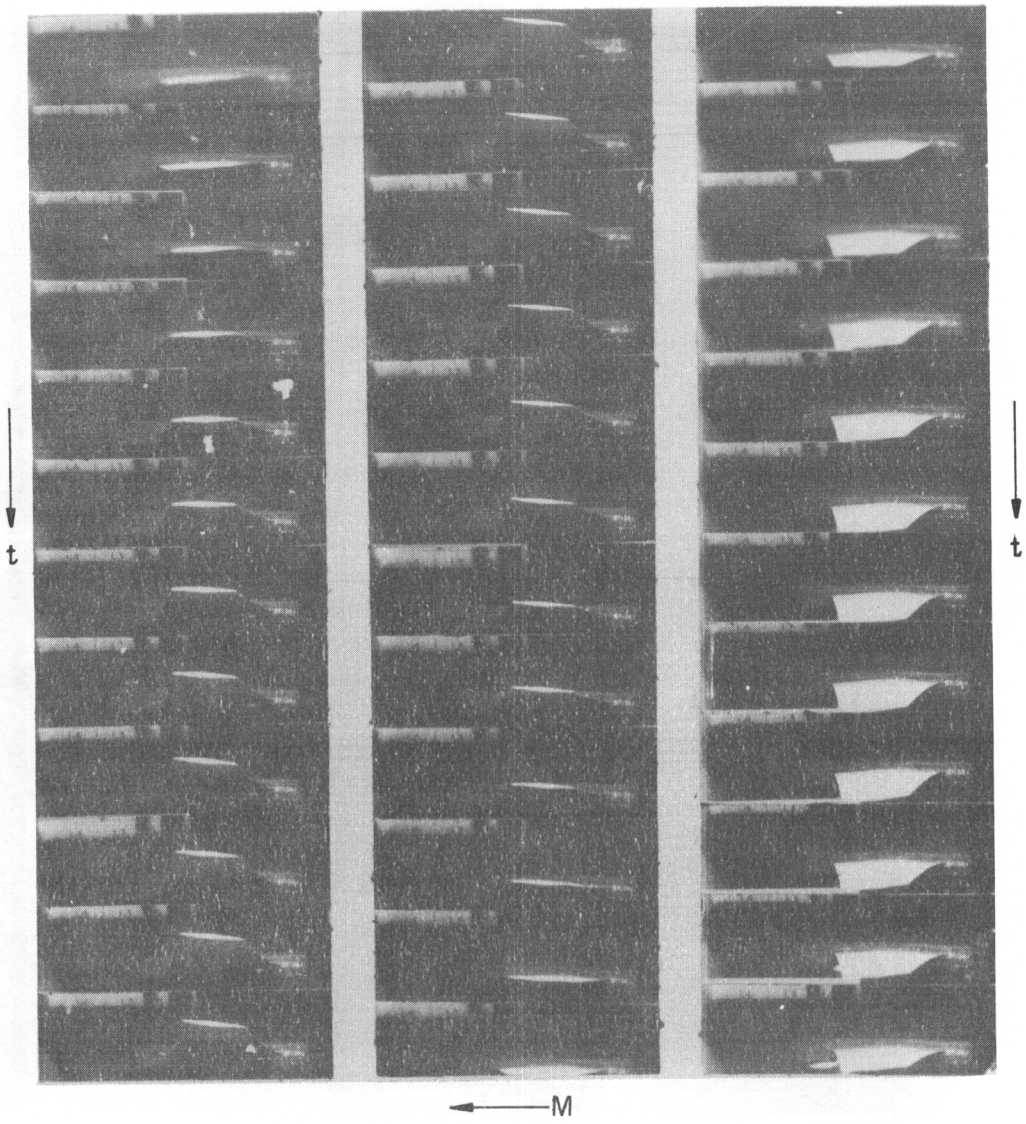

b) At destruction

Fig. 16. High-speed movies of ST-13-A1 model during flutter. (cont.)

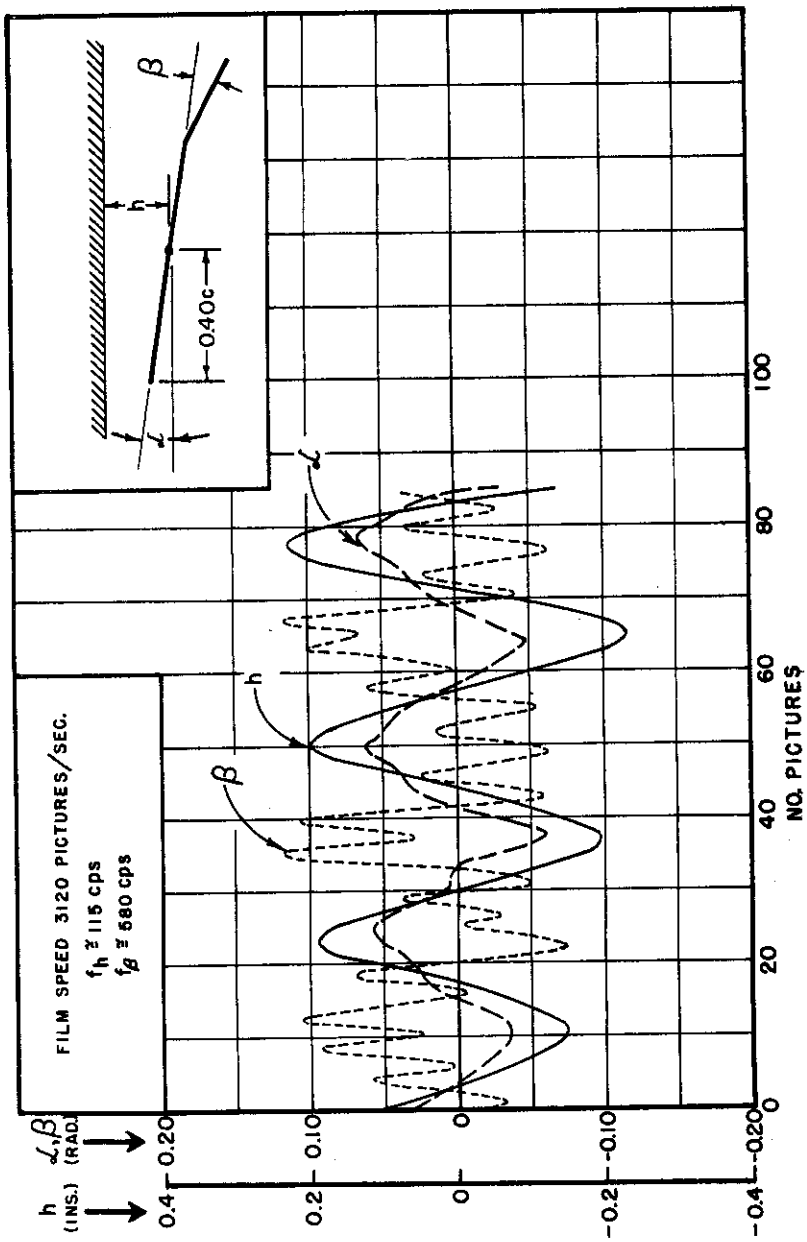

Fig. 17. Wing-aileron motion at start of tunnel test of ST-13-A1 model from high-speed movies. M = 1.88.

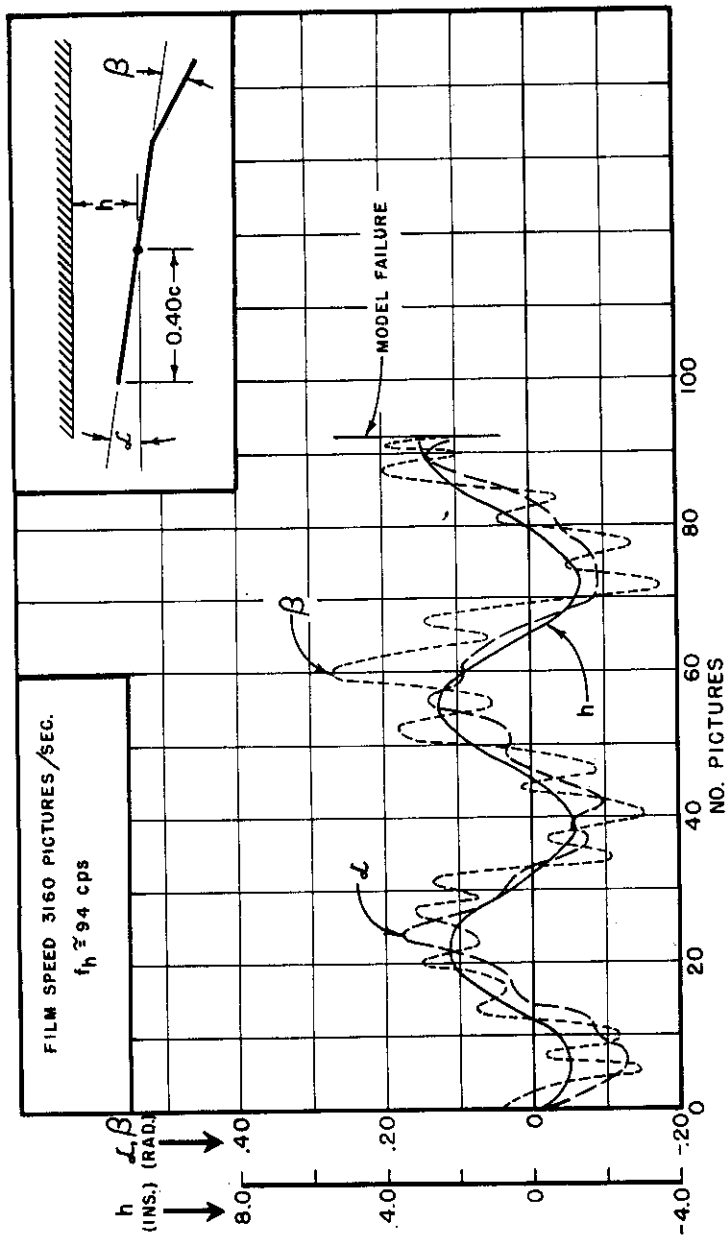

Fig. 18. Wing-aileron motion during flutter of ST-13-A1 model from high-speed movies. M = 1.30.

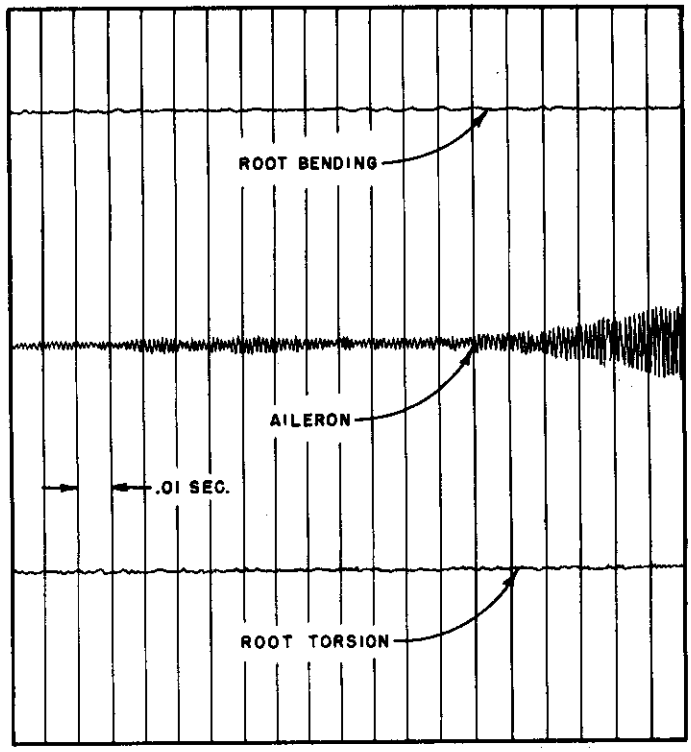

Fig. 19. Traces of strain gage recordings during flutter of ST-13-A model.

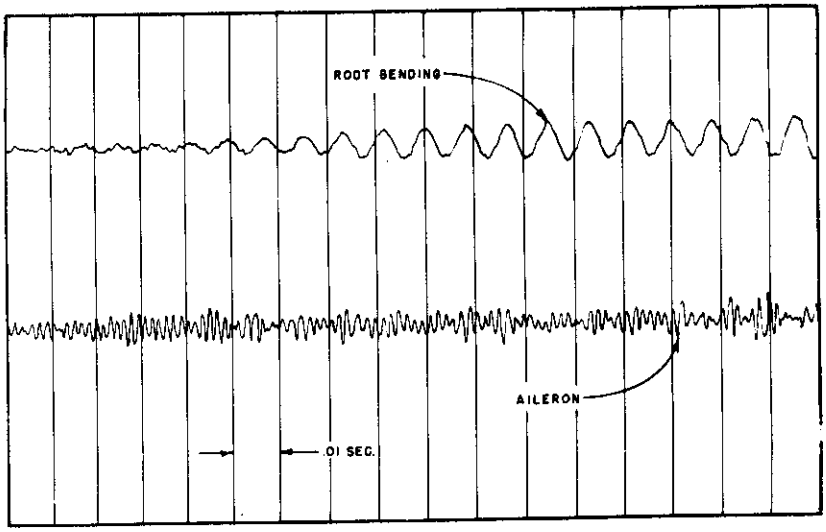

Fig. 20. Traces of strain gage recordings during flutter of ST-13-A1 model.

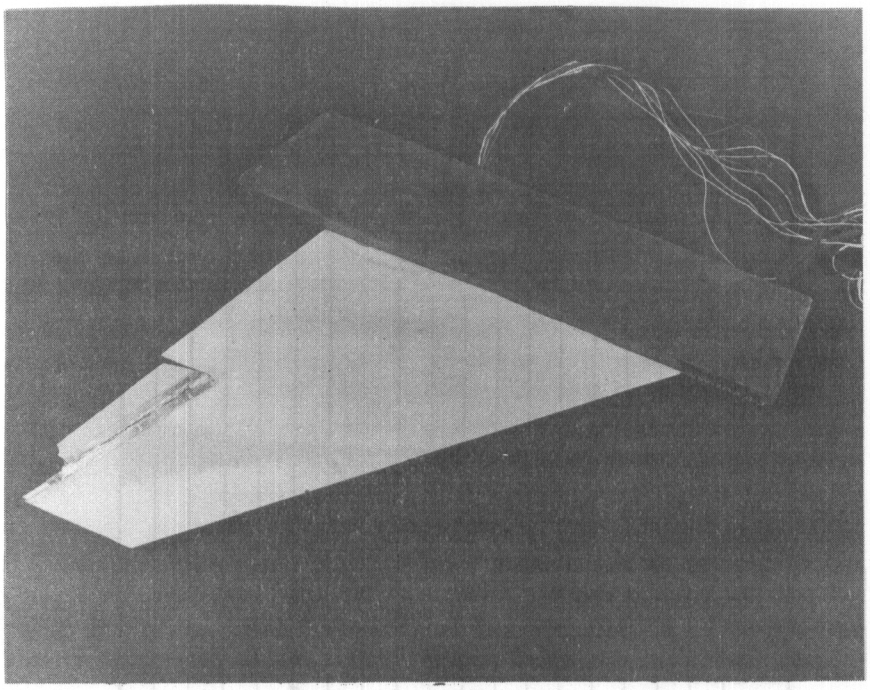

Fig. 22. Lightweight swept wing-aileron model after destructive high-frequency aileron flutter.

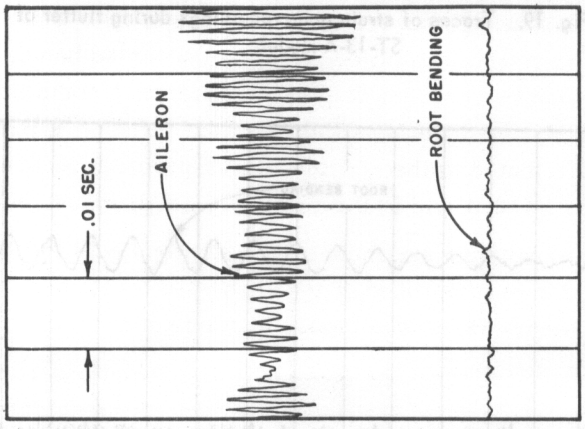

Fig. 21. Traces of strain gage recordings during flutter of ST-13-A2 model.

APPENDIX III

DETERMINATION OF REFERENCE TORSIONAL FREQUENCY FOR MODEL WINGS

In the theoretical flutter analysis for the straight wing with aileron (Appendix I) the frequencies of the simple uncoupled bending, torsion and aileron modes of vibration are used as parameters. The results are presented using the torsional frequency as a significant reference value. On the other hand the measured vibration frequencies of the models correspond to the lower coupled modes of a complex elastic system. In order to compare theory and experiment in terms of dimensionless parameters it was necessary to estimate a reference torsional frequency for the models which corresponded to the one used in presenting the theoretical results.

In the case of the straight wings without ailerons of Ref. 1 the two lowest coupled frequencies were found to differ from the uncoupled bending and torsion frequencies by less than two percent so that the difference could be ignored (see Section D. 7 of Ref. 1). This small effect of coupling on primary natural frequencies can be attributed to the considerable separation between the frequencies $(\omega_{h_1}/\omega_{\alpha_1}) \cong 0.3$ and to the relatively small mass coupling. However, when the same basic straight wings incorporate ailerons with the uncoupled aileron frequency in the neighborhood of the uncoupled torsional frequency, the frequencies of the primary measured modes may be strongly affected.

The following analysis forms the basis of a simplified procedure for estimating an uncoupled torsional frequency for each of the series of models by extrapolation of the measured torsional frequencies. Although the need for the procedure stemmed from the comparison between theory and experiment for the straight wings, it was also applied to the swept and delta wings in the hope that it would aid in interpretation of the results.

If we assume that the major effect of the aileron degree of freedom on the primary torsional behavior of the models can be represented by the simple two

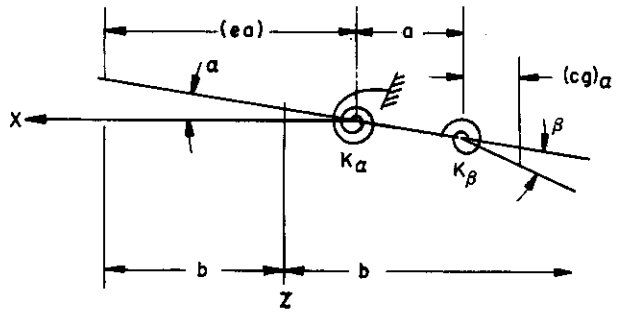

Fig. 23. Two-degree-of-freedom wing-aileron model.

degree-of-freedom model shown in Fig. 23, the two equations of motion are:

$$\ddot{\alpha}\, I_\alpha + \alpha\, K_\alpha + \ddot{\beta}\, (I_{HL} + a\, S_{HL}) = 0 \tag{9}$$

$$\ddot{\alpha}\, (I_{HL} + S_{HL}\, a) + \ddot{\beta}\, I_{HL} + \beta\, K_\beta = 0 \tag{10}$$

where the dot stands for differentation with respect to time, K_α and K_β are spring stiffnesses, the I's are the appropriate mass moments of inertia, and S_{HL} is the static unbalance of the aileron about the hinge line. If simple harmonic motion is assumed by taking:

$$\alpha = \bar{\alpha}\, e^{i\omega t} \tag{11}$$

$$\beta = \bar{\beta}\, e^{i\omega t} \tag{12}$$

where $\bar{\alpha}$ and $\bar{\beta}$ are the complex amplitudes of the angle of attack and angle of aileron deflection respectively, then the resulting eigenvalue problem can be solved for the two values of frequency given by Eq. (13).

$$\omega^2_{1,2} = \frac{1}{2\left[1 - \dfrac{(I_{HL} + S_{HL}\, a)^2}{I_{HL}\, I_\alpha}\right]} \times \left[(\omega^2_{\alpha_1} + \omega^2_\beta) \pm \sqrt{(\omega^2_{\alpha_1} + \omega^2_\beta)^2 - 4\,\omega^2_{\alpha_1}\,\omega^2_\beta \left[1 - \frac{(I_{HL} + S_{HL}\, a)^2}{I_{HL}\, I_\alpha}\right]}\right] \tag{13}$$

where $\omega^2_{\alpha_1}$ and ω^2_β are given by:

$$\omega^2_{\alpha_1} = \frac{K_\alpha}{I_\alpha} \tag{14}$$

and

$$\omega^2_\beta = \frac{K_\beta}{I_{HL}} \tag{15}$$

and are the uncoupled torsion and aileron frequencies respectively for our simple system. If for a given value of ω_{α_1}, ω, and ω_2 are plotted for various values of ω_β, two curves result. The lower branch (ω_1) approaches ω_β when ω_β approaches zero and ω_{α_1} as ω_β gets very large. A second branch at higher frequency (ω_2) also occurs approaching a value of frequency slightly higher than ω_{α_1} as ω_β approaches zero and approaching ω_β as ω_β approaches infinity These curves are plotted for a value of ω_{α_1} = 290 cps in Fig. 24 for a typical unbalanced aileron case.

Insofar as this simplified analysis applies to the straight wing vibration data of Appendix II, the two branches of Eq. (13) are represented by the two lowest modes with predominantly torsional node lines. If the frequencies of these modes are plotted for increasing values of uncoupled aileron frequency ω_β the asymptotic value of the lower branch is taken as the nominal uncoupled torsional frequency of the wing, ω_{α_N}.* Figure 24 shows the experimental curves for the straight wing models and also shows the theoretical curves derived from Eq. (13). The agreement between the theoretical curve from Eq. (13) and the test data is surprisingly good for the lower frequency branch. Furthermore, the asymptotic value of 290 cps which was used as the nominal uncoupled torsional frequency for the straight wings, agrees very well with the value of first torsional frequency that was measured for the ST-13 wing in Table 8 of Appendix II. The ST-13 wing is the basic straight wing without an aileron.

Figure 25 shows similar experimental curves for the swept wing models. The asymptotic values of 300 cps and 295 cps were chosen as the nominal first torsion frequencies for the swept wings with unbalanced and balanced ailerons

*It should be noted that a more comprehensive analysis including many more modes would predict the same asymptotic behavior of the lower torsional branch with the limiting frequency that of the primary torsion mode of the base wing. It was mentioned earlier in this appendix that this frequency of the base straight wing is within a few percent of its uncoupled torsional frequency.

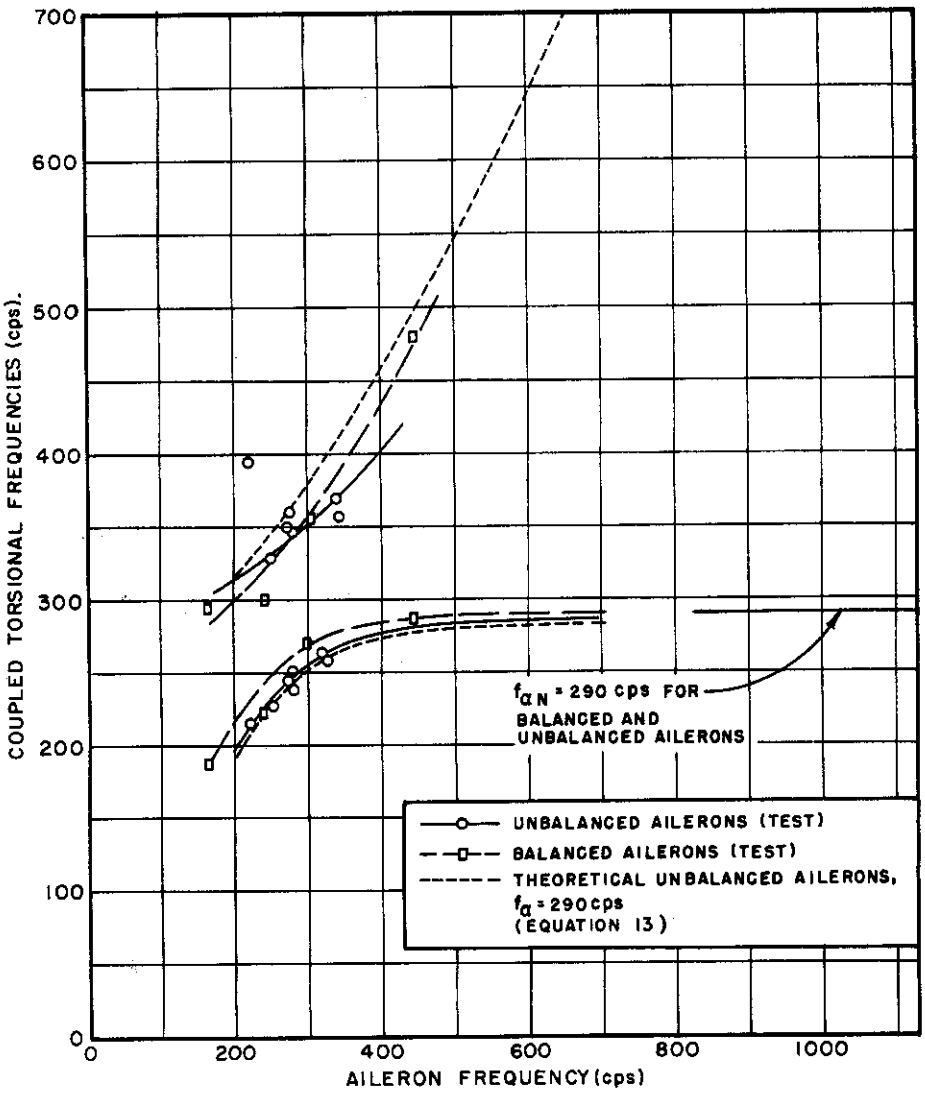

Fig. 24. Effect of aileron-torsion coupling on straight wing torsional frequencies.

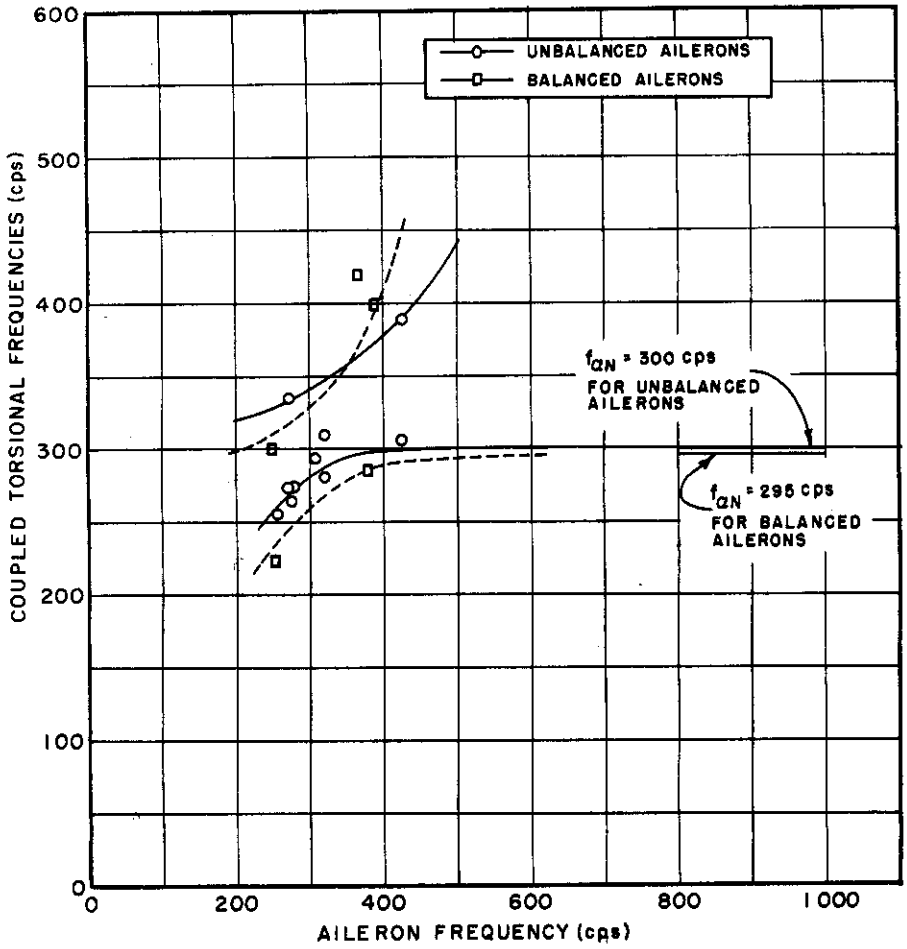

Fig. 25. Effect of aileron-torsion coupling on swept wing torsional frequencies.

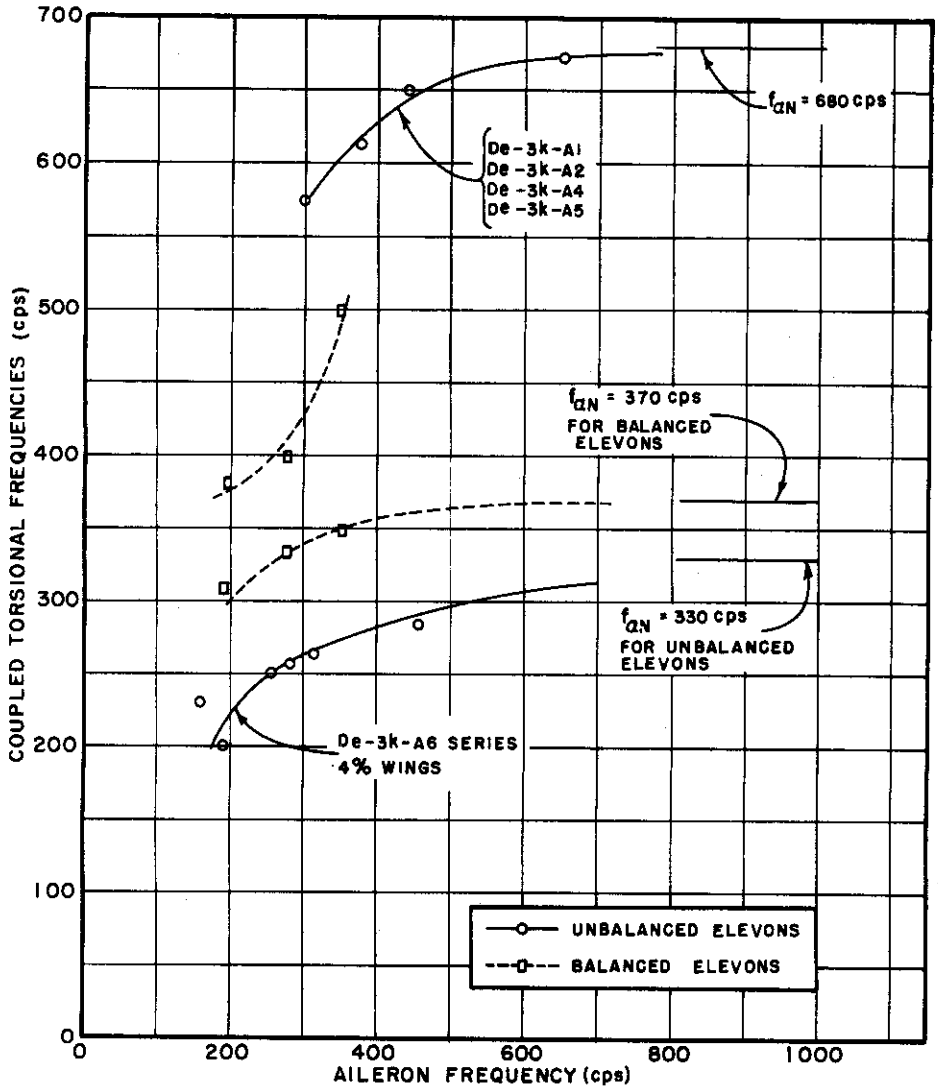

Fig. 26. Effect of elevon-torsion coupling on delta wing torsional frequencies.

respectively. Since none of the SW-10 series models were tested without an aileron a direct comparison of these asymptotic values with a locked aileron case is not possible. However, the agreement between these values and the measured first torsional frequency of the SW-9 wing is quite good. The SW-9 wing is slightly different structurally from the SW-10 series wings, but has no aileron.

Figure 26 shows the experimental curves for the delta wings. Only the lower torsional frequency was recorded for the unbalanced delta wing series. The asymptotic value for the De-3k-A6 through -A14 series is 330 cps and agrees quite well with that measured for the De-3k-A6 model with the elevon locked. The balanced aileron delta wings show a higher asymptotic value of 370 cps. The difference between the two wings is a reflection of the difference in balsa wood used to construct the models. The asymptotic value for the De-3k-A1 through -A5 series wings of 680 cps is of somewhat academic interest since none of these wings fluttered. The uncoupled first torsional frequency for the De-3k-A15 model was estimated by extrapolation of the De-3k-A6 curve by using static influence coefficient data.

The method outlined in this appendix for finding the nominal uncoupled first torsional frequency from the asymptotic value of the lower torsional frequency branch depends to a large extent on the judgment of the person analyzing the vibration test results. It could not be used except where a relatively large number of similar wings differing only in aileron frequency are tested. However, the method does have the advantage of depending only on the measured vibration data and not on measurements of model mass properties. For wings of varying basic structure, the uncoupled torsional frequency can be obtained only by locking the aileron to the wing in a manner which does not disturb the mass balance of the wing or by using Eq. (13) or a similar one to find ω_{α_1} and ω_β where ω_1 and ω_2 and the mass properties of the model are known.